Szent István Egyetem
Állatorvos-tudományi Doktori Iskola

THE GONADOTROPIN SURGE: ON THE ROLE OF ESTROGEN-INDUCED SYNAPTIC PLASTICITY AND RAPID, NON-GENOMIC REGULATORY MECHANISMS.

PhD Thesis

By:

Attila Zsarnovszky

2005

Szent István Egyetem
Állatorvos-tudományi Doktori Iskola

Témavezető és témabizottsági tagok:

Prof. Dr. Péter Sótonyi
SzIEÁOTK Anatómiai és Szövettani Tanszék

Dr. Papp Zoltán
SzIEÁOTK Állathigiéniai TanszékMhely

Dr. Szalay Ferenc
SzIEÁOTK Anatómiai és Szövettani Tanszék

Készült 8 példányban. Ez az 1. sz. példány.

.....
dr. Zsarnovszky Attila

TABLE OF CONTENTS

SUMMARY

Hypothalamic mechanisms maintain the reproductive cycle and fertility in all mammalian species. In females, the cyclic nature of the reproductive functions is based upon the responsiveness of the neuroendocrine hypothalamus to the fluctuating levels of estrogen (E_2), and the responsiveness of the ovaries to the fluctuating levels of gonadotropins. This cyclic and reciprocal function is maintained by alternating negative- and positive feedbacks. Failure of the positive feedback results in anovulation and sterility. The regulatory effect of E_2 on pituitary gonadotropin release is mediated by a complex neuronal system located in the mediobasal hypothalamus (MBH).

It is well established that excitatory amino acid (EAA) neurotransmission is an essential component in the regulation of the gonadotropin-releasing hormone (GnRH) delivery system. However, the morphological interconnection of these systems is not fully understood. The first objective of the present study was to determine whether or not alpha-amino-3-hydroxy-5-methyl-4-isoxazole propionic acid (AMPA) receptors – as indicators of aspartate/glutamatergic innervation – are present in the major neuronal populations, such as the neuropeptide-Y- (NPY), galanin- (GAL) and tyrosine-hydroxylase- (TH) containing neurons of the arcuate nucleus (AN) of the female rat. The results of our experiments suggest that an excitatory aspartate/glutamatergic input is implicated in the regulation of the examined neuropeptide containing AN neurons but not in that of TH-IR cells of the same area.

Previous studies indicate that an E_2-induced synaptic plasticity (EISP) is part of the mechanism through which E_2 regulates the function of hypothalamic neurons. To better understand the mechanism of the EISP, we aimed to determine the identity of hypothalamic neurons that undergo EISP, and compare the findings with simultaneous changes in plasma E_2- and LH-concentrations. Our results indicate that in non-human primates (Cercopithecus aethiops) E_2 induces a characteristic pattern of changes in the number of axo-somatic synapses in the MBH that plays a major role in the regulation of the secretion/release of gonadotrop hormone-releasing hormone (GnRH).

The E_2-responsiveness of MBH neurons has been explained by their expression of estrogen receptors. However, some of the E_2-dependent regulatory mechanisms of the basal forebrain are mainly associated with rapid and short-lived events that occur during the midcycle positive gonadotropin feedback. The rapid events that take place in MBH

neurons occur within minutes after exposure to E_2, and are mediated by signaling systems upstream of gene-activation. Rapid E_2-induced effects on the activation of intracellular signaling systems have been observed in a variety of brain regions. We focused on identifying the activated form of the extracellularly regulated kinases 1 and 2 (ERK1/2) in the developing and adult rat cerebellum. To ensure the validity of the applied concentrations of E_2 on neurons, we chose to test the rapid effects of E_2 on the activation of the ERK-pathway in cerebellar cells, which are known to lack aromatase (estrogen-synthase) at any age, and characterized the time-, dose- and age dependency of these rapid effects, both in cultured cerebellar granule cells and in intact live cerebellum.

Our in vitro and in vivo results provided evidence that E_2 can rapidly activate neuronal ERK1/2 intracellular signaling. It is suggested that the activation of the ERK1/2-pathway within the MBH can also be modulated rapidly by E_2, as it occurs in other brain areas.

GENERAL INTRODUCTION

Hypothalamic mechanisms maintain the reproductive cycle and fertility in all mammalian species. In females, the cyclic nature of the reproductive functions is based upon the responsiveness of the neuroendocrine hypothalamus to the fluctuating levels of estrogen (E_2), and the responsiveness of the ovaries to the fluctuating levels of gonadotropins. This cyclic and reciprocal function is maintained by two distinct and alternating regulatory mechanisms: 1) Negative feedback, when E_2 down-regulates the release of gonadotropins, and 2) The midcycle positive feedback, when the sharply rising plasma concentration of E_2 results in a surge in the release of pituitary gonadotropins that leads to ovulation. Failure of the positive feedback results in anovulation and sterility. The regulatory effect of E_2 on pituitary gonadotropin release is mediated by a complex neuronal system located in the basal forebrain. In the rat, this system consists of two major components: a neuronal circuit in the mediobasal hypothalamus (MBH), concentrated mainly in and around the arcuate nucleus (AN), and another circuit of gonadotrop hormone-releasing hormone- (GnRH) producing neurons and functionally associated cells that are concentrated in and around the medial preoptic area (MPOA). The MBH circuit is responsive to changing levels of E_2 and regulates the function of the GnRH neurons of the MPOA circuit and thus, is responsible for shaping the pattern of secretion and release of GnRH into the pituitary portal vasculature. GnRH, in turn, stimulates the release of luteinizing hormone (LH) from the pituitary gonadotrops that are sensitized by E_2.

Previous studies indicate that the fluctuation of plasma E_2-concentrations during the estrous cycle induces changes in the number of synapses in the hypothalamus, suggesting that this estrogen induced synaptic plasticity (EISP) is part of the mechanism through which E_2 regulates the function of hypothalamic neurons in the MBH. To better understand the mechanism of the EISP, in the studies described in the present work we aimed to determine the identity of hypothalamic neurons that undergo EISP, and compare the findings with simultaneous changes in plasma E_2- and LH-concentrations. Our results, in consistence with relevant peer studies, indicate that E_2 induces changes in the number of axo-somatic synapses in the MBH that plays a major role in the regulation of the secretion/release of GnRH, in an alternating positive- and negative feedback fashion. Since EISP was observed in both rodents and non-human primates (**1-**

12), it is assumed that EISP could be a key regulatory mechanism in the human MBH as well. Therefore, further research aiming at elucidating the mechanism of hypothalamic EISP is crucial for understanding the regulation of female reproductive biology.

As part of the present studies we demonstrated that in rat, the EISP observed in the MBH is confined to a distinct population of neurons that directly project to regions of the brain where the blood-brain barrier is absent (neurohaemal regions), mainly the pituitary portal vasculature (**1**). Therefore, it was reasonable to assume that this cell population represents the first link in the hypothalamic chain of neurons that regulates the secretory function of GnRH neurons and thus, plays a key role in the regulation of the entire GnRH-regulating hypothalamic circuit. To better understand the functional attributes of the intrinsic connectivity of this hypothalamic circuit, we determined some of the biochemical characteristics of its neurons (**13**, and references therein). Those studies clearly indicate that excitatory amino acid (EAA) neurotransmission, at the level of the AN, is highly involved in the complex regulation of GnRH. Our results also show that there are at least two populations of neurons within the AN, one of which (most of the neuropeptide-containing neurons) is under an aspartate/glutamatergic "supervision," while the other (dopaminergic neurons) is not. It is also suggested that the inhibitory neurons of the AN are in a key position to regulate the cyclic, EAA-induced female reproductive processes in the neuroendocrine hypothalamus.

The estrogen-responsiveness of the MBH neurons has been explained by their expression of estrogen receptors (mostly ERα in the arcuate nucleus) that function as ligand-activated transcription factors regulating the expression of E_2-responsive genes. However, some of the E_2-dependent regulatory mechanisms of the basal forebrain could not yet been explained. These mechanisms are mainly associated with rapid and short-lived events that occur during the midcycle positive gonadotropin feedback. In fact, the driving force of the mechanism which rapidly turns the reciprocal (negative) feedback into positive feedback is far from being understood. The rapid events that take place in MBH neurons, such as a change in the structure of the plasma membrane (change in the number of intramembranous protein particles and the number of endo- and exocytotic pits (e.g., **14-16**), increased internalization (endocytosis, [**14**]), occur within minutes after exposure to E_2, and are apparently initiated and mediated by signaling systems upstream of gene-activation. Rapid E_2-induced effects on neuronal excitability (**17-19**)

and the activation of a number of intracellular signaling systems have been observed in a variety of brain regions (**20**). These observations prompted us and many other scientists to search for a plasma membrane-associated ER that, upon binding to E_2, could activate intracellular signaling cascades (**21**). While the identity of such membrane-incorporated ERs remains to be determined, accumulating evidence indicates that plasmamembrane-associated structure(s), upon binding to E_2, can rapidly (within minutes) activate a number of intracellular signaling systems, including the extracellular signal regulated kinases 1 and 2 (ERK1/2) (**20**). We focused on identifying the activated, dually phosphorylated form of ERK1/2 in the developing and adult rat cerebellum (**22-25**). The ERK1/2 system has been identified in the MBH and its activation by E_2 has been reported (**26**). Nevertheles, in order to characterize the effects of E_2 on the activation of the ERK1/2-pathway, we chose the cerebellum as an experimental model system because this brain region lacked aromatase activity at any age examined, therefore the 'de novo' estrogen synthesis that could mask the real effects of the experimental E_2-treatments could be discounted. We investigated the rapid effects of E_2 on the activation of the ERK-pathway and characterized the time-, dose- and age dependency of these rapid effects, both in cultured cerebellar granule cells and in intact live cerebellum. We should remark that in order to better understand the role and the nature of E_2-induced ERK-activation in neurons, and thus keeping away from the possibility of confusion during the evaluation of the results, several aspects of the matter were taken under investigation (see below).

Our in vitro and in vivo results were consistent and provided evidence that E_2 can rapidly activate the ERK1/2 intracellular signaling system even in a brain region that does not belong to the neuroendocrine part of the brain. Studies in the cerebellum and other parts of the central nervous system suggest that the activation of the ERK1/2-pathway (that in the hypothalamus is affected by E_2 24 hours after the treatment [**26**]) can also be modulated rapidly by E_2, as it occurs in other brain areas.

AIMS OF THE THESIS

1. Identification and biochemical characterization of MBH neurons that are regulated by excitatory amino acid (EAA) neurotransmission in female rats (Zsarnovszky et al., 2000; [**13**]):

a. Immunohistochemical identification of alpha-amino-3-hydroxy-5-methyl-4-isoxazole propionic acid (AMPA) receptors GluR1 and GluR2/3, as indicators of aspartate/glutamatergic innervation in the arcuate nucleus of female rats;

b. Immunohistochemical co-localization of AMPA receptors with neuropeptide-Y (NPY), galanin (GAL) and tyrosine-hydroxylase (TH);

c. Assessment of the possible role of EAA-neurotransmission in the neuroendocrine hypothalamus;

2. Determination and analysis of estrogen-induced synaptic plasticity (EISP) in the primate and rat arcuate nucleus (AN):

a. Identification of neurons undergoing EISP (Parducz et al., 2003; [**1**]);

b. Determination of the number of synaptic connections on gonadotrop hormone-releasing hormone- (GnRH) and other neurons in the AN of ovariectomized versus ovariectomized plus estrogen-treated monkeys (Zsarnovszky et al., 2001; [**2**]);

c. Determination of the number of synaptic connections on glutamic-acid-decarboxylase-immunoreactive (GAD-IR) inhibitory GABAergic neurons in the AN of monkeys (Zsarnovszky et al., 2000; [**3**]);

d. Assessment of the role of EISP in the regulation of gonadotropin-release;

3. Identification and characterization of rapid, non-genomic estrogen effects on non-neuroendocrine neurons: estrogen-induced rapid modulation of the extracellularly regulated kinases 1 and 2 (ERK1/2) MAPK- (mitogen-activated protein kinase) pathway in the rat cerebellum:

a. Determination of rapid estrogen effects in primary neuronal cell cultures (Wong et al., 2003; [**22, 25**]);

b. Determination of the spatiotemporal distribution of activated, dually phosphorylated ERK1/2 (pERK) in the rat cerebellum (Zsarnovszky and Belcher, 2004; [**27**]);

c. Identification of direct in vivo estrogen effects on the activation of cerebellar ERK1/2-activation: analysis of dose- and age-dependency (Zsarnovszky and Belcher, 2003 [**25**, **28**]).

MATERIALS AND METHODS

1. *Identification and biochemical characterization of MBH neurons that are regulated by excitatory amino acid (EAA) neurotransmission: Immunohistochemical identification of alpha-amino-3-hydroxy-5-methyl-4-isoxazole propionic acid (AMPA) receptors GluR1 and GluR2/3, as indicators of aspartate/glutamatergic innervation in the arcuate nucleus of female rats and immunohistochemical co-localization of AMPA receptors with neuropeptide-Y (NPY), galanin (GAL) and tyrosine-hydroxylase (TH);*

Animals and tissue preparation

Four immunohistochemical co-localization studies were conducted (co-localization of GluR2/3 with GluR1, NPY, GAL and TH) using five normal cycling adult female Sprague-Dawley rats (200-250 g body weight) for each study. Animals were kept under standard laboratory conditions, with tap water and regular rat chow ad libitum in a 12-h light, 12-h dark cycle. Twenty-four hours before sacrifice, under deep ketamine (75 mg/kg, i.m.) anesthesia, animals were fixed in a stereotaxic apparatus (David Kopf Instruments, Tujunga, CA) and, using a Hamilton microsyringe (Hamilton Co., Reno, NV), a single injection of colchicine (80 μg in 20 μl saline) was applied into the lateral ventricle to enable perikaryal labeling of NPY and GAL. Rats were killed 24 h later under deep ether anesthesia by transcardial perfusion with 50 ml heparinized saline followed by 250 ml fixative (4% paraformaldehyde, 0.1% glutaraldehyde and 15% saturated picric acid, in 0.1 M phosphate buffer [PB], pH 7.4). Brains were removed from the skull and a tissue block containing the entire hypothalamus was dissected out and postfixed for 2 h in a similar, but glutaraldehyde-free fixative. After fixation, the tissue blocks were rinsed several times in PB and, in order to recognize the two sides of the slices, they were trimmed asymmetrically with a razor blade. Sixty-micrometer-thick coronal vibratome sections were cut from the entire rostrocaudal extent of the AN, and the adjacent sections were arranged in pairs. This was followed by 4X15-min rinses in PB. In order to eliminate unbound aldehydes, sections were incubated for 20 min in 1% sodium borohydride, then washed 6X7 min in PB.

Immunostaining

One section of each pair was immunostained for GluR2/3, whereas their counterparts were single immunostained for either GluR1, NPY, GAL or TH. Sections were incubated overnight at room temperature in primary antisera (rabbit-anti-GluR1, -GluR2/3; 1:500, Chemicon; mouse-anti-TH; 1:5000, Chemicon; rabbit-anti-NPY; 1:20000; rabbit-anti-GAL; 1:5000, Peninsula Laboratories, San Carlos, CA; all in PB containing 1% normal serum produced in the species of the second antibodies). After several rinses in PB, sections were further incubated in biotinylated goat-anti-rabbit second antibody for GluR1, GluR2/3, NPY and GAL; in biotinylated horse-anti-mouse second antibody for TH (all at a dilution of 1:250 in PB, at room temperature, for 2 h). A subsequent rinse in PB for 3X10 min was followed by incubation in avidin-biotin-peroxidase, at room temperature, for 2 h (ABC Elite Kit, Vector Labs). After 3X10 min rinses in PB, the immunoreaction was visualized as brown by a diaminobenzidine reaction. Pairs of sections were thoroughly rinsed in PB and mounted with their matching surfaces on the upper side. Sections were then dehydrated through increasing ethanol concentrations and, finally, coverslipped.

Co-localization

The “mirror” technique allows immunostaining for two different cytoplasmic antigens within a cell that is vibratome-cut into two halves. The immunostained material was examined at the light microscopic level. Focusing on the upper surface of each section, at a magnification of X200, camera lucida drawings were made using a drawing tube attached to an Olympus BH-2 microscope. Examination of the corresponding areas on the adjacent sections allowed us to determine to what extent the GluR2/3-containing neurons also express GluR1, NPY, GAL and TH, and vice versa. Then, the number of cell bodies immunoreactive for both GluR2/3 and one of the examined antigens were counted and expressed as percentages. This gave us an approximation of the degree of co-localization of the above mentioned substances with GluR2/3. All the preceding animal procedures were carried out under a protocol approved by the Yale University Animal Care Committee.

2. *Determination and analysis of estrogen-induced synaptic plasticity (EISP) in the primate and rat arcuate nucleus (AN):*

2.a. *Identification of neurons undergoing EISP.*

Animals and surgical procedures

Two-months-old female Sprague-Dawley rats were used for this study, housed and fed as described previously. Animals were ovariectomized under nembutal anesthesia and one month later were given a single i.p. fluorogold injection (2 mg/100 g body weight), dissolved in saline (Fluorochrome, Inc., Englewood, CO). Five days post-injection the animals were s.c. injected either with a single dose (100 μg/100 g body weight) of 17β-estradiol (Sigma Chemical Co., St. Louis, MO) dissolved in sesame oil or with a single injection of the oil vehicle.

Immunocytochemistry

Twenty four hours after the estradiol injection, the animals were anesthetized with Nembutal and perfusion-fixed as described above. After perfusion the brains were removed from the skull and post-fixed for 3 h (see above). The above immunostaining protocol was followed, using a rabbit anti-fluorogold primary antibody (Biogenesis, Inc., Franklin, MA, 1:5000). For electron microscopy, sections were osmicated (1% OsO_4 in PB) for 30 min, dehydrated through increasing ethanol concentrations and flat-embedded in Araldite between liquid release-coated (Electron Microscopy Sciences, Fort Washington, PA) slides and coverslips. After capsule embedding, blocks were trimmed and ribbons of serial ultrathin sections were collected on Formvar-coated single-slot grids, contrasted by uranyl acetate and lead citrate, and examine using a Zeiss EM 902 electron microscope.

Quantitative analysis

The analysis was performed in a double-blind fashion on electron micrographs from rats of the different experimental treatments. To obtain a complementary measure of the number of axo-somatic synaptic contacts, unbiased for possible changes in synaptic size, the dissector technique (**29**) was used. On consecutive 90-nm-thick sections, we determined the average projected height of the synapses and used about 30% of this value as the distance between the disectors. On the basis of this calculation, the number

of axo-somatic synapses was counted in two consecutive serial sections about 270 nm apart ("reference" and "look-up" sections) of 12-15 perikaryal profiles in each block. In order to increase the sampling, the procedure was repeated in such a way that the reference and look-up sections were reversed. We considered a structure as a synapse if the bouton and the perikaryal membrane were in direct contact and at least three synaptic vesicles were present in the presynaptic bouton.

Synaptic densities were evaluated according to the formula

$N_v=\Sigma Q/V_{dis}$

Where ΣQ represented the number of synapses present in the "reference" section that disappeared in the "look-up" section. V_{dis} is the disector volume (volume of reference), which is the area of the perikaryal profile multiplied by the distance between the upper faces of the reference and look-up sections (**29**), i.e., the data are expressed as numbers of synaptic contacts per unit volume of perikaryon. Section thickness was determined by using the Small's minimal fold method.

There were six rats in each experimental group and three blocks/animal were counted. Data from the same animals were pooled since no variations were detected in the three blocks from any of the animal groups. In each experimental group, normal distribution was checked by means of the Kolmogorov test. Since the hypothesis of a normal distribution was not rejected, the Student's t-test was used to determine the significance of differences between the mean values of data groups. A level of confidence of $P<0.05$ was adopted for statistical significance.

2.b. *Determination of the number of synaptic connections on gonadotrop hormone-releasing hormone- (GnRH) and other neurons in the AN of ovariectomized versus ovariectomized plus estrogen-treated monkeys.*

Animals

Sixteen female monkeys (Cercopithecus aethiops) were used for this study. Monkeys were housed in social groups (four monkeys in each, according to the experimental groups, see below) in a building which had indoor/outdoor housing. There were also perches and barrels for playing and hiding. Monkeys were maintained on a controlled diet of Purina monkey chow and fresh fruit. Tap water was available ad libitum. Ten days before the study, the animals were ovariectomized (anesthesia: ketamine

hydrochloride, 10 mg/kg, i.m.; atropine 0.01mg/kg, i.m., followed by intravenous infusion of penthobarbital, 10 mg/kg; monkeys had been intubated and respiration had been controlled throughout the operation) and separated into four experimental groups, each consisting of four monkeys (n=4 per group). The first group served as control OVX, without further estrogen-treatment, while the monkeys of the second, third and fourth groups were given a single i.m. injection of estradiol benzoate (50 μg/kg) 24 h, 48 h and 8 days, respectively, before sacrifice. Subsequently, monkeys were tranquilized with ketamine hydrochloride (15 mg/kg, i.m.) and butorphanol (0.025 mg/kg, i.m.) and blood samples were taken from the femoral vein of each for later determination of blood concentrations of estradiol and LH. Monkeys were then euthanized by phenobarbital and promptly fixed by transcardial perfusion of a fixative containing 4% paraformaldehyde and 0.1% glutaraldehyde. Brains were removed and postfixed overnight in 3% paraformaldehyde. All of the mentioned procedures were carried out in the St. Kitts Biomedical Research Facility, under a protocol approved by the facility's commettee and the Yale University Animal Care Committee.

Tissue procedures

A tissue block containing the entire arcuate nucleus was dissected from each brain. Fifty μm thick vibratome sections were cut and immunostained for GnRH as described above (Materials and Methods 1.), using a highly specific mouse-anti GnRH monoclonal antibody (a generous gift of Dr. Henryk Urbanski, Oregon Primate Research Center). The tissue-bound peroxidase was visualized by DAB-reaction. After the immunostaining, the sections were osmicated (15 min in 1% osmic acid in PB), and dehydrated in increasing ethanol concentrations. During the dehydration, 1% urany-acetate was added to the 70% ethanol to enhance ultrastructural membrane contrast. Dehydration was followed by flat-embedding in Araldite (Electron Microscopy Sciences, Hatfield, PA). Ultrathin sections were cut on a microtome, collected on Formvar-coated slot grids and contrasted with lead-citrate for further electron microscopic examination.

Quantitative analysis

A total of 20 GnRH- and 50 randomly chosen non-GnRH neurons in close proximity to the GnRH cells from each monkey were selected for analysis. One cross-section of each

selected neuron was randomly chosen for synapse counting and characterization. Synapse characterization was performed at X20,000 magnification, while all quantitative measurements were done on electron micrographs at a magnification of X4,500. For the synapse characterization, we followed the guidelines provided by Palay and Chan-Palay (**30**) and Colonnier (**31**). Symmetric and asymmetric synapses were counted on all selected neurons only if the pre- and post-synaptic membrane specializations were clearly seen and synaptic vesicles were present in the presynaptic bouton. Synapses with neither clearly symmetric nor asymmetric membrane specializations were excluded from the assessment. The plasma membranes of selected cells were outlined on photomicrographs and their length was measured with the help of a chartographic wheel. Plasma membrane length values measured in the individual monkeys were added and the total length was corrected to the magnification applied. The synaptic counts were expressed as numbers of synapses on a membrane length unit of 1,000 μm. Since an F-test analysis of our synaptic counts in the arcuate nucleus of the monkeys has revealed a significant nonhomogeneity of variances between groups, the Kruskal-Wallis one-way nonparametric analysis of variance test was selected for multiple statistical comparisons. The Mann-Whitney U-test was used to determine significance of differences between groups. A level of confidence of $P<0.05$ was employed for statistical significance. The morphometric analysis was carried out without knowledge of the experimental group from which the pictures were taken.

Plasma estrogen concentrations were measured by specific radioimmunoassay described elsewhere (**32**). Plasma LH concentrations were determined by the mouse Leydig cell bioassay (**33**). The above mentioned statistical methods were applied for the analysis of blood estrogen- and LH concentrations.

2.c. *Determination of the number of synaptic connections on glutamic-acid-decarboxylase-immunoreactive (GAD-IR) inhibitory GABAergic neurons in the AN of monkeys.*

Animals and Tissue Procedures

Animal species and animal handling were as described above (see section 2.b.). Tissue fixation was as described above (see section 2.b.). Double immunolabeling for glutamic-acid-decarboxylase and GnRH was carried out as follows:

A tissue block containing the entire AN was dissected out from each brain. Fifty µm thick vibratome sections were cut and thoroughly washed in 0.1 M phosphate buffer (PB). In order to eliminate unbound aldehydes, sections were incubated in 1% sodium-borohydride for 15 min, then rinsed in PB for 6X7 min. Next, sections were placed in a highly specific mouse-anti GAD (a key enzyme in GABA-biosynthesis) monoclonal antibody (dilution: 1:5,000 in PB; Boehringer-Mannheim) and incubated with gentle motion overnight at room temperature. A 3X10 min wash in PB was followed by 2 h incubation in biotinylated horse-anti mouse second antibody (dilution: 1:250 in PB; Vector Laboratories, Burlingame, CA) at room temperature. After a thorough wash in PB, the sections were placed in avidin-biotin-complex (2 h, room temperature; ABC Elite Kit, Vector Labs), then washed again in PB for 3X10 min. The tissue bound peroxidase was visualized by a nickel-intensified diaminobenzidine reaction. Because the animals were not colchicine-pretreated, the first immunoreaction resulted in the black labeling of only GAD-IR axon terminals, but not perikarya.

The second immunostaining was performed using the protocol described above, except that the primary antibody was a monoclonal mouse-anti-GnRH (a generous gift of Dr. Henryk Urbanski [Oregon Primate Research Center], dil: 1;1,000). Visualization of the immunoperoxidase was accomplished by diaminobenzidine reaction. After the double staining, the sections were osmicated (15 min in 1 % osmic acid in PB), and dehydrated in increasing ethanol concentrations. During the dehydration, 1 % uranyl-acetate was added to the 70 % ethanol in order to enhance ultrastructural membrane contrast. Dehydration was followed by flat-embedding in Araldite (Electron Microscopy Sciences, Hatfield, PA). Ultrathin sections were cut on a Reichert-Jung Ultracut-E microtome, collected on Formvar-coated slot grids and contrasted with lead-citrate for further electron microscopic examination.

Quantitative analysis

Twenty GnRH- and twenty randomly chosen putative GABA (P-GABA) neurons in close proximity to the GnRH cells from each animal were selected for analysis. One cross-section (in which the nucleus could be recognized) of each selected neuron was randomly chosen for synapse counting and characterization. Synapse characterization was performed at X20,000 magnification, while all quantitative measurements were done on electron micrographs at a magnification of X4,500. For the characterization of the synapses we considered the guidelines provided by Palay and Chan-Palay, 1975 (**30**) and Colonnier, 1968 (**31**). GAD-IR and immunohistochemically unidentified asymmetric and symmetric synapses were counted on all selected neurons if the pre- and postsynaptic membrane specializations were clearly seen and if synaptic vesicles were present in the presynaptic bouton. The plasma membranes of selected cells were outlined on photomicrographs and their perimeter was measured with the help of a chartographic wheel. Plasma membrane length values of distinct neurons (GnRH and P-GABA, respectively) measured within an individual animal were added and the total length was corrected to the magnification applied. The synaptic counts were expressed as numbers of synapses on a perikaryal membrane length unit of 1,000 µm. The morphometric analysis was carried out without knowledge of the experimental group from which the pictures were taken.

Plasma estradiol- and LH concentrations were measured as described in refs **32** and **33**, statistical analysis was done as presented in section 2.b. as well.

2.d. *Assessment of the role of EISP in the regulation of gonadotropin-release.*

Since the methodology of the data analysis and drawing inferences was mainly theoretical, and there is no clear-cut border between this act and the evaluation of the results, Aim 2.d. will be presented in the **Discussion** section.

3. *Identification and characterization of rapid, non-genomic estrogen effects on non-neuroendocrine neurons: Estrogen-induced rapid modulation of the extracellularly regulated kinases 1 and 2 (ERK1/2) MAPK- (mitogen-activated protein kinase) pathway in the rat cerebellum.*

3.a. *Determination of rapid estrogen effects in primary neuronal cell cultures.*

Animals

Timed pregnant Sprague Dawley rats were obtained from the supplier (Charles River, Wilmington, MA) at least 48 h before they gave birth. The postnatal age of the litter was calculated by using the day on which pups first appeared as postnatal day 0 (P0). On P7-P9 the sex and wieght of each age-matched animal were determined and recorded before granule cell preparation. At this age the mean weight of the pups was 18-20 g; pups weighing significantly less than the average were excluded from study. All animal procedures were performed in accordance with protocols approved by the University of Cincinnati Institutional Animal Care and Use Commettee and followed NIH guidelines.

Preparation of primary cultures of cerebellar neurons

Primary cerebellar cultures were prepared from P7-P9 male or female rat pups without enzymatic treatment and were maintained under serum- and steroid-free conditions as previously described (**22**). Cerebellar cells were diluted serially in an appropriate volume of culture media and seeded at an initial density of $1.5X10^5$ granule cells/cm^2. For analysis of mature primary cerebellar granule cells, a final concentration of 10 μM cytosine β-D-arabinofuranoside (AraC; Sigma, St. Louis, MO) was added 24 h after seeding to inhibit the proliferation of non-neuronal cells; treatments were performed after 7 d in culture. Cell counting indicated that greater than 90-95% of the cells contained in these cultures were granule cell neurons. Dissociated primary explant

cultures were prepared identically to primary cultures of granule cell neurons except that AraC was not added and drug treatments were performed immediately after cell attachment.

Drug treatments

Cerebellar cultures were exposed for various times to 1,3,5(10)-estratrien-3,17β-diol (17β-estradiol), 1,3,5(10)-estratrien-3,17α-diol (17α-estradiol), 4-pregnen-2,20-dione (progesterone, Sigma), 4-androsten-17β-ol-3-one (testosterone, Steraloids, Newport, RI), or 7α-{9-(4,4,5,5,5-pentafluoro-pentylsulphinyl)nonyl}oestra-1,3,5(10)-triene-3,17β-diol (ICI182,780) (Tocris Cookson, Ellisville, MO) at indicated concentrations (serially diluted in DMSO vehicle). 1,3,5(10)-estratrien-3,17β-diol 17-hemisuccinate/BSA (E_2-BSA; Sigma) and BSA (1 μM, fraction V, BSA; USB, Amersham Biosciences, Cincinnati, OH) were diluted in PBS, pH 7.4, with potentially contaminating free estradiol removed by microfiltration (30 kDa cutoff; Micron YM-30, Millipore, Bedford, MA). For pulse-chase estradiol treatments, after incubation with drug, the treatment medium was removed; then the cultures were washed with phenol red-free HBSS (Invitrogen, Carlsbad, CA) or PBS, and fresh estrogen-free culture medium was added.

Positive controls for ERK1/2 activation included treatment with 10% fetal calf serum (Invitrogen) or brain-derived neurotrophic factor (BDNF; 100 ng/ml; Promega, Madison, WI); for activation of p38 and JNK the cultures were exposed to 30 ng/ml anisomycin for 30 min. The involvement of the MAPK signaling pathway was assessed in cultures that were pretreated for 30 min with the MEK1 inhibitor U0126 (10 μM; Promega). Additional control or antagonist treatments included staurosporine (100 nM; Sigma), zVAD-fmk (12.5 μM; Promega), and PD150606 (50 μM; Calbiochem, La Jolla, CA), with each serially diluted to the desired concentrations in the appropriate vehicle. In experiments that used antagonists the vehicle-treated negative controls were exposed to concentrations of vehicle identical to those present in experimental cultures receiving both antagonist and agonist.

Generation of cerebellar cell lysates and Western blot analysis.

After treatment, the medium was aspirated, and the attached cells were washed with ice-cold HBSS or PBS. Cells were detached on ice with cold 2 mM EDTA in PBS and

collected at 2 °C by centrifugation at 600 X *g* for 10 min. Pelleted cells were resuspended and homogenized on ice in (in mM) 20 Tris-HCl, pH 7.5, 150 NaCl, 1 PMSF, 1 EDTA, 1 EGTA, 2.5 sodium pyrophosphate, 1 β-glycerol phosphate, and 1 Na_3VO_4 plus 1 mg/ml Pefabloc, 10 μg/ml leupeptin, 10 μg/ml pepstatin, 1 μg/ml aprotinin, 1% Triton X-100, 0.05% sodium deoxycholate, and phosphatase inhibitor mixture 1 (Sigma). Homogenates were sonicated on ice for 5 sec a total of six times. Alternatively, cell lysis was achieved by three freeze/thaw cycles in liquid N_2. Lysates were cleared by centrifugation at 14,000 X *g* for 1 min at 2°C. Total protein present in each lysate was quantified by using a modified Lowry assay (DC protein assay; Bio-Rad, Hercules, CA).

SDS-PAGE, Western blotting, and densitometric analysis were performed by standard protocols (**34**). For ERK1/2 analysis 5–10 μg/lane of each protein lysate was fractionated on 10% gels by SDS-PAGE and then electrotransferred to nitrocellulose or polyvinylidene difluoride membranes. For analysis of the stress-activated protein kinase/Jun terminal kinase (SAPK/JNK) and p38 MAP kinase activation, 50 μg/lane of control or cerebellar lysate was analyzed. Membranes were blocked with 5% nonfat dry milk for 1 hr in TBS-T and incubated with appropriate phospho-specific antisera (Table 1) overnight at 4°C. Antigens bound by primary antibodies were detected with appropriate HRP-conjugated anti-IgG secondary antibodies (1:30,000 dilution; Kirkegaard and Perry Laboratories, Gaithersburg, MD), and immunoreactive bands were visualized onto preflashed x-ray film by enhanced chemiluminescence, using the SuperSignal West Pico Substrate (Pierce, Rockford, IL). Multiple exposures of each blot were collected, and those in the linear range of the film were used for densitometric analysis. Digital images of appropriate films were captured with the EDAS290 imaging system (Kodak, New Haven, CT), and the optical density of each immunoreactive band was determined with Kodak 1D Image Analysis software. Optical densities were calculated as arbitrary units after local area background subtraction, normalized to the density of the phospho-independent MAPK immunoreactivity, and reported as fold induction relative to control.

Table 1. Primary antisera

Antigen	Source	Species	Designation	Dilution
Phospho-ERK1/2 (Thr202/Tyr204)	Cell Signaling	Rabbit	9101	1:1000; 1:400*
ERK1 (K-23)	Santa Cruz	Rabbit	SC-94	0.2 μg/ml
ERK2 (C-14)	Santa Cruz	Rabbit	SC-154	0.2 μg/ml
Phospho-p38 (Thr180/Tyr182)	Cell Signaling	Rabbit	9211	1:1000
p38 MAP kinase	Cell Signaling	Rabbit	9212	1:1000
Phospho-SAPK/JNK (Thr183/Tyr185)	Cell Signaling	Rabbit	9251	1:1000
SAPK/JNK	Cell Signaling	Rabbit	9252	1:1000
GFAP	Sigma	Mouse	GA5	1:1000*

*Dilutions used for immunohistochemistry

Immunocytochemical analysis of MAPK activation.

Cerebellar cell cultures were prepared from 8-d-old female Sprague-Dawley rat pups as described above and seeded into poly-L-lysine-coated eight-well chamber slides (Lab Tek; Nunc, Naper-ville, IL) at a density of 100,000 –140,000 cells/ cm^2 in a final volume of 300 μl/well. Cultures were maintained in a humidified incubator in 5% CO_2 at 37 °C for 7 d in the presence of a final concentration of 10 μM AraC. On the seventh day in culture one-half of the culture medium was removed from each experimental and vehicle control well. A final concentration of 2 X 10^{-11} M 17 β-estradiol or an equal volume of DMSO vehicle was added to the removed medium, mixed, and readded to the wells. Culture media were mixed gently by orbital rotation for 30 sec and incubated in 5% CO_2 at 37 °C for 13 min. This treatment resulted in a total exposure time of 15 min. A third group of control cultures remained untreated. After incubation the cultures were fixed with –20 °C methanol for 20 min and washed with PBS (3X10 min). Cultures then were incubated at room temperature for 2 hr with anti-phospho-ERK1/2 and anti-glial fibrillary acidic protein (GFAP) primary antibodies (Table 1). After 3X10 min washes in PBS the cultures were incubated with FITC-conjugated goat anti-mouse and Texas Red-conjugated goat anti-rabbit IgG antisera (Jackson ImmunoResearch Laboratories, West Grove, PA), each at a dilution of 1:60 in PBS/0.2% Triton X-100. Cultures were washed thoroughly in PB and then coverslipped with Vectashield mounting medium with DAPI (Vector Laboratories, Burlingame, CA). Microscopic examination of immunostained material was performed with a Nikon TE 2000 inverted microscope. Fluorescence of FITC, Texas Red, and DAPI was examined by epifluorescence microscopy, using a filter configuration for sequential excitation/emission imaging via 488 (green), 568 (red), and 405 (blue) nm channels (Chroma Technology, Brattleboro, VT). Digital images were captured with a SpotRT

(Media Cybernetics, Silver Spring, MD) CCD camera, using Image-Pro Plus version 4.5 software. Final graphics were generated and labeled with Photoshop version 6.01 (Adobe, San Jose, CA) software, with triple-stained material generated by an overlay of the individual blue, red, and green images.

Analysis of granule cell viability.

Dissociated explant cultures were seeded onto 24-well plates and exposed to drug or vehicle for the indicated times. For each sample, the culture medium was collected before cell counting, and the amount of lactate dehydrogenase (LDH) released into the medium as a result of cell lysis was determined as previously described (**35**). Cells then were washed and detached by incubation on ice for 2 min with 200 µl of ice-cold 2 mM EDTA in PBS, pelleted by centrifugation at 600 X g, resuspended into an appropriate volume of HBSS, and lightly stained with trypan blue. Viable granule cell numbers were determined by direct cell counting of small (≅5 µm diameter) trypan blue-excluding granule cells with a hematocytometer, using standard methods. For each experiment the mean ±SEM of four independent samples was determined for each treatment group; triplicate cell counts were made for each sample, with each experiment repeated at least three times. Granule cell viability was also assessed by the previously described MTS reduction assay (**35**).

Analysis of propidium iodide permeability.

Cell cultures were seeded and maintained as described above in 60 mm cell culture dishes in 3 ml of growth medium. At 3 hr after seeding, the granule cell cultures were pulse-treated for 15 min with a final concentration of 10^{-11} M 17β-estradiol or an equal volume of DMSO vehicle. After treatment, the medium was removed, and the cultures were washed two times with steroid-free growth medium. A final volume of 3 ml of steroid-free growth medium was added, and the cultures were incubated at 37 °C in 5% CO_2 until the required time after treatment. At each time point that was analyzed, a final concentration of 1.5 µM propidium iodide (PI; Molecular Probes, Eugene, OR) was added to each culture. After a 4 min incubation period digital red fluorescent images were captured, and PI-permeable cell numbers were determined (Image-Pro software, version 4.5) for each sample. Results for each time point are reported as the mean values from six randomly selected 0.27 mm^2 fields from three different samples.

Analysis of granule cell proliferation; BrdU incorporation.

Dissociated explant cultures were seeded into 96-well plates without AraC, allowed to attach for 2 hr, treated with 10^{-11} M 17β-estradiol or DMSO vehicle for 15 min, washed with HBSS, and then incubated with fresh medium containing a final concentration of 10 μM 5-bromo-2'-deoxyuridine (BrdU). Additional cultures were exposed to 10^{-11} M estradiol or vehicle for the entire incubation period. The amount of BrdU incorporated into newly synthesized DNA at each time point was monitored by an ELISA-based approach (BrdU Labeling and Detection Kit III, Roche Molecular Biochemicals, Indianapolis, IN).

Analysis of caspase-3 activity.

Dissociated explant cultures were seeded in 60 mm dishes at $1.5X10^5/cm^2$ and allowed to attach for 2 hr. Cultures were treated with 17β-estradiol for 15 min and washed with HBSS; treatment medium was replaced with fresh steroid-free medium and then incubated for 24 hr. Staurosporine-treated (100 nM) cultures were used as positive controls, and additional control cultures were treated with the pan-caspase inhibitor zVAD-fmk (12.5 μM). After incubation, the cell lysates were prepared, and caspase-3 activity was determined for 40 μg of lysate on the basis of the liberation of a colored p-nitroaniline (pNA) from the caspase-3 substrate Ac-DEVD-pNA (Colorimetric CaspACE

Assay System, Promega). Specific caspase-3 activity (pmol of pNA/hr per microgram of protein) of each sample was calculated from a standard pNA curve generated from a dilution series of known concentrations of pNA.

Statistical analysis.

Unless noted otherwise, all data that have been presented are representative of at least three independent experiments. Statistical analysis was conducted with a Student's *t* test or by one-way ANOVA with post-test comparison, using Newman–Keuls or Dunnett's multiple comparison tests as appropriate. The level of statistical significance between

treatment groups is indicated as follows: *p< 0.05; **p< 0.01; ***p< 0.001. Data were analyzed with Excel (Microsoft, Redmond, WA) and GraphPad Prism version 3.01 (GraphPad Software, San Diego, CA).

3.b. *Determination of the spatiotemporal distribution of activated, dually phosphorylated ERK1/2 (pERK) in the rat cerebellum.*

Animals

All animal procedures were done in accordance with protocols approved by the University of Cincinnati Institutional Animal Care and Use Committee and followed NIH

guidelines. Timed pregnant Sprague–Dawley rats were obtained from the supplier (Charles River) at least 48 h before giving birth. The age for each litter was calculated using the day on which pups first appeared as postnatal day 0 (P0). Pups were reared by their mothers with the size of each litter being adjusted to 10 pups per litter on P0. Representative results are presented from 6 to 10 animals per age group. All age groups contained between 3–5 males and female, and no sex-differences in pERK-IR were detected at any age examined.

Tissue fixation

Animals were anesthetized with a mixture of ketamine (P4–P12: 230 mg/kg, s.c.; P15–16: 215 mg/kg, s.c.; adults: 200 mg/kg, i.m.) and 6.6 mg/kg xylazin. In preliminary control studies, when animals were sacrificed by rapid decapitation without prior anesthesia, it was found that neither the pattern nor the nature of pERK-IR was influenced by anesthesia. Following rapid decapitation cerebella were rapidly dissected, immersion-fixed in an ice cold mixture of 4% paraformaldehyde and 3% acrolein in 0.1 M phosphate buffer (pH 7.4; PB) overnight and then postfixed in 4% paraformaldehyde until tissue processing. Using this fixation protocol tissue penetration and complete fixation was accomplished within 3 min of sacrifice.

Immunohistochemistry

Immunohistochemical staining of 50-µm-thick free-floating sections has been described previously. The following primary antibodies were used at the indicated dilutions: rabbit anti-phospho-p44/42 MAP Kinase (1:400; cat. # 9101, Cell Signaling Technology, Beverly, MA); mouse anti-GFAP (1:1000; G-A-5, Sigma, St. Louis, MO); mouse anti-β-tubulin (1:1000; TU24, Babco, Richmond, CA). Bound antibodies were visualized with nickel-intensified 3,3'-diamino-benzidine by the avidin–biotin peroxidase complex method following standard protocols (Vector Laboratories, Burlingame, CA). For double-labeling experiments, 20-µm sections were analyzed with antigen-bound antibodies visualized with fluorescein isothiocyanate (FITC) conjugated goat anti-mouse IgG (12.73 µg/ml) and Texas Red conjugated goat anti-rabbit IgG (13.64 µg/ml) (Jackson Immunoresearch Laboratories, West Grove, PA). Sections were coverslipped with Vectashield mounting medium with DAPI (Vector Laboratories). Specificity of all antisera has been previously validated by Western blotting and immunohistochemical analysis (**22**). In negative control experiments, omission of the primary antibodies or pre-absorption of p44/42phosphoMAPK antibody with immunogenic peptide (phospho-ERK2, Control Protein Kit, cat. # 9103, Cell Signaling Technology) resulted in no specific immunostaining.

Microscopic examination of immunostained material was carried out using a Nikon 2000 TE inverted microscope. Fluorescence of FITC, Texas Red and DAPI was examined by epifluorescence microscopy using a filter configuration for sequential excitation/emission imaging via 488-, 568- and 405-nm channels (Chroma Technology, Brattleboro, VT). Digital images were captured with a SpotRT (Bridgewater, NJ) CCD camera using Image Pro Plus v4.5 software. Final graphics were generated and labeled using Photoshop v6.01 (Adobe, San Jose, CA), with double- and triple-stained figures generated by an overlay of the individual blue, red and green images.

Quantitative analysis

To determine the densities of pERK-IR cerebellar cells at various postnatal days and in the adult, digital images of one mid-sagittal section per animal was analyzed using Image Pro Plus v4.5. Numerical density of pERK-IR granule cells in the internal

granular layer and the number of pERK-IR Purkinje cells was determined in cerebellar foliae II–X. The area of the internal granular layer and the row occupied by Purkinje cells was outlined for each folium, and immunopositive cells or cell clusters were manually tagged. Cell number, areas and length measurements were determined with Image Pro Plus v4.5 using the count/size, area, size functions, respectively. The following parameters were determined: the number of pERK-IR granule cells per unit area; the number of pERK-IR Purkinje cells per unit length of the Purkinje cell layer; and the number of pERK-IR Bergmann glia clusters per unit length of the Purkinje cell layers; resulting values are referred to as ‘‘pERK-IR cell density’’ or ‘‘Bergmann glia cluster density’’. Statistical analysis and graphic representations of data were prepared using Prism v4.0 (GraphPad) software. The level of significance between different age groups was determined by one-way analysis of variance (ANOVA) with post-test comparison using Tukey’s multiple comparison test.

3.c. *Identification of direct in vivo estrogen effects on the activation of cerebellar ERK1/2-activation: analysis of dose- and age-dependency.*

Animals

All animal procedures were done in accordance with protocols approved by the University of Cincinnati Institutional Animal Care and Use Committee and followed NIH guidelines. Male and female Sprague-Dawley rats of various ages (postnatal day 4 [P4] - P19, and adult) were used for this study. Rat pups were kept with their mothers and maintained under standard laboratory conditions (12-h dark-light cycles, standard rat chow and tap water *ad libitum* for the mothers and adult animals).

Animal surgery and tissue fixation

Animals were anesthetized with a mixture of ketamine and 6.6 mg/kg xylazin (ketamine for P4-P12 animals: 230 mg/kg, s.c.; for P15-16 animals: 215 mg/kg, s.c.; for adults: 200 mg/kg, i.m.). Heads were fixed in a stereotaxic apparatus equipped with a small animal adaptor, as described elsewhere (**36**). The occipital bone was cleaned from the fasciae and cervical musculature and was separated from the surrounding bones of the

calvaria, dorsally along the interparietooccipital suture, and bilaterally along the dorsal half of the temporooccipital suture. Bilateral separation lines were directed ventromedially crossing the dorsal condyllar fossa to the dorsal arch of the foramen magnum, just above the occipital condyles. To separate the occipital bone from the first cervical vertebra, the dorsal atlantooccipital membrane was transversely cut. The occipital bone was removed and the exposed external meninges (dura mater and arachnoidea) were cut along the midsagittal plane. The dorsocaudal cerebellar surface exposed this way allowed easy identification of foliae VI. and VII., which were used as injection points. To allow injection needle access in adults, a hole was drilled in the midline, on the dorsal surface of the skull 12.3 mm behind the bregma. Injections were done using a 5 µl Hamilton syringe, attached to the stereotaxic apparatus. The needle was vertically lowered in the midsagittal plane to reach the suprafastigial region where the cerebellar foliae merge together and pulled back about 0.5 mm to create a cavity for the injected material. Three µl of 17β-estradiol (water soluble, cyclodextrin-encapsulated, catalog number: E-4389, Sigma, St. Louise, MO) at each concentration (10^{-12}-10^{-6} M) was injected into the cerebella of P4-10 animals, while in older animals 5 µl was injected. Un-injected, mock-injected and cyclodextrin vehicle-injected (2-hydroxypropyl-β-cyclodextrin, catalog number: C-0926, Sigma, St. Louise, MO, at equal concentrations present in each estrogen-dilution) animals were used as controls. Six minutes after the initiation of injections, animals were rapidly decapitated, brains dissected and placed in ice-cold fixative (4% paraformaldehyde/3% acrolein in 0.1 M phosphate buffer [PB], pH 7.4). Brains were fixed overnight and postfixed in 4% paraformaldehyde until tissue processing.

Immunohistochemistry for brightfield microscopy

Immunohistochemical staining of 50-µm-thick free-floating sections has been described previously (3.b.).

Analysis of estrogen-induced rapid modulation of cerebellar phospho-ERK1/2-immunoreactivity

Considering the very limited means and unreliability of qualitative measurements in this case, results were not expressed in numerical values at this time. Instead, one mid-sagittal representative cerebellar section, from the site of injection from each animal, was selected for qualitative comparison of estrogen-effects.

RESULTS

1. *Identification and biochemical characterization of MBH neurons that are regulated by excitatory amino acid (EAA) neurotransmission: Immunohistochemical identification of alpha-amino-3-hydroxy-5-methyl-4-isoxazole propionic acid (AMPA) receptors GluR1 and GluR2/3, as indicators of aspartate/glutamatergic innervation in the arcuate nucleus of female rats and immunohistochemical co-localization of AMPA receptors with neuropeptide-Y (NPY), galanin (GAL) and tyrosine-hydroxylase (TH).*

GluR immunoreactivity

The immunostaining for GluR1 and GluR2/3 (Fig. 1 A,C,E,F) revealed a widespread and mostly homogeneous distribution of immunoreactive (IR) cells in the AN that corresponded with an earlier description (**37**). A majority of the AN neurons were found to contain these AMPA receptor subunits. Although their distribution was mostly homogeneous, it is worthy of note that the subependymal and ventromedial subdivisions of the AN contained relatively fewer IR somata. Also, a distinct non-IR zone surrounded and outlined the AN on its lateral and dorsal sides (not shown).

NPY immunoreactivity

A distinct perikaryal NPY immunopositivity was observed throughout the AN (Fig. 1 D) with the greatest number of cells observed in the central and caudal aspects of the nucleus. Immunoreactive perikarya were spherical or oblong in shape. In coronal sections, several NPY-IR cell bodies were seen across the entire mediolateral extent of the subependymal and internal zones of the median eminence.

GAL immunoreactivity

A large group of small to medium-sized GAL-IR perikarya were seen in the AN (Fig. 1B). GAL-IR cells were distributed ventrally to the ventromedial hypothalamic nucleus, with more intense immunoreactivity at the ventrolateral aspects of the AN. In more

caudal sections IR cells were found ventral to, and extending into, the ventral premamillary nucleus.

TH immunoreactivity

The distribution of TH-IR neurons was largely consistent with that previously reported by many authors (**38-40**).

A total of 4440 GluR2/3-IR cells were examined in the present study (750 for TH, 1860 for GAL, 1080 for NPY, and 750 for GluR1 content). GAL was found in 31.72% and NPY in 38.72% of GluR2/3-IR cells (Fig. 1A–D), whereas all of the examined GluR2/3-IR cells were also IR for GluR1 (Fig. 1E, F).

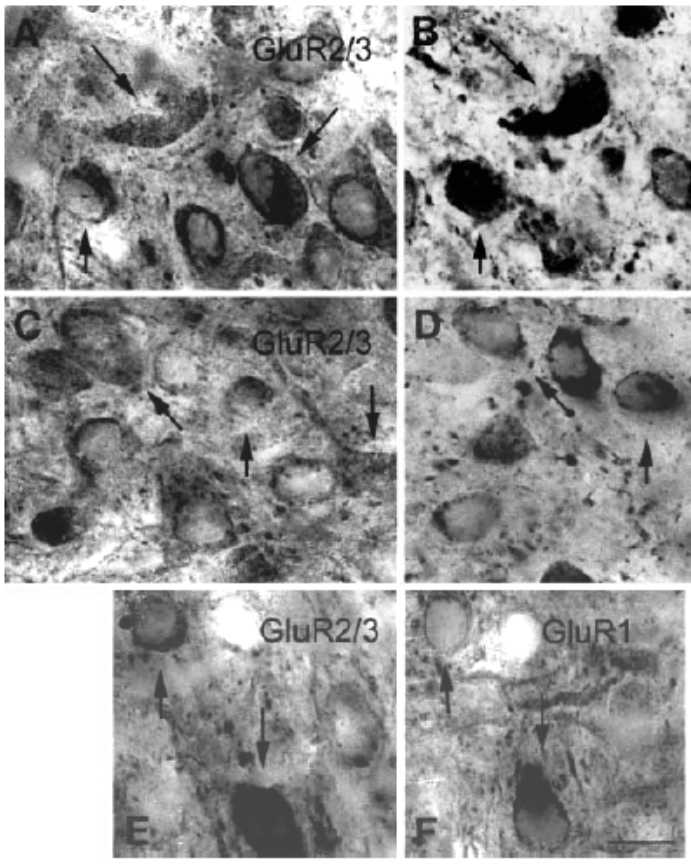

Figure 1. Colocalization of GluR2/3 with GAL, NPY and GluR1. Parallel arrows point to matching cell halves. Bar 20 µm

Percentages of co-localizations are illustrated in Fig. 2.

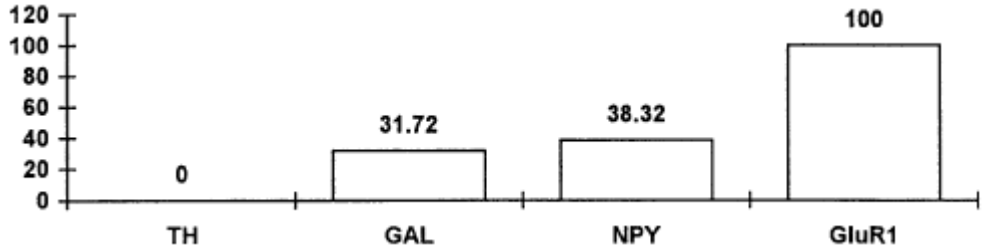

Figure 2. Numerical calculation of TH, GAL, NPY and GluR1 immunoreactivity in 100 GluR2/3-IR neurons.

We also determined the rate of GluR2/3 co-localization with 1050 examined GAL- and 510 NPY-IR neurons of the AN. More than half (56.19%) of the GAL and the majority of NPY (79.41%) neurons co-expressed GluR2/3 (Fig. 3).

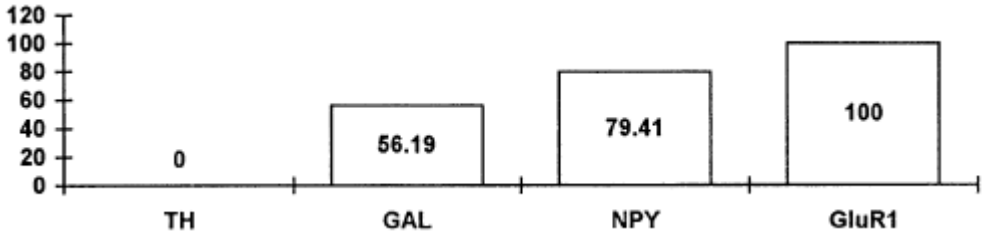

Figure 3. Numerical calculation of GluR2/3 immunoreactivity in 100 TH, GAL, NPY and GluR1-IR neurons.

We were not able to find TH immunoreactivity within the GluR2/3-containing neurons (Fig. 4).

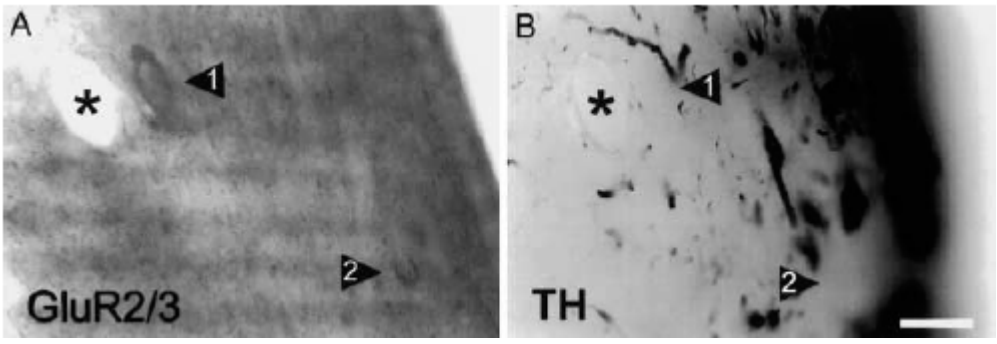

Figure 4. TH does not co-localize with GluR2/3. Arrowheads point to GluR-IR neurons that are not stained for TH. Asterisks label the same vessel in adjacent sections. Bar 20 µm.

A summary of proposed neuronal circuit is illustrated in Figure 5.

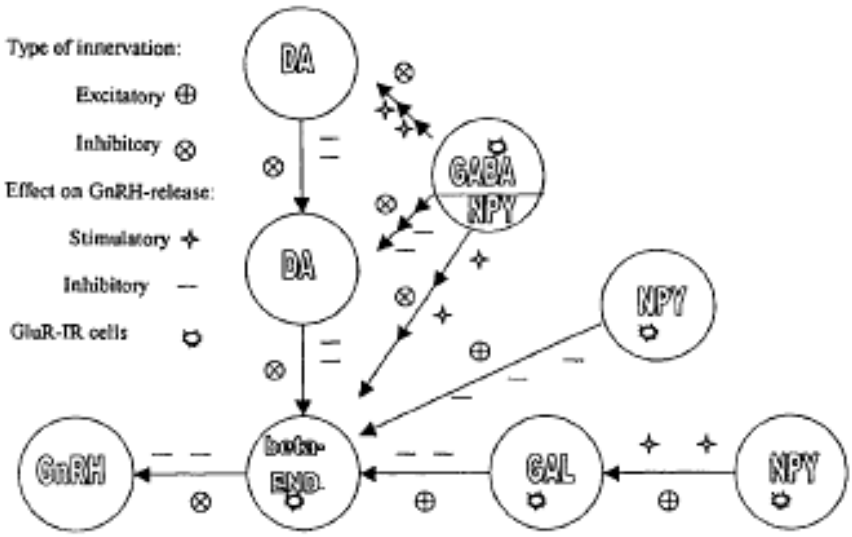

Figure 5. Schematic illustration of the connectivity between TH- (dopamine, DA), NPY-, GAL-, GABA- and beta-END neurons involved in the regulation of GnRH cells.

2. *Determination and analysis of estrogen-induced synaptic plasticity (EISP) in the primate and rat arcuate nucleus (AN):*

2.a. *Identification of neurons undergoing EISP.*

The pattern of fluorogold (FG) immunopositivity and the number of labeled cells were similar in ovariectomized and ovariectomized plus 17β-estradiol-treated animals. FG-positive cells were found scattered around the entire nucleus with a tendency of being clustered near the ventricular wall. In the morphometric studies we excluded the ventrolateral part, because the number of FG-containing neurons was low. In ultrathin sections, the densely stained cytoplasm contained the usual array of organelles and the cells were partly ensheathed by glial lamellae. We observed axo-somatic synapses on both labeled and unlabelled neurons. These synapses contained mainly round, densely packed clear vesicles of homogenous size, mitochondria and occasionally a few larger dense core vesicles (Fig. 6A). We could not find any fine structural alterations in the arcuate neurons from animals fixed 24 h after 17β-estradiol administration, but the surface density of axo-somatic synapses was lower (Fig. 6B), therefore we performed the unbiased stereological measurement according to the disector method to determine the synapse number.

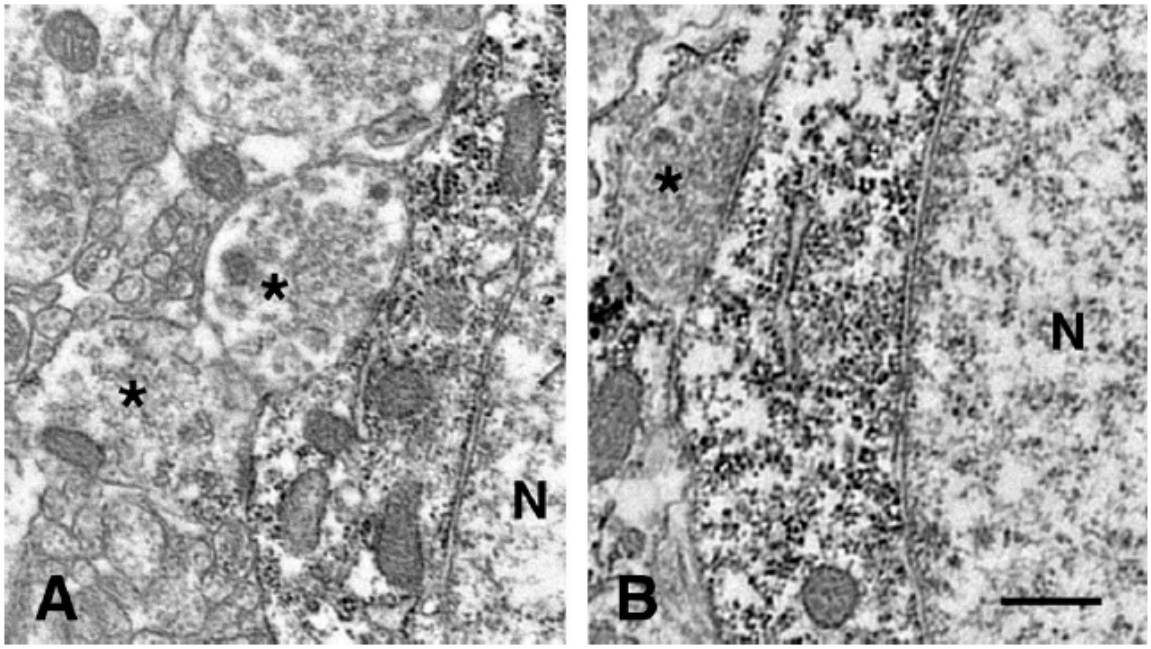

Figure 6. Electron micrographs of arcuate neurons immunostained for fluorogold from ovariectomized (A) and ovariectomized+E_2-treated (B) rats. Fluorogold-immunorective cells and processes contain dense precipitates. N, nucleus; asterisk, axo-somatic synapses; bar= 1 µm.

The data of this analysis show that the numerical density of axo-somatic synapses terminating on labeled or unlabelled neurons of ovariectomized animals differs significantly. The FG-immunoreactive cells receive less axosomatic synaptic inputs (16.1±1.9/1,000 μm^3 of perikaryon) than do other cells which do not contain this retrograde tracer (22.8±2.6/1,000 μm^3 of perikaryon). The two groups of neurons react differently to the estradiol treatment. There were no changes in the number of axo-somatic synapses on unlabelled neurons after 24 h of 17β-estradiol treatment (21.6±2.2/1,000 μm^3 of perikaryon), while there was a significant decrease of nerve endings on labeled ones (8.6±1.2/1,000 μm^3 of perikaryon). Data are summarized in Fig. 7.

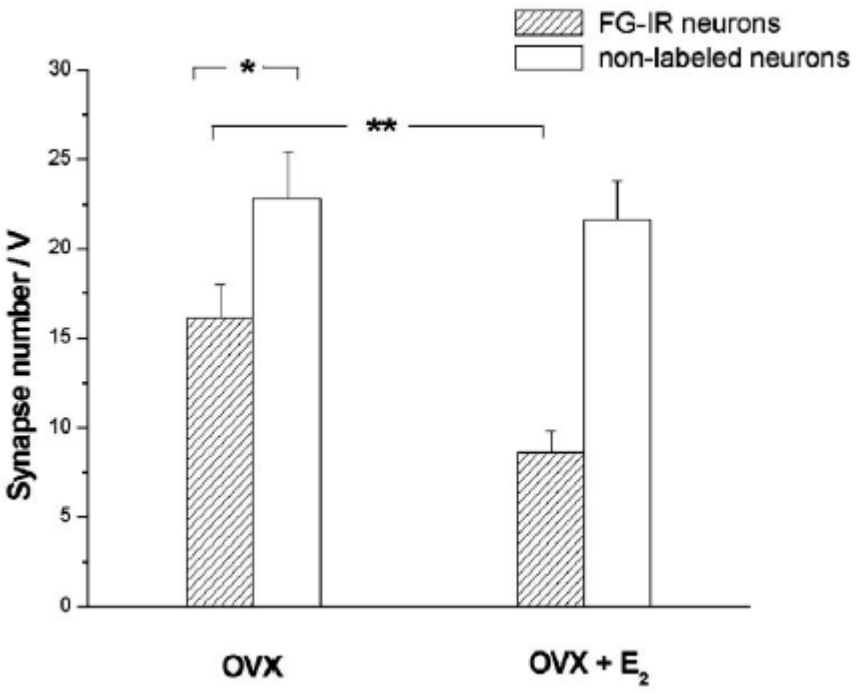

Figure 7. Numerical density of axo-somatic synapses in the arcuate nucleus on fluorogold-labeled and non-labeled neurons of ovariectomized (OVX) and ovariectomized+E_2-treated (OVX+E_2) rats. The number of synapses were counted by the Sterio method and the data are expressed as number of synaptic contacts per unit volume of perikaryon (1000 μm^3) * P<0.05, ** P<0.01.

2.b. *Determination of the number of synaptic connections on gonadotrop hormone-releasing hormone- (GnRH) and other neurons in the AN of ovariectomized versus ovariectomized plus estrogen-treated monkeys.*

Synaptic plasticity on GnRH and other neurons

The immunoperoxidase reaction resulted in brown immunolabeling of GnRH neurons, as seen under the light microscope, where their appearance was largely consistent with previous descriptions (**41, 42**). The ultrastucture of the arcuate nucleus was similar to that described in previous studies (**12, 43**). We were unable to detect synapses on GnRH neurons of OVX monkeys. Instead, a massive glial ensheathing of their plasma membrane was seen (Fig. 8A), as also described by Witkin et al. (**44**).

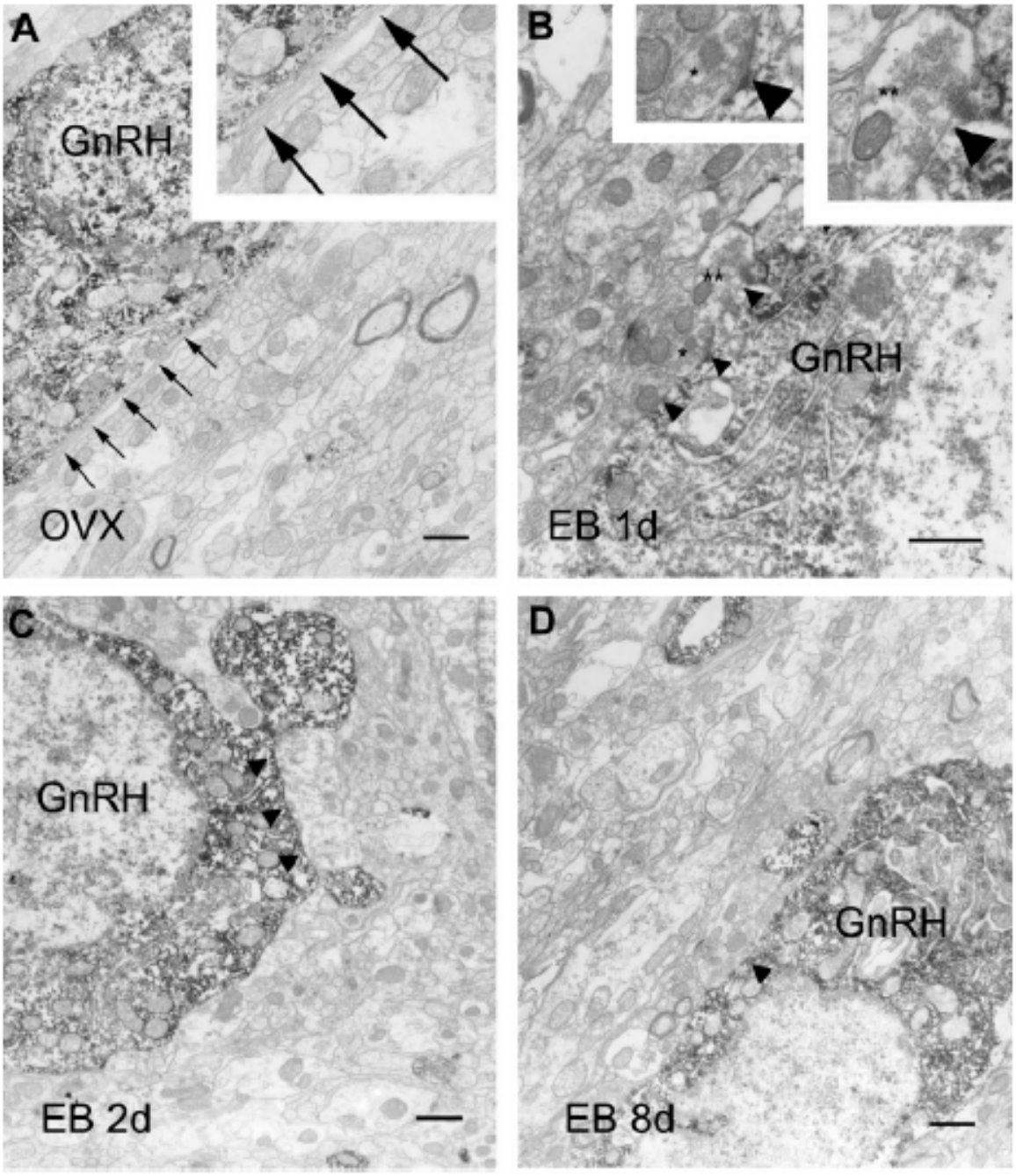

Figure 8. (A) Gondotropin releasing hormone (GnRH) cell in ovariectomized (OVX) monkey. Arrows point to the surrounding glial sheath, also shown at a higher magnification in the insert. (B) GnRH cell in estradiol benzoate day 1 animal. Arrowheads point to synaptic structures. Inserts illustrate examples of axonal boutons establishing asymmetric (one asterisk) or symmetric (two asterisks) synapses with GnRH cells; (C and D) GnRH cells in estradiol benzoate day 2 and estradiol benzoate day 8 animals. Arrowheads point to synaptic connections. Bars represent 1 µm.

Synaptic counts and their temporal distribution are presented in (Fig. 9A-D).

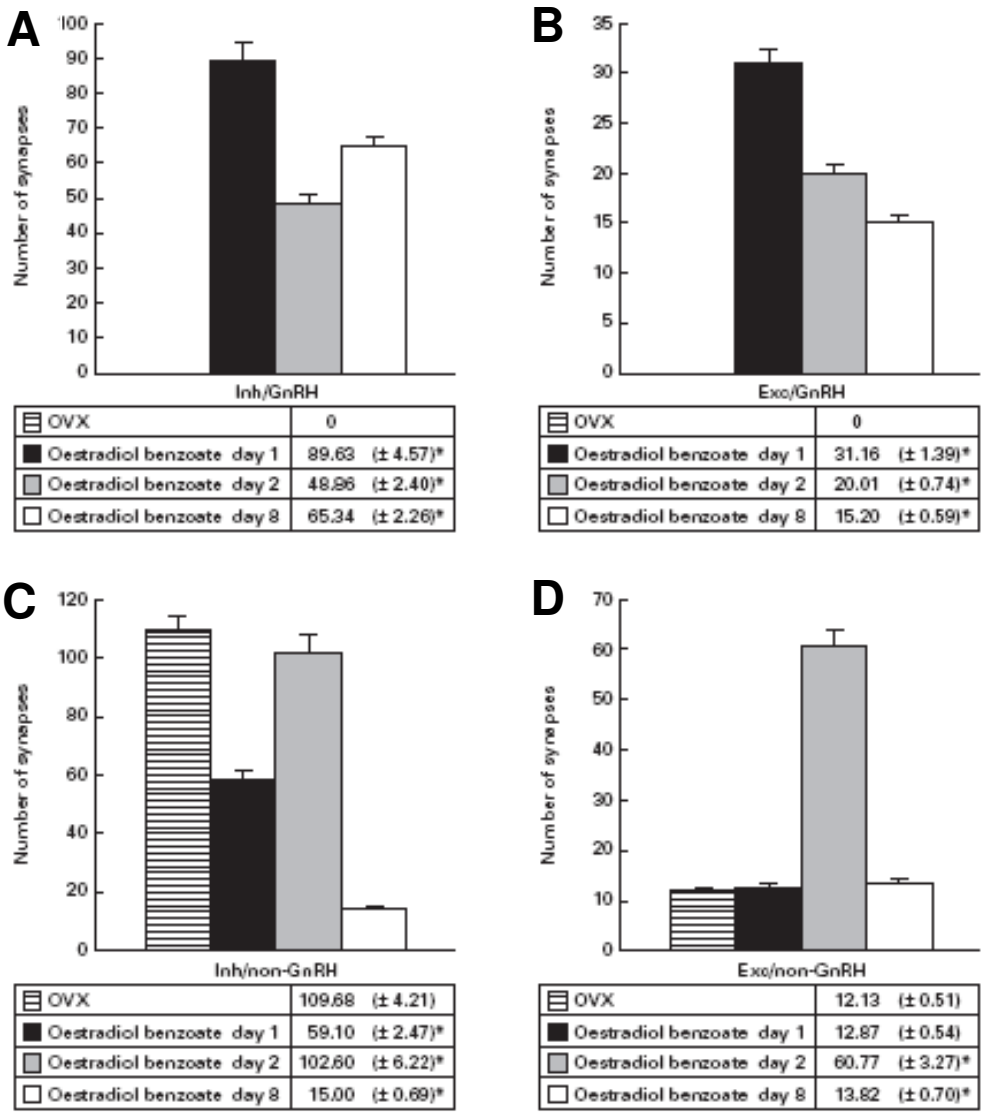

Figure 9. Numbers of: Inh (inhibitory, A) and Exc (excitatory, B) synapses on gonadotropin releasing hormone (GnRH) cells; Inh (C) and Exc (D) synapses on non-GnRH neurons (all 1000 µm of perikaryal membrane). Columns represent mean values; error bars illustrate the standard error of the mean (SEM). Values are also displayed in data tables (SEM values in parentheses). Asterisks indicate statistically significant differences from the values of the previous experimental group ($P<0.05$).

As an example, Fig. 10 illustrates a non-GnRH neuron of the estradiol benzoate day 2 group. Estrogen has a pivotal role in the negative/positive feedback-based regulation of LH-release. This regulatory function involves an estrogen-responsive neuronal circuit within the arcuate nucleus.

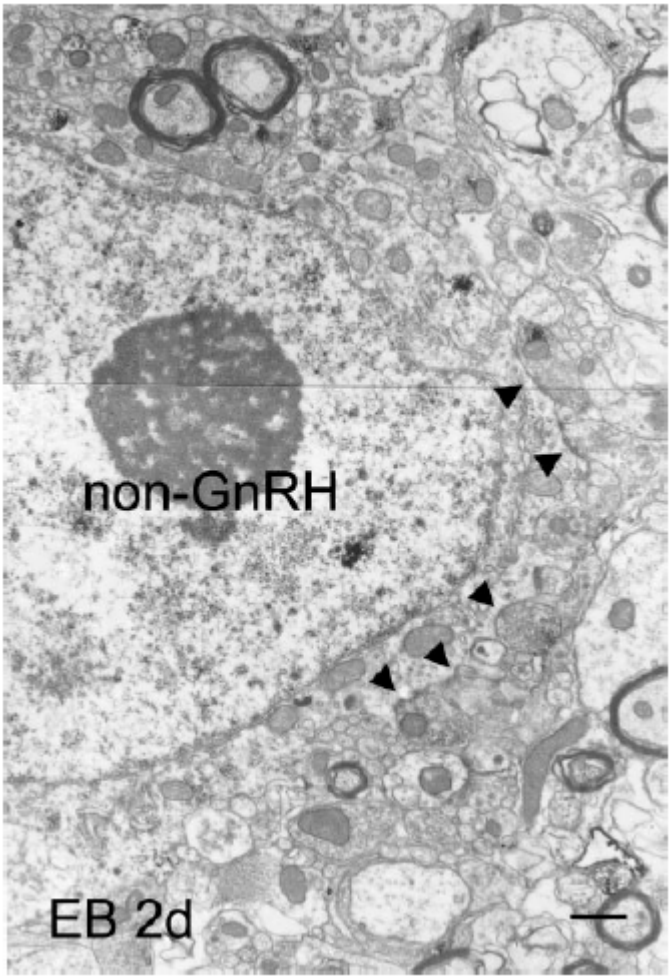

Figure 10. Non-gonadotropin releasing hormone (GnRH) cell from an estradiol benzoate day 2 animal. Arrowheads point to synaptic structures. Bar represents 1 µm.

Therefore, it was important to compare the temporal changes in plasma estrogen-concentrations to the synaptic plasticity observed at both GnRH- and non-GnRH neurons. Because the GnRH surge generated by this mechanism evokes a subsequent surge in LH-release, it was important to follow the temporal events in the plasma LH concentrations. Plasma estrogen- and LH levels are shown on Fig. 11. In order to make the present results comparable to our earlier description (**12**), we averaged the synaptic counts from day 1 to day 8 for each experimental group.

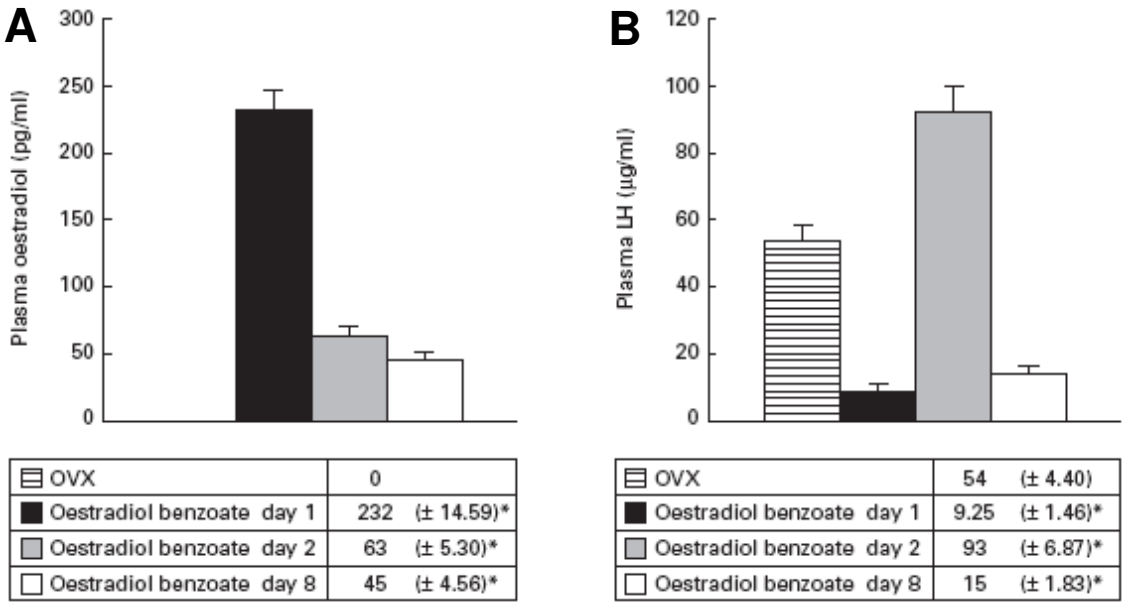

Figure 11. Plasma-estradiol (A) and -luteinizing hormone (LH) (B) levels. Columns represent mean values, error bars illustrate the standard error of the mean (SEM). The values are also displayed in data tables (SEM in parentheses). Asterisks designate a statistically significant difference from the values of the previous experimental group.

The averages were calculated as follows: the number of all types of synapses/1000 µm plasma membrane within an experimental group divided by the number of monkeys in that group (n=4) and further divided by the number of synapse-assessments [2:GnRH and non-GnRH; differences between groups expressed in percentage are the same if averages are calculated by summing the mean values of synaptic counts in a group, and dividing this sum by four (n=4)]. This gave an average of 96.38 synapses per 1000 µm plasma membrane in monkeys 1 day after estradiol benzoate treatment, with a transitional elevation (116.12 at 2 days), followed by a decrease of 43.3% at 8 days after treatment (54,65).

2.c. *Determination of the number of synaptic connections on glutamic-acid-decarboxylase-immunoreactive (GAD-IR) inhibitory GABAergic neurons in the AN of monkeys.*

Synaptic plasticity on putative GABA (P-GABA) neurons

While no synapses were found on GnRH cells of the OVX animals, P-GABA neurons of this group were contacted by numerous axon terminals. Synaptic counts are presented in Figures 12 and 13.

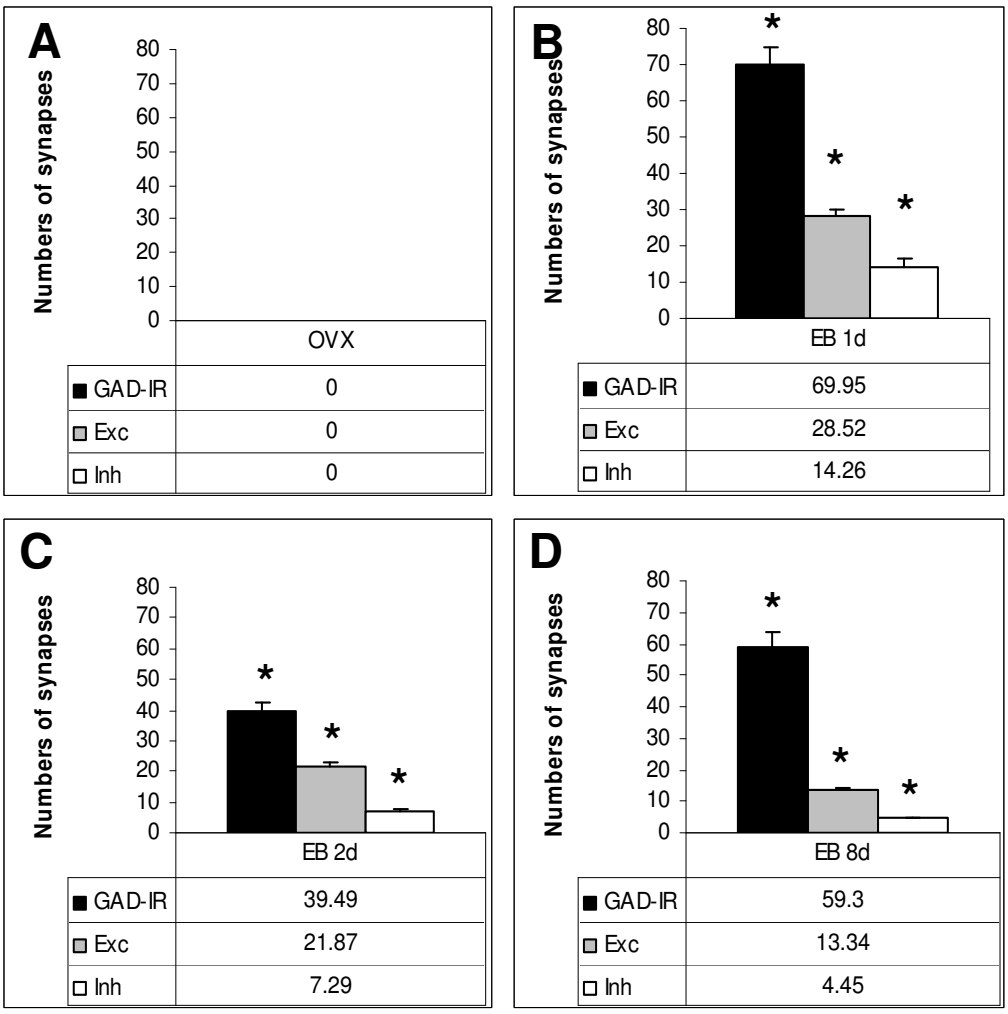

Figure 12. Numbers of synapses on GnRH neurons of OVX (A), EB 1d (B), EB 2d (C) and EB 8d (D) animals. Columns represent mean values; error bars illustrate the standard error of the mean. Values are also displayed in data tables. Asterisks indicate statistically significant differences from the values of synapses of the same type in the previous experimental group.

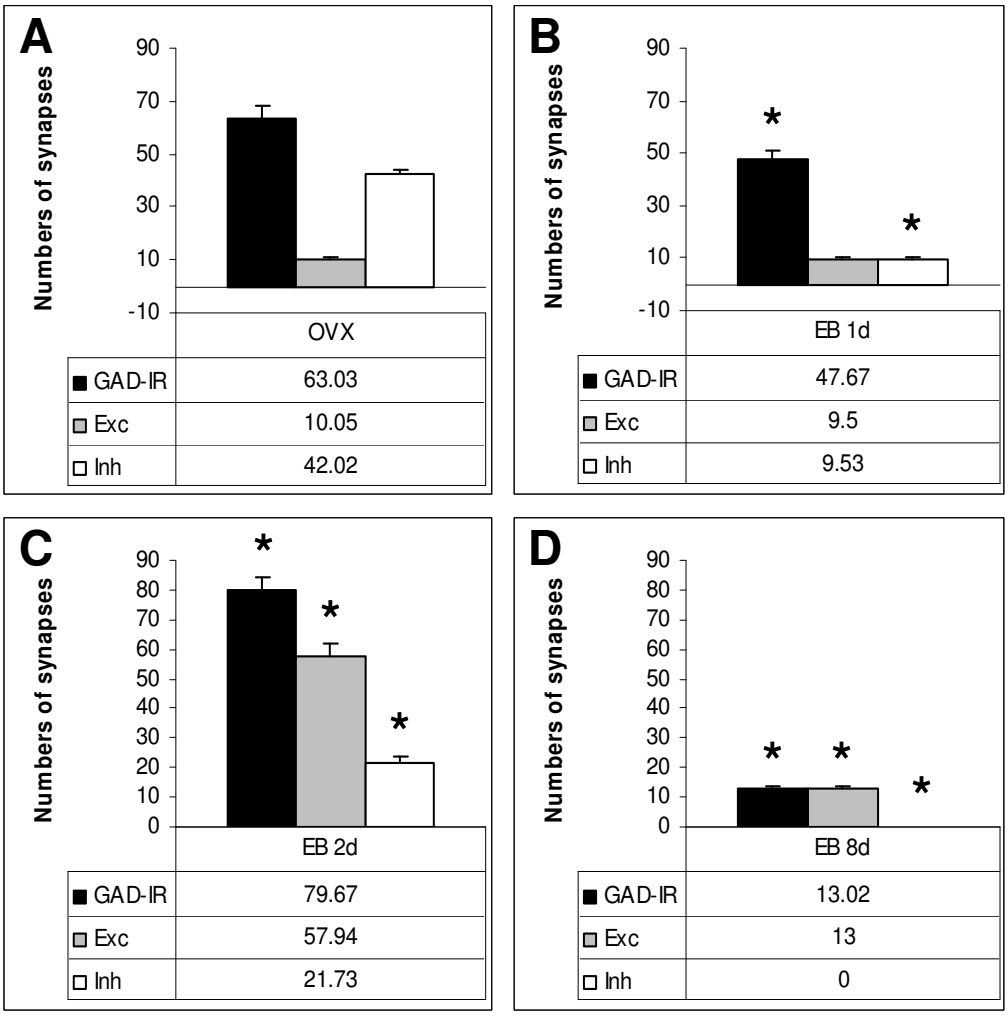

Figure 13. Numbers of synapses on P-GABA neurons of OVX (A), EB 1d (B), EB 2d (C) and EB 8d (D) animals. Columns represent mean values; error bars illustrate the standard error of the mean. Values are also displayed in data tables. Asterisks indicate statistically significant differences from the values of synapses of the same type in the previous experimental group.

Figure 14 gives an example of a non-GnRH neuron that has infolded nucleus (non-GnRH-IN) and therefore considered to be a P-GABA neuron (EB 2d).

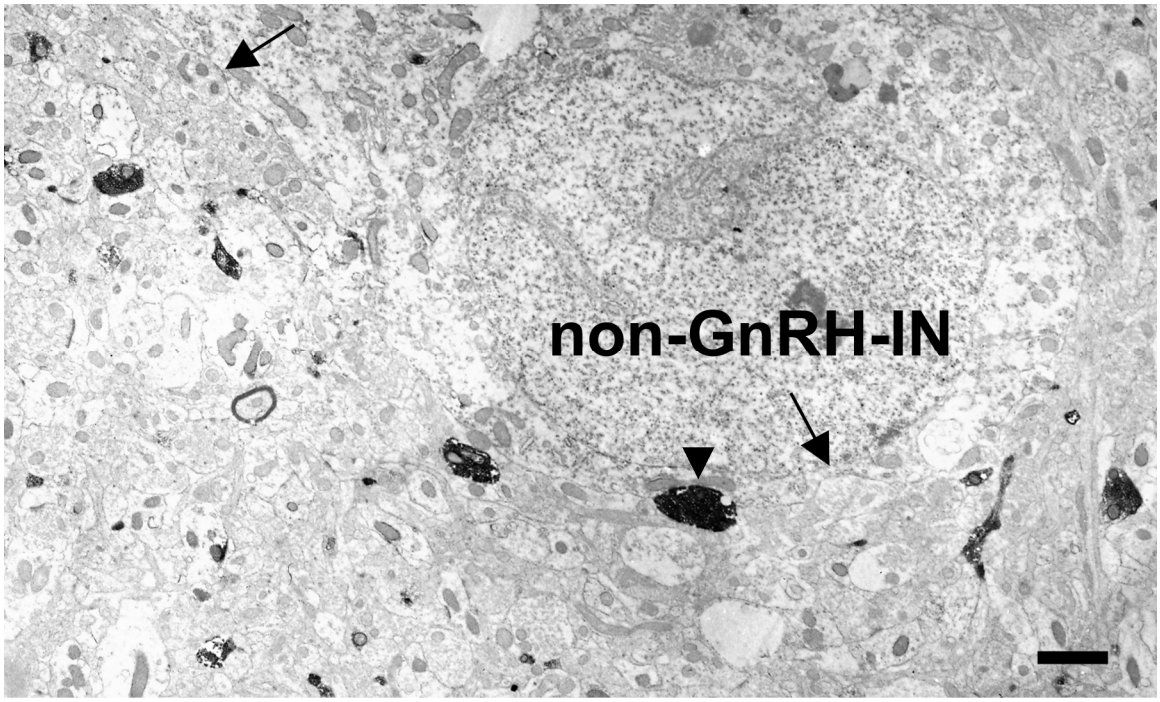

Figure 14. Representative electron micrograph of a putative GABA neuron two days after the estrogen-treatment. Only few GAD-immunoreactive (arrowhead) and unidentified (arrows) synaptic boutons contact cells that have infolded nucleus in the EB 2d experimental group. Bar represents 1 µm.

It is generally believed that the trend of action of neural elements depends upon the balance of their incoming inhibitory and excitatory stimuli. In order to better understand the synaptological status of examined neurons in relation to blood E- and LH concentrations, we established the concept of synaptic balance value, which expresses the ratio of inhibitory/excitatory (Inh/Exc) synapses on examined cell types. These values for both GnRH- and P-GABA neurons demonstrate that an inhibitory influence predominates; this inhibitory input on P-GABA neurons gradually decreases from OVX to day 8 after E_2-treatment, while on GnRH cells, it increases by EB 2d, followed by a slight fall by EB 8d (Fig. 15). It has been described that the vast majority of AN GABAergic axon terminals are of local origin (**45**). However, the scope of the present study did not allow us to provide evidence that the examined P-GABA neurons directly innervate GnRH cells. In the absence of such evidence, we sought to determine the relationship (whether it seems functional or not) between the synaptological status of the P-GABA- and GnRH neurons by comparing the synaptic balance values and then, seeing whether there is a resemblance to the blood E_2- or LH-levels. (In short, in OVX animals LH levels were high [54 µg/ml, mean value] and blood E_2 was below

measurable. By 24 hours, the LH had been inhibited [9.25 µg/ml] by the E_2 [232 pg/ml, mean value]. By 48 hours after EB administration the blood E_2 had begun to fall [63 pg/ml], having already triggered an LH surge [93 µg/ml]. In EB 8d animals, both the E_2 [45 pg/ml] and LH [15 µg/ml] decreased.)

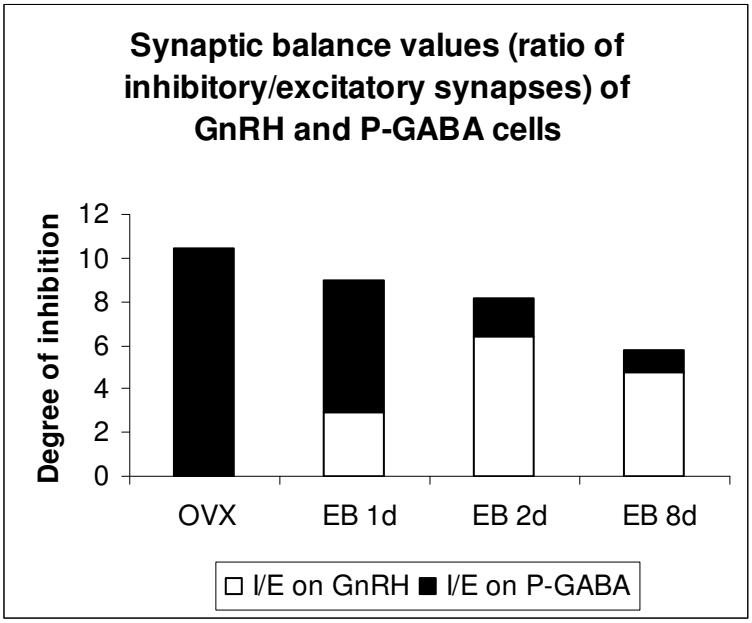

Figure 15. The gradual decrease and reversal of the inhibitory dominance on P-GABA neurons and simultaneous changes of synaptic balance values on GnRH cells.

With the purpose of comparing our present results to the changes in blood hormone levels, we illustrated the values of plasma E_2 and LH levels in Figure 16A-B. Also, to this end, we determined the ratio of synaptic balance values between the examined cell types ([P-GABA Inh/Exc] / [GnRH Inh/Exc]) and presented in Figure 16C-D. While we can only imply from these data a possible functional and/or morphological relationship between the GnRH and P-GABA cells, the trend of changes in synaptic balance values (synaptic status) of GnRH cells resemble those seen in blood LH levels, while temporal changes in the synaptic status of P-GABA neurons follow the trend displayed by E_2 levels; these observations suggest that E_2 targets hypothalamic GABAergic cells, as a consequence of which the synaptic status of GnRH cells changes, followed by the adequate release of LH. The ratio of synaptic balance values (Fig. 16D) further suggests that the overall synaptological changes in the AN are also dictated by the actual concentration of blood E_2.

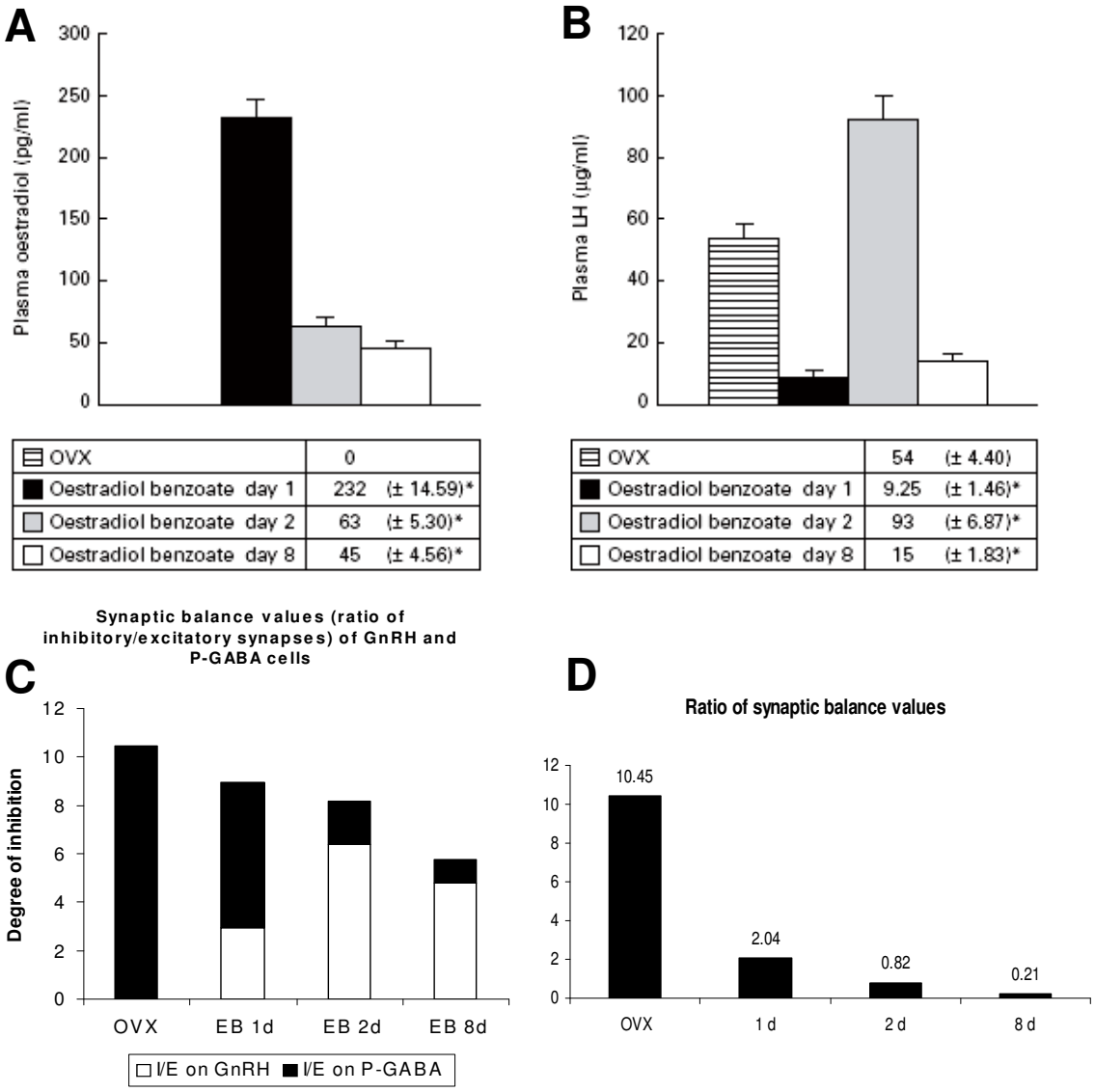

Figure 16. Comparison of the temporal changes in blood hormone levels (estrogen, A) and the synaptic balance values of GnRH cells (C, white columns) and P-GABA neurons (C, black columns). Overal temporal changes in the synaptic status of the arcuate nucleus (D) implies an estrogen-driven mechanism during the course of the negative gonadotropin feedback.

3. *Identification and characterization of rapid, non-genomic estrogen effects on non-neuroendocrine neurons: Estrogen-induced rapid modulation of the extracellularly regulated kinases 1 and 2 (ERK1/2) MAPK- (mitogen-activated protein kinase) pathway in the rat cerebellum.*

3.a. *Determination of rapid estrogen effects in primary neuronal cell cultures.*

Preliminary studies with an accepted physiological concentration of estradiol (10^{-8} M) indicated that the ERK1/2 MAPK signaling pathway in primary cultures of cerebellar neurons was variably responsive to estradiol treatment (data not shown). Dose–response analysis of rapid E_2-induced ERK1/2 activation was performed to characterize fully the rapid activation of ERK1/2 by estradiol (Fig. 17).

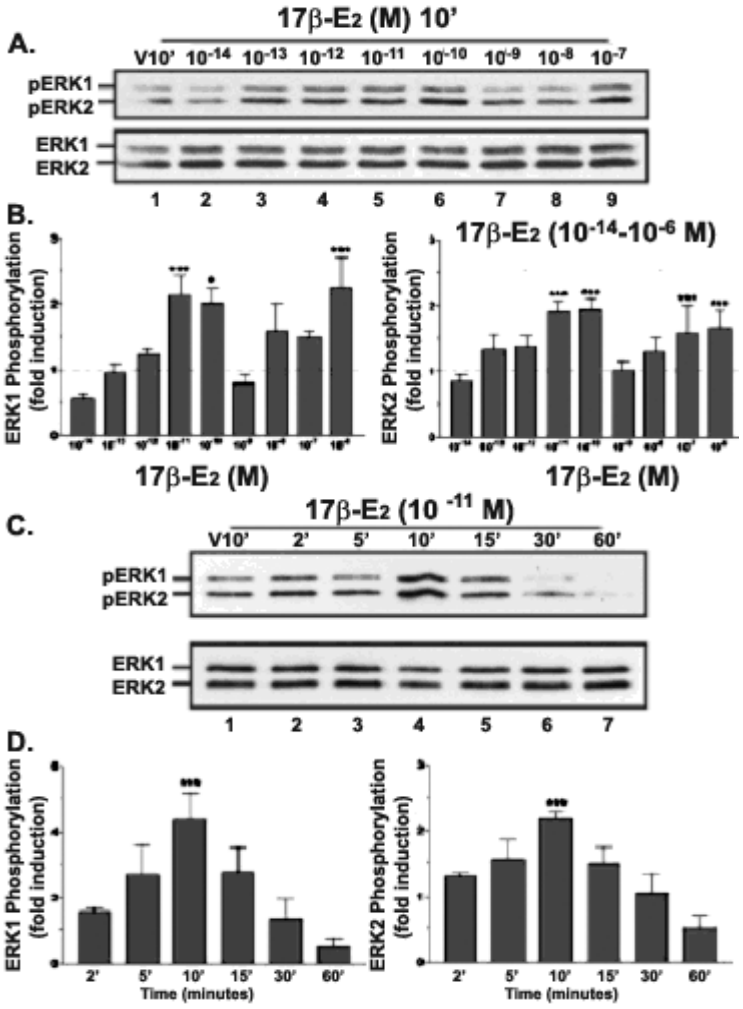

Figure 17. The dose dependency and kinetics of 17β-estradiol (E_2)-induced ERK1/2 activation. *A*, E_2 dose–response analysis: representative Western blots. Shown are protein lysates (≈5 µg/lane) from cerebellar granule cell cultures treated for 10 min with vehicle (V10') or increasing concentrations of E_2 (10^{-14} to 10^{-7} M). E_2 concentrations are indicated above each lane, and the positions of ERK1-IR and ERK2-IR are indicated to the left of each panel. *B*, E_2 dose–response analysis: densitometric analysis. Levels of E_2-induced ERK1/2 activation, expressed as fold increase above the baseline of vehicle-treated control, were determined by densitometric analysis of pERK1-IR and pERK2-IR. Results are expressed as the means±SEM of the fold induction as compared with control from nine independent experiments. Baseline levels are indicated with a dashed line. *C, D*, Time course analysis. ERK1/2 phosphorylation was increased significantly 10 min after the addition of 10^{-11} M E_2. With longer E_2 exposures the phosphorylation rapidly returned to baseline or lower levels.

In granule cell cultures that were exposed to various concentrations of E_2 for 10 min, analysis of multiple experiments revealed that E_2 stimulated significant ERK1/2 activation in two different concentration ranges. An initial biphasic, or hormetic, stimulation of ERK-phosphorylation was observed at 10^{-11} to 10^{-10} M, and a second significant increase in MAPK signaling was induced by high (10^{-7} to 10^{-6} M) concentrations of E_2 (Fig. 17A-B). A highly variable and insignificant responsiveness was observed at the 10^{-8} M concentration.

At the lowest concentration of E_2 that induces maximal effects (10^{-11} M), the time dependence of E_2-stimulated ERK1/2 phosphorylation was investigated (Fig. 17C-D). Increased ERK1/2 phosphorylation was often detectable as early as 2 min after treatment, with increases reaching significance by 10 min. Increases in ERK1/2 phosphorylation were transient and returned to baseline levels or below after 15 min of exposure. Neither the time course nor dose dependency of E_2-induced ERK1/2 activation was influenced by the sex of the animal from which the granule cell cultures were derived.

To determine whether cell-impermeable E_2 elicits a rapid increase in ERK-activation, we treated granule cell cultures with E_2 covalently bound to BSA (E_2-BSA). As was observed for free E_2, after a 10 min treatment with E_2-BSA (E_2 concentration of 10^{-11} M) a rapid increase in ERK1/2-phosphorylation was observed (Fig. 18A), suggesting that E_2-induced ERK1/2-activation is initiated at the extracellular surface of the plasma membrane.

The involvement and specificity of the MAPK signaling pathway also was confirmed. In the presence of 10 μM U0126, a specific inhibitor of the upstream MAPK kinase (MEK), ERK1/2 responsiveness to E_2 was abrogated completely (Fig. 18B). Western blot analysis that used phosphorylation state-specific antisera for the SAPK/JNK and p38 MAP kinases indicated that SAPK/JNK and p38 were not activated by E_2-treatment (Fig. 18C-D), thus demonstrating that the rapid MAPK response to estradiol is specific to the ERK1/2 MAPK pathway.

Because these granule cell cultures contain a small number (<5% of the total cells) of contaminating glia-like cells (**35**), immunofluorescence analysis of E_2-induced ERK activation was performed to identify unambiguously which cell type was responsive to E_2. In cultures treated with 10^{-11} M E_2 for 15 min, increased MAPK phosphorylation was detected in only the small granule cell neurons (Fig. 19A-D). Further, in cultures immunostained for both phosphorylated ERK1/2 and the glia-specific antigen GFAP, increased phosphorylated ERK1/2 was observed only in the GFAP-negative granule cells (Fig. 19E-F), clearly demonstrating that in granule cell neurons, but not cerebellar glia, ERK1/2 phosphorylation was increased rapidly by estradiol treatment.

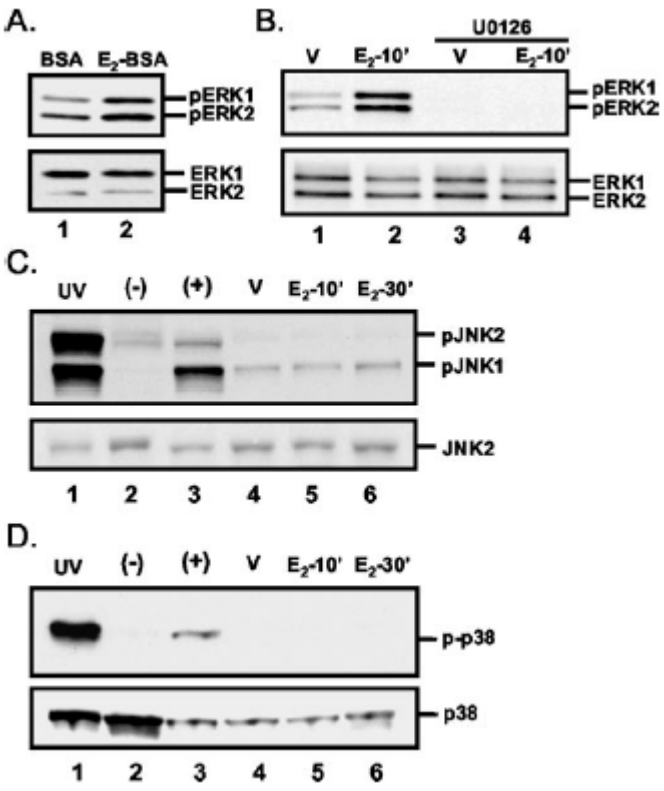

Figure 18. Analysis of the specificity and nature of estradiol-induced ERK1/2 activation. **A**, Cell-impermeable E_2-BSA induces ERK1/2 phosphorylation. Shown are representative Western blots of protein lysates sequentially probed for pERK1/2 and total ERK1/2. Lysates were isolated from granule cell cultures after a 10 min treatment with equal molar concentrations of BSA or BSA-conjugated E_2 (final E_2 concentration of 10^{-11} M). **B**, Representative Western blots of cell lysates from cultures treated with 10^{-11} M E_2 (E_2-10') or vehicle (V) for 10 min with or without a 30 min preexposure to 10 µM U0126 or vehicle. The presence of U0126 blocks estrogen-induced ERK phosphorylation, indicating that estrogen effects are MEK-dependent and mediated via the MAPK pathway. **C**, Analysis of estradiol-induced SAPK/JNK MAPK activation. Representative Western blot analyses demonstrate that treatment with 10^{-11} M E_2 does not induce detectable increases rapidly in SAPK/JNK MAPK activation. HEK 293 cell lysates exposed (lane 1) or unexposed (lane 2) to UV light and granule cell cultures treated for 30 min with 30 ng/ml anisomycin (lane 3) served as controls. Granule cell cultures were treated with vehicle for 10 min (lane 4; V) or 10-^{11} M estradiol for 10 and 30 min (lanes 5, 6, respectively). The top panel was probed with antiserum specific for the phosphorylated forms of JNK1 and JNK2. The bottom panel was probed with antiserum that recognizes JNK2 independently of phosphorylation state. The positions of the 54 and 46 kDa JNK1 and JNK2 immunoreactive bands are indicated. **D**, Analysis of estradiol-induced p38 MAPK activation. Representative Western blot analyses demonstrate that treatment with 10^{-11} M E_2 does not induce detectable increases in p38 MAPK activation. Activation of the p38 MAP kinase was analyzed with phospho-p38 antiserum (p-p38) as described for JNK1/2 and similarly was found to be unaffected by E_2 treatment. All presented results are representative of at least three independent experiments.

To characterize further the pharmacological properties of E_2-induced ERK1/2 phosphorylation in cerebellar granule cells, we examined the responsiveness to other steroids. As was observed for 17β-E_2, the "nonestrogenic" estradiol isomer 17α-estradiol (17α-E_2) rapidly induced ERK1/2-phosphorylation (Fig. 20A). At concentrations that induced maximal effects, 17α-E_2 and 17β-E_2 were comparably

efficacious; however, 17α-E_2 was markedly less potent than 17β-E_2, with a single peak of maximal activation observed in the concentration range of 10^{-9} to 10^{-8} M. The phosphorylation state of ERK1/2 in cerebellar granule cells was unresponsive to progesterone or testosterone across a concentration range of 10^{-13} to 10^{-6} M (Fig. 20C-D).

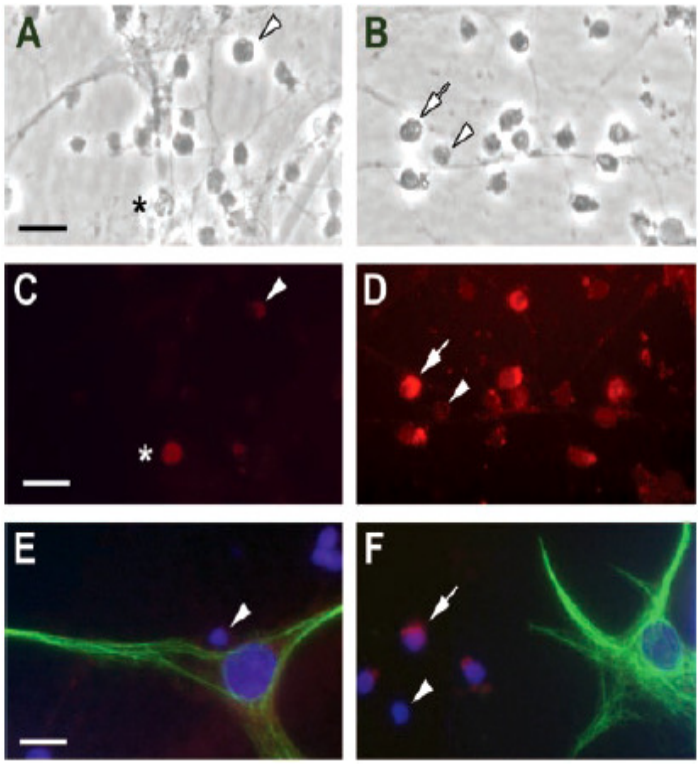

Figure 19. Immunofluorescent analysis of the cell-type specificity of estradiol- (E_2) induced rapid ERK phosphorylation in cerebellar granule cell cultures. Shown are representative photomicrographs of control (left) and experimental (right) cerebellar granule cell cultures treated with vehicle or 10^{-11} M E_2 for 15 min. Bright-field images of control (**A**) and E_2-treated (**B**) cultures and corresponding epifluorescent images were immunostained for phospho-ERK1/2 and visualized with a Texas Red-conjugated goat anti-rabbit secondary antibody (**C**, control; **D**, E_2-treated). E_2 treatment resulted in increased cytoplasmic and nuclear staining of granule cells (white arrows), whereas only scattered cells with markedly lower levels of fluorescence could be seen in untreated or vehicle-treated cultures (white arrowheads). Asterisk indicates a dead granule cell that shows homogeneous autofluorescence. No phospho-ERK1/2-IR was detected in GFAP-immunoreactive glial cells (E, F, green fluorescence).

When cultures were co-treated or pretreated for 5 min with 1 μM ICI182,780, E_2-induced MAPK phosphorylation was not blocked at any E_2 concentrations that were tested (data not shown). However, when cultures were pretreated with ICI182,780 for 30 min, increases in ERK1/2-activation were not detectable 10 or 30 minutes after treatment with 10^{-11} M E_2 (Fig. 21A). On the basis of the rapid and transient kinetics of estradiol-induced ERK1/2-activation, we hypothesized that ICI182,780 also was inducing rapid and transient ERK1/2-phosphorylation.

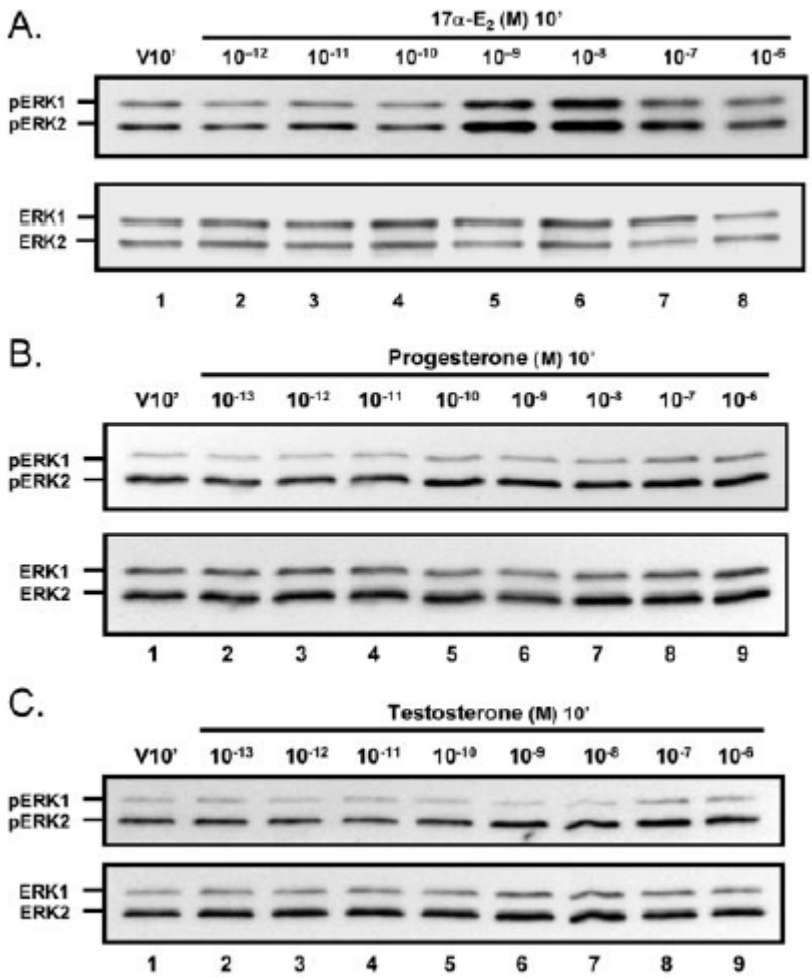

Figure 20. Dose–response analysis of ERK1/2 activation by 17α-estradiol, progesterone, and testosterone. Shown are representative Western results of ERK1/2 activation analysis in primary cultures of cerebellar granule cells treated for 10 min with increasing concentrations of the nonestrogenic estrogen isomer 17α-estradiol (**A**), progesterone (**B**), or testosterone (**C**). ERK1/2 phosphorylation was induced rapidly by 17α-E_2. Maximal activation was right-shifted by two orders of magnitude as compared with 17β-E_2, with significant ($p<0.05$; n=3) stimulation of ERK1/2 phosphorylation at 10^{-9} and 10^{-8} M 17α-E2 but with insignificant effects at the higher concentrations. Neither progesterone nor testosterone stimulated ERK1/2 phosphorylation. Results are representative of at least three experiments.

Analysis of ICI182,780 dose dependency experiments demonstrated that a 10 min exposure to 10^{-9} to 10^{-7} M ICI182,780 increased ERK1/2 phosphorylation (Fig. 20B). Further, time course studies indicated that 10^{-8} M ICI182,780 induced a significant rapid and transient increase in ERK1/2 phosphorylation with temporal characteristics similar to those observed for E_2 (Fig. 20C-D). Rather than acting as a true competitive antagonist, these results suggest that, in the presence of higher concentrations of ICI182,780, 10^{-11} M E_2 cannot re-stimulate ERK1/2 signaling after transient ICI182,780-induced ERK1/2-phosphorylation.

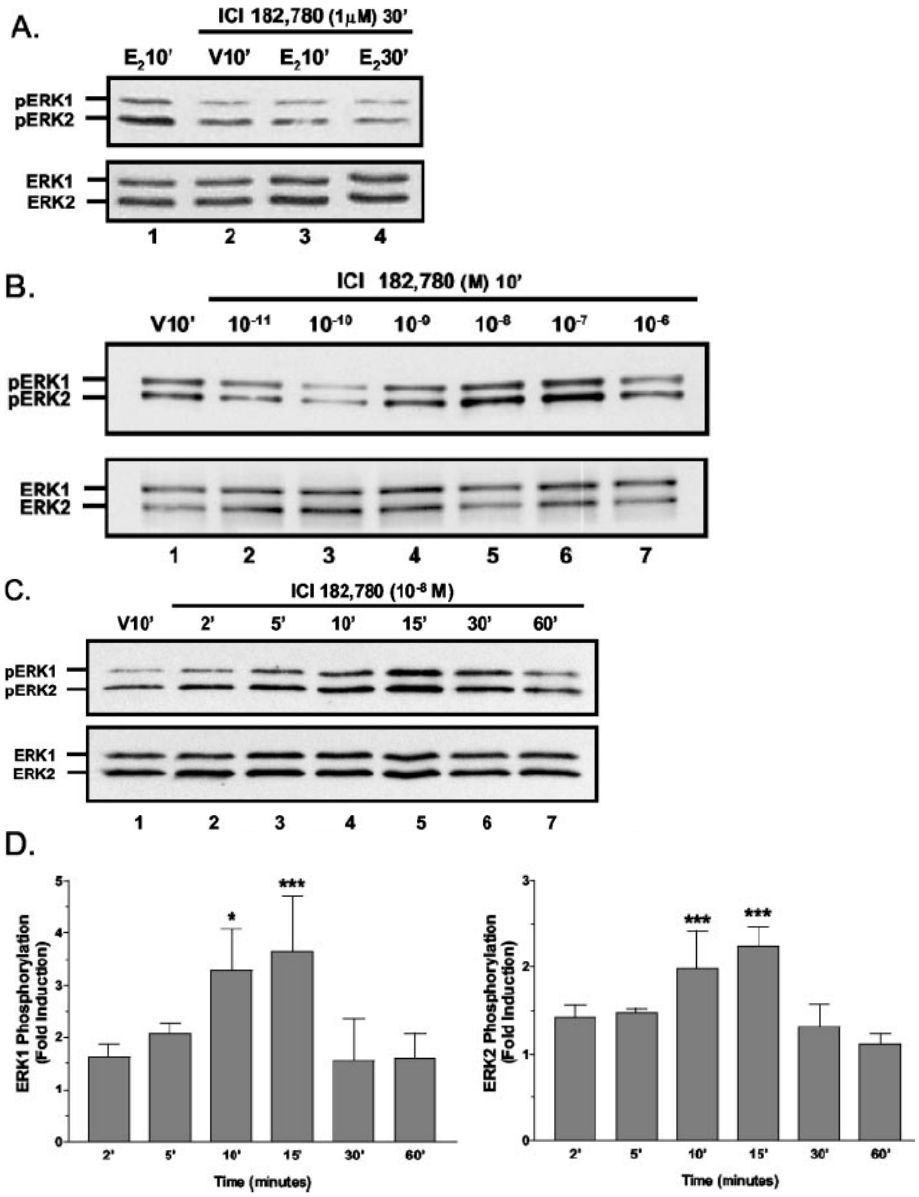

Figure 21. Analyses of ICI182,780-mediated activation of ERK1/2. **A**, ICI182,780 blockade of E_2-mediated MAPK stimulation; Western blot analyses of E_2-induced ERK1/2 phosphorylation in cell lysates from cultures pretreated for 30 min with 1 μM ICI182,780. This increased duration of ICI182,789 pretreatment abrogates estradiol-stimulated ERK1/2 phosphorylation. **B**, ICI182,780 dose–response analysis. Shown are representative Western blot results of the dose dependency of rapid ICI182,780-induced ERK1/2 phosphorylation. In primary cultures of cerebellar granule cells treated for 10 min with increasing concentrations of ICI182,780, rapid increases in ERK1/2 phosphorylation are observed with concentrations between 10^{-9} and 10^{-7} M, indicating that ICI182,780 is a highly potent agonist of rapid ERK1/2 phosphorylation. **C**, **D**, Time course analysis of ERK1/2 phosphorylation stimulated by 10^{-8} M ICI182,780 revealed that ERK1/2-phosphorylation increases significantly at 10 and 15 min after the addition of 10^{-8} M ICI182,780, and with longer exposure ERK1/2 phosphorylation rapidly returnes to baseline levels. For each
Experiment, the results are normalized to total ERK-IR and are the mean fold induction ± SEM of six different experiments. *,***See Materials and Methods.

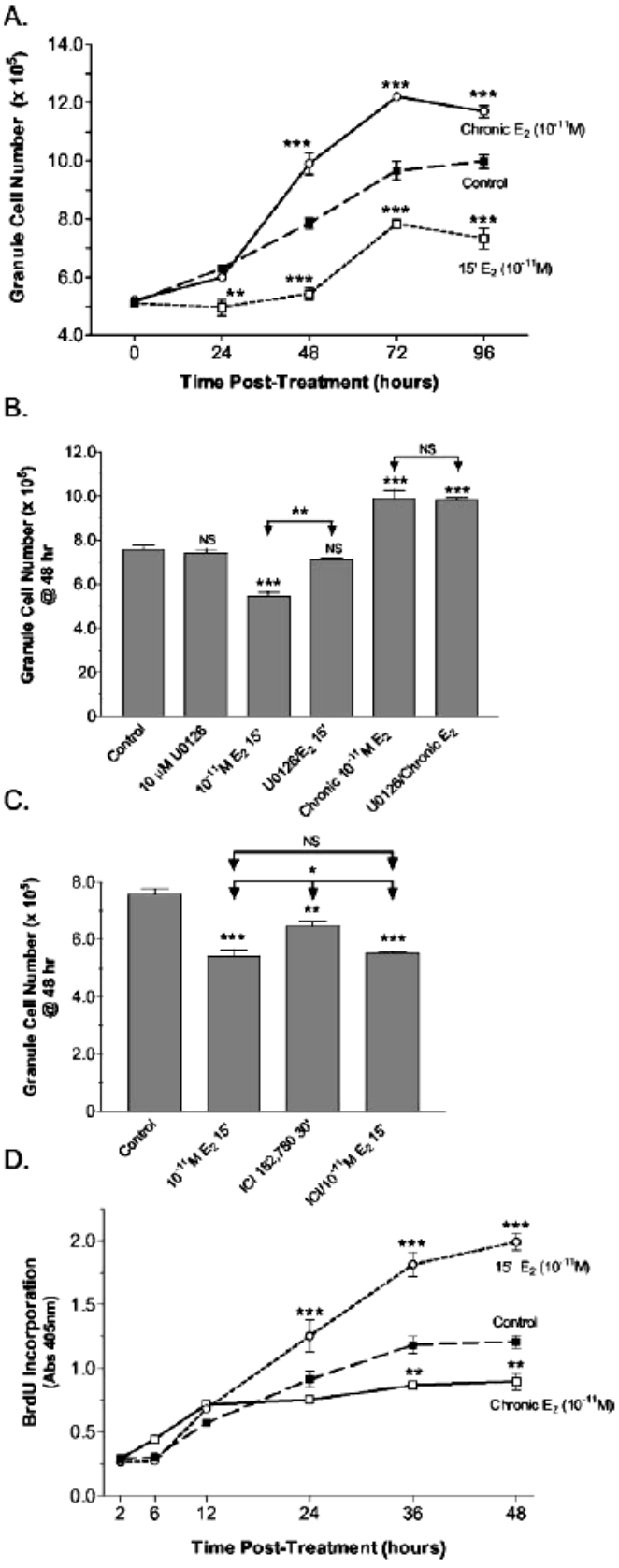

Figure 22. Analysis of E_2-effects on developing granule cell viability and mitogenesis. **A**, At different time points after a 15 min pulsed (15' E_2) or continuous (Chronic E_2) treatment with 10^{-11} M E_2 or vehicle control, the number of viable cells was determined. After 48 hr of treatment a significant increase in granule cell numbers resulted from continuous E_2 exposure. In pulse-treated cultures significant decreases in viable cells were observed, with net increases in cell numbers not observed until 72 hr after treatment. Values are average cell number per culture ± SEM from three independent experiments. No significant difference was observed between cultures that were control pulse-treated or treated continuously with vehicle. For each time point the level of significance between the cell numbers determined for the control and each experimental group is indicated. **B**, The role of E_2-induced MAPK activation was demonstrated by pretreatment of the cultures with the MEK1 inhibitor U0126. At the time of maximal differences in viable granule cell numbers (48 hr) U0126 significantly blocked E_2-induced decreases in viable granule cells. Pretreatment with U0126 did not influence increased granule cell viability resulting from chronic exposure to 10^{-11} M E_2. U0126 alone had no effect on granule cell viability. Values are average cell number per culture ± SEM from three independent experiments. The level of significance between control and experimental treatment groups is indicated directly above the error bar (NS, no significant difference). Levels of significance between the E_2 and U0126+E_2 treatment groups are indicated with arrows. **C**, A significant reduction in granule cell viability was detected 48 hr after a 30 min treatment with 1 μM ICI182,780, which was augmented further by an additional 15 min exposure to 10^{-11} M E_2. Levels of significance are indicated as above. **D**, At different time points after a 15 min pulsed (15' E_2) or continuous (Chronic E_2) treatment with 10^{-11} M E_2 or vehicle, the amount of BrdU incorporated into newly synthesized DNA of dividing cerebellar cells was assessed via an ELISA-based method. Pulsed exposures induced additional rounds of mitosis, whereas chronic exposure was anti-mitogenic. Values are expressed as the means ± SEM from three independent experiments, with the level of significance for the difference between control and each experimental value indicated. *,**,***See Materials and Methods.

Direct cell counting of viable granule cells at different times after either a 15 min pulse treatment of 10^{-11} M E_2 followed by an estrogen-free chase period or after continuous exposure to 10^{-11} M E_2 indicated that this low concentration of estradiol significantly altered the number of viable cells present. In control cultures and cultures continuously exposed to E_2 significant increases in viable cells were detected 24 hr after treatment. In pulse-treated cultures increases in the number of viable granule cells were not observed until 72 hr after treatment (Fig. 22A). In all cases by 72 hr after treatment granule cell numbers had reached a plateau. In terms of the number of viable granule cells, chronic treatment with E_2 resulted in significant increases in viable granule cells after 48 hr in culture. In contrast, there were significantly fewer viable granule cells in pulse-treated cultures at all time points (Fig. 22A).

The role of ERK1/2-activation in the observed changes in granule cell numbers was investigated by determining whether U0126 could block the E_2-induced changes in granule cell viability (Fig. 22B). At 48 hr after treatment (the time of maximal differences in viable granule cell numbers) significantly fewer viable granule cells were present in cultures pulse-treated with E_2. In the presence of 10 μM U0126, however, 15 min of exposure to 10^{-11} M E_2 had no significant influence on the number of viable granule cells. In cultures chronically treated with E_2 for 48 hr the presence of U0126 during the entire incubation period did not inhibit E_2-induced increases in viable granule cell numbers. These results indicate that pulsed E_2-treatment caused a decrease in granule cell numbers that was mediated by rapid ERK1/2-activation, whereas the effects of chronic E_2 treatment were independent of MEK–ERK signaling.

As with E_2, pulsed treatment with 1 μM ICI182,780 resulted in a significant decrease in viable granule cells 48 hr after treatment (Fig. 22C). When ICI182,780 treatment was followed by an additional 15 min exposure to 10^{-11} M E_2 before the chase period, an additional significant decrease in cell numbers was observed. This result suggests that ICI182,780 does not inhibit E_2-dependent decreases in granule cell viability, but rather the effects of ICI182,780 and estradiol are additive.

To determine whether pulsed or continuous E_2 exposures differentially influence the mitogenesis of immature granule cell precursors, we analyzed DNA synthesis during the first 48 hr in culture by measuring BrdU incorporation. Surprisingly, the results of BrdU incorporation experiments revealed that exposure to 10^{-11} M E_2 for 15 min was

mitogenic compared to vehicle-treated control cultures (Fig. 22D). In contrast, chronic exposure to the same concentration of E_2 significantly decreased granule cell mitogenesis.

In vivo and in culture the cerebellar granule cells normally undergo apoptotic and oncotic/necrotic forms of programmed cell death during development (**46-48**). Therefore, we initially sought to determine whether increased granule cell death occurred after pulsed estradiol treatment. Initial observations revealed increased cytoplasmic vacuolization of granule cell neurons in estradiol-treated cultures, a feature consistent with oncotic cell death (**49**). Because the loss of plasma membrane integrity is an additional hallmark of oncotic forms of cell death, the permeability to propidium iodide (PI) and the release of LDH into the culture media were used to determine whether increases in oncosis/necrosis were induced by pulsed E_2 treatment. Significant increases in PI permeability were detected at 3, 12, and 24 hr after a 15 min pulse treatment with 10^{-11} M E_2 (Fig. 23A-C). However, at 48 and 72 hr after treatment, times when rapid and significant increases in viable granule cells and granule cell mitogenesis occur (Figs. 21, 22), PI permeability was decreased significantly as compared with control (Fig. 23C).

Analysis of LDH at 24 hr after a 15 min pulsed exposure to 10^{-11} M E_2 revealed that a significant MAPK-dependent increase in LDH release also occurred (Fig. 23D). Pulsed treatment with 1 μM ICI 182,720 also resulted in significant LDH release; this effect was not increased further by the addition of E_2. Similar to the results obtained for the analysis of PI permeability, in E_2-treated cultures decreased LDH release was detected at the 48 hr time point (Fig. 23E). However, at 48 hr a significant LDH release was detected in cultures treated with ICI182,780. This last observation suggests that later proliferative and protective actions of pulsed E_2 treatment may involve ligand-activated transactivational activity that involves the ERs. In mature cultures of granule cells neither viability nor LDH-release was influenced by either pulsed or continuous exposure to any concentration of E_2 between 10^{-11} and 10^{-6} M (Fig. 24A-D).

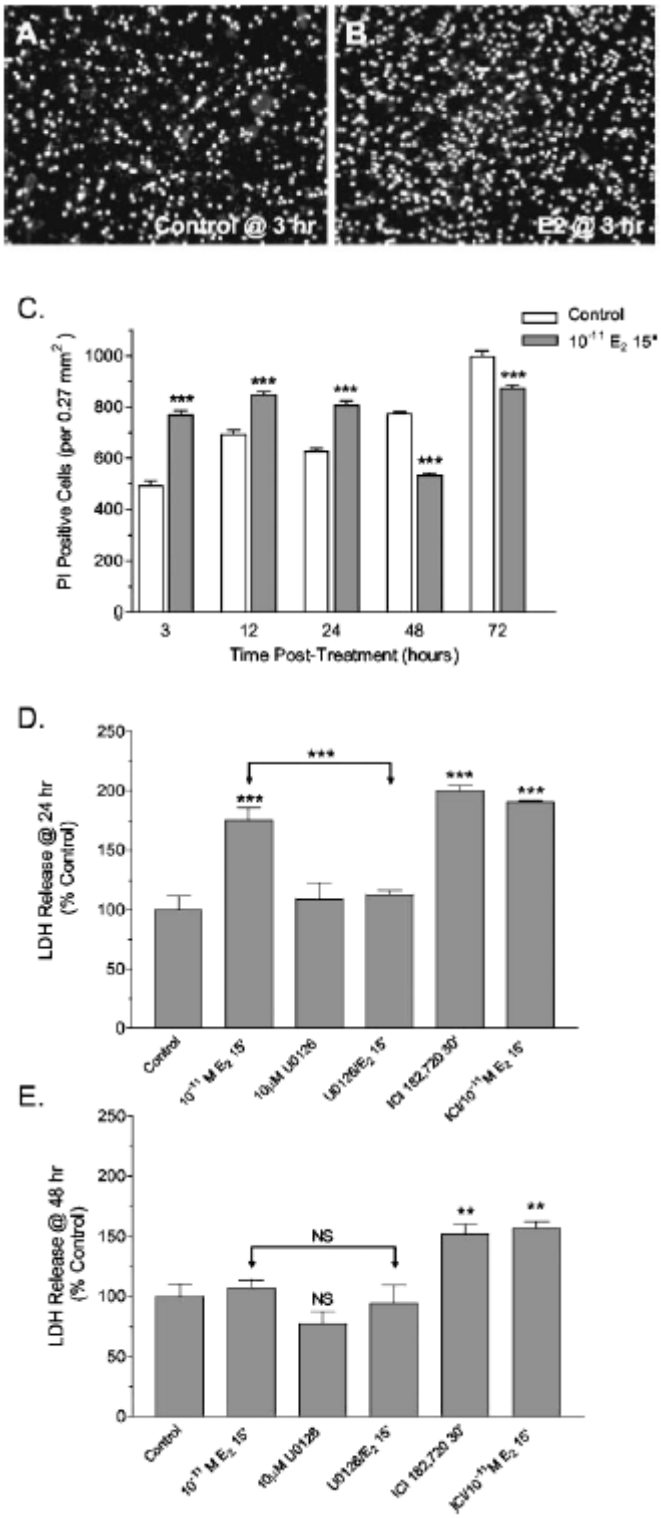

Figure 23. Effects of pulsed E_2 treatment on granule cell permeability. Compared with control cultures (**A**), propidium iodide (PI) permeability, a measure of oncotic cell death, significantly increased in cultures of granule cells 3 hr after a 15 min exposure to 10^{-11} M E_2 (**B**). **C**, Quantitative determination of the number of PI-permeable granule cells revealed that estradiol treatment induced significant changes in permeability. Increased oncotic profiles were observed at the 3, 12, and 24 hr post-treatment time points, whereas at the 48 and 72 hr time points significant decreases in PI permeability were observed. Results are reported as the means ± SEM for six 0.27mm^2 fields randomly selected from three different samples for each time point. At 24 hr (**D**) and 48 hr (**E**) after 15 min of exposure to 10^{-11} M E_2 the amount of LDH released into culture media was determined and used as a measure of necrotic cell death. LDH release was increased significantly in E_2-treated cultures at 24 hr, but not at 48 hr. Pretreatment with U0126 completely blocked E_2-induced increases in LDH release at 24 hr, indicating that E_2 was acting via activation of the MAPK pathway. At both times a robust increase in LDH release was observed after a 30 min exposure to 1 µM ICI182,780, an effect not accentuated by an additional 15 min of exposure to ICI182,780 and 10^{-11} M E_2. Results are expressed as the means ± SEM (*n*=8 – 9), with significance assessed by a one-way ANOVA and Dunnett's or Newman–Keuls post-test. The level of significance between control and experimental treatment groups is indicated directly above the error bar (NS, no significant difference). **,***See Materials and Methods.

Results of chromosomal fragmentation analysis and counting of fluorescently labeled condensed chromatin structures confirmed that granule cells in both vehicle and E_2-treated cultures were undergoing apoptotic-like programmed cell death. However, neither chronic nor pulsed E_2 treatments appeared to increase apoptotic cell morphologies (data not shown). To confirm that caspase-dependent apoptosis was not increased by a 15 min pulsed treatment with 10^{-11} M E_2, we determined caspase activity at 24 hr after treatment and found it to be unaffected by E_2 treatment (Fig. 25A). Treatment with the nonspecific PKC inhibitor staurosporine resulted in a robust increase in caspase activity. In staurosporine-, vehicle-, and E_2- treated cultures the caspase activity was inhibited completely by the pan-caspase inhibitor zVAD-fmk. Nearly identical levels of caspase activity were detected in vehicle and E_2-treated cultures. Caspase activity similarly was unaffected by a blockade of MAPK signaling before E_2 treatment (Fig. 25A).

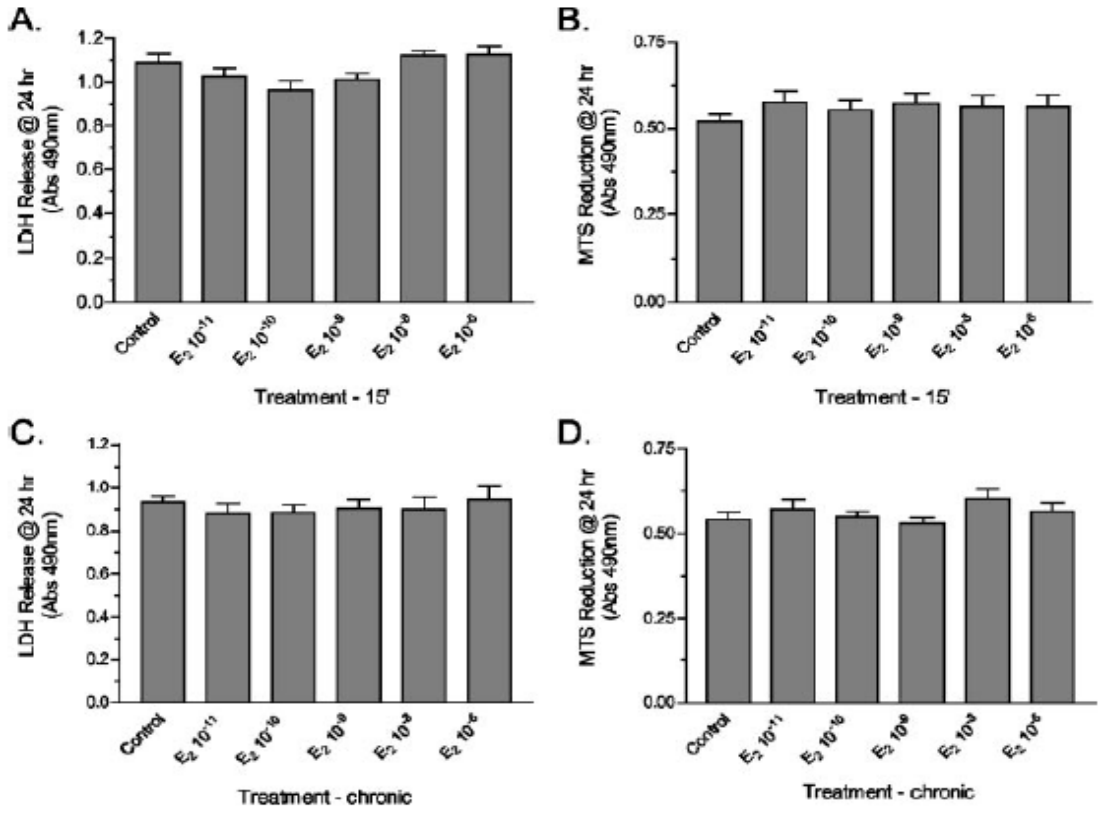

Figure 24. Effects of E_2 on mature cerebellar granule cells. Changes in granule cell permeability were assessed by LDH release; granule cell viability was determined by the MTS reduction assay in mature cell cultures 24 hr after either a 15 min pulsed treatment or a continuous exposure to different concentrations of E_2 from 10^{-11} to 10^{-6} M. At all of the E_2 concentrations, no differences in cell lysis or viability were detected in response to either pulsed 15 min exposures (**A**, **B**) or a continuous 24 hr exposure (**C**, **D**). Results expressed as the means ± SEM (n=24). (One-way ANOVA and Dunnett's post-test.)

Finally, the role of Ca^{2+}-activated cysteine proteases, calpains, for which the intracellular activation is known to play an important role in oncotic cell death (**50, 51**), was investigated 24 hr after a 15 min exposure to 10^{-11} M E_2. Compared with control, significant increases in LDH release were observed in E_2-treated cultures with and without the addition of zVAD-fmk (Fig. 25B-C), indicating that estradiol-induced LDH release was independent of caspase activity. Pretreatment with U0126 completely blocked E_2-induced increases in LDH release, further indicating that E_2 was acting via activation of the MAPK pathway. The irreversible calpain inhibitor PD150606 similarly blocked E_2-induced LDH release (Fig. 25B), and PD150606 blockade of LDH release was not enhanced by the inhibition of caspase activity by zVADfmk (Fig. 25C). Together, these results show that E_2-mediated LDH release is a MAPK-dependent consequence of oncotic-like programmed cell death and not a secondary consequence of increased apoptosis.

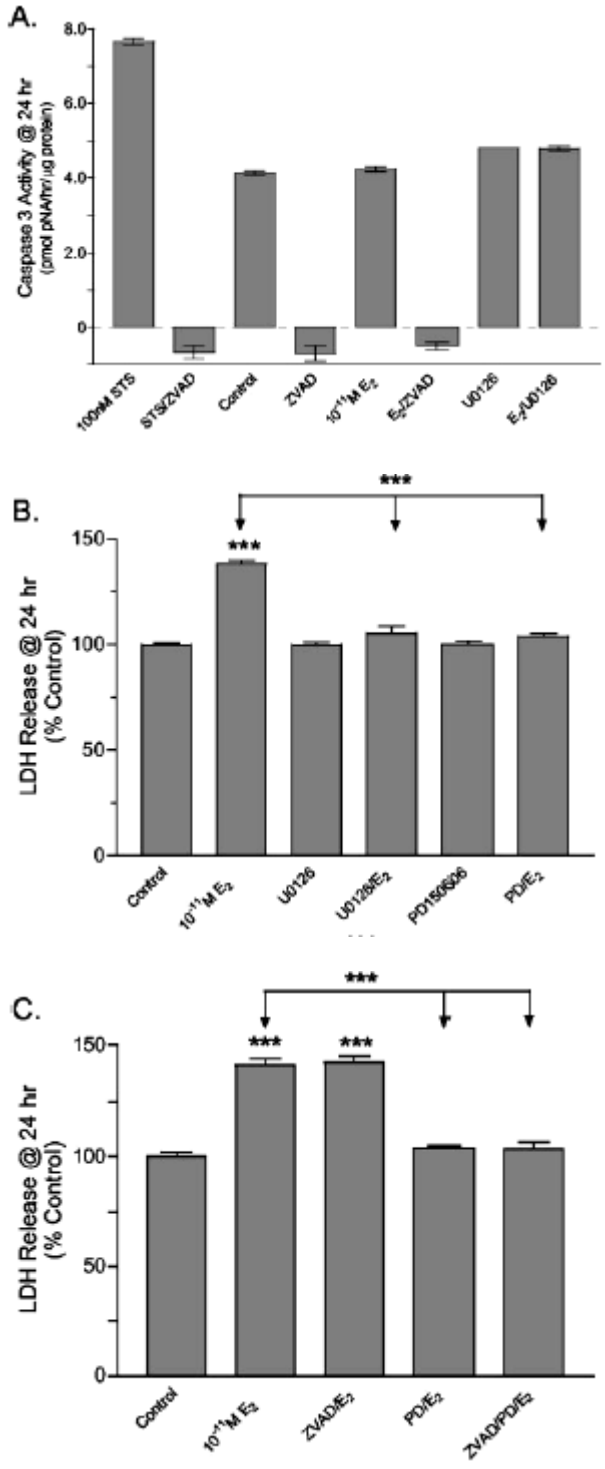

Figure 25. Analysis of the role of caspase or calpain activity in the mechanism of E_2-mediated granule cell neurotoxicity. **A**, Immature granule cell cultures were pulse-treated with 10^{-11} M E_2, and caspase activity was determined 24 hr after treatment. Compared with control, E_2 treatment did not increase caspase activity. The nonspecific PKC inhibitor staurosporine (STS) was used as a positive control to stimulate apoptosis by activation of caspases and resulted in a robust increase in caspase activity. In staurosporine-, vehicle-, and E_2-treated cultures the caspase activity was inhibited completely by the pan-caspase inhibitor zVAD-fmk (12.5 µM). Caspase activity similarly was unaffected by the blockade of MAPK signaling before E_2 treatment. **B**, At 24 hr after 15 min of exposure to 10^{-11} M E_2 the amount of LDH released into culture media was determined as an indicator of oncotic cell death. LDH release was increased significantly in E_2-treated cultures. Pretreatment with U0126 (10 µM) completely blocked E_2-induced increases in LDH release, confirming that E_2 was acting via activation of the MAPK pathway. The irreversible calpain inhibitor PD150606 (50 µM) similarly blocked E_2-induced LDH release. **C**, E_2-induced LDH release was independent of the pan-caspase inhibitor zVAD-fmk. Compared with control, significant increases in LDH release were observed in E_2-treated cultures with and without the addition of zVAD-fmk. In the presence of PD150606 the LDH release in cultures treated with E_2 was not significantly different from control. zVAD-fmk did not enhance PD150606 blockade of LDH release. Results indicate that E_2-mediated LDH release is a MAPK-dependent consequence of necrosis-like programmed cell death and not a secondary consequence of apoptosis. In all cases the results are expressed as the means ± SEM (n=24), with significance assessed by a one-way ANOVA and Dunnett's or Newman–Keuls post-test. The level of significance between control and experimental treatment groups is indicated directly above the error bar. ***See Materials and Methods.

3b. *Determination of the spatiotemporal distribution of activated, dually phosphorylated ERK1/2 (pERK) in the rat cerebellum.*

Postnatal day 0

In the developing cerebellar cortex on P0 scattered migrating Purkinje cells in proximity of the forming Purkinje cell layer were immunopositive for pERK (Fig. 26A). At this age, GFAP-IR was restricted to the dissolute pretrigonal- and subisthmal-glial matrices (Fig. 26B); pERK-IR was not observed in these proliferating glial cells that were abundant in the ventral half of the cerebellum.

Postnatal day 1

By P1, a variable degree of pERK immunostaining was detected in scattered Purkinje cells (Fig. 26C, black arrowhead). Immunostaining was most prominent in immature Purkinje cells in the anterior and posterior cerebellar lobes. Phospho-ERK staining was also present in Bergmann glia cells organized into a proliferating layer just beneath and intermingled with the forming Purkinje cell layer (Fig. 26C, white arrowhead). Scattered clusters of spindle-shaped immunopositive Bergmann glial cells were localized in the forming Purkinje cell layer (Fig. 26C1). These clusters consisted of 3–10 closely packed cells, without Purkinje cells positioned between them. Discontinuous rows of small pERK-IR cells, presumably maturing post-mitotic granule cells, were observed near the differentiating subdivision of the external germinal layer (EGL; Fig. 26C2).

Postnatal days 2-3

On P2, pERK-IR remained in scattered cells of the differentiating subdivision of the EGL. Immunostaining in Purkinje cells was reduced on P2, and was further reduced to background levels on P3. In contrast, staining was retained in proliferating Bergmann glia, with numerous intensely stained clusters of Bergmann glial cells being observed (Fig. 26D arrow heads; Fig. 26D1). By P3, the proliferating layer of Bergmann glial cells was thicker (Fig. 26E).

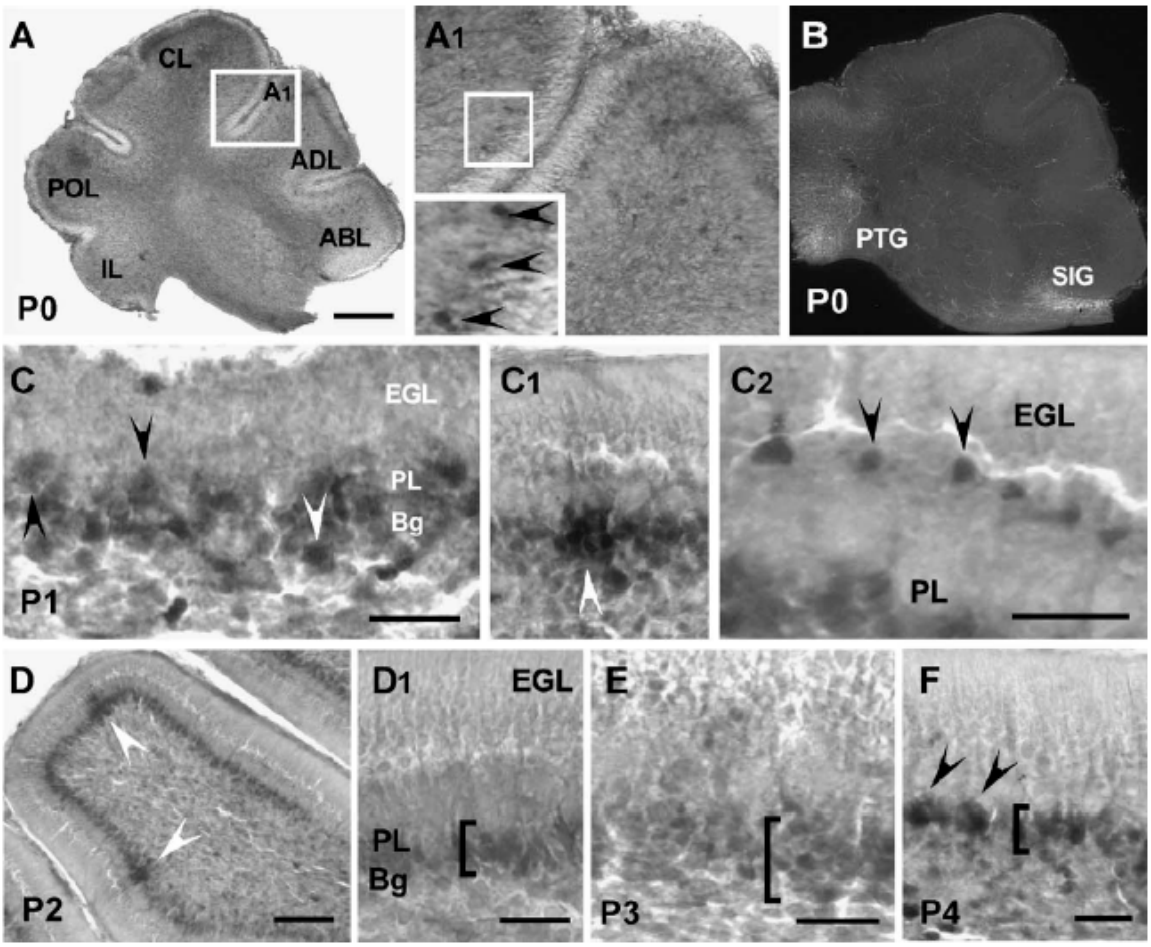

Figure 26. Developmental changes of pERK-immunoreactivity (IR) in the cerebellum from birth to P4. (**A**) At P0, only scattered, migrating Purkinje cells, within the cerebellar matrix and in the proximity of the forming Purkinje cell layer, were pERK- IR (A1 inset, black arrowheads). (**B**) At P0, glial fibrillary acidic protein- IR was detected in the vicinity of the pretrigonal (PTG) and subisthmal glial matrix (SIG), no pERK- IR was observed. (**C**) By P1, scattered Purkinje cells near the forming Purkinje cell layer (PL) were pERK- IR (black arrowheads). Phospho-ERK- IR Bergmann glial cells (Bg) were organized in a proliferating layer associated with the forming PL (white arrowhead—a Bergmann glia cell just beneath the PL). Additionally, scattered groups of 3–10 densely packed spindle-shaped maturing Bergmann glia-like cells, without intervening Purkinje cells (**C**1, white arrowhead) stained in the forming PL. Scattered pERK- IR cells, presumably postmitotic, maturing granule cells, were observed in the differentiating part of the external germinal layer (EGL; **C**2, black arrowheads). (**D**) At P2, intense staining was seen in the proliferating layer of Bergmann glial cells. Numerous immunoreactive clusters of Bergmann glial cells were observed in the PL (white arrowheads). (**E**) By P3, the proliferating Bergmann glia layer was thicker than at P2 and the intensity of the staining was considerably decreased compared to that seen at P2 (compare **D**1 and **E**). (**F**) At P4, the proliferating Bergmann glial cells were heavily stained and organized in a 2– 3-cell-deep layer (compare **D**1, **E** and **F**). Scale bars: (**A**) 200 µm; (**C**, **C**2) 25 µm; (**D**) 100 µm; (**D**1, **E**, **F**) 25 µm. ABL: anterobasal lobule; ADL: anterodorsal lobule; CL: central lobule; POL: posterior lobule; IL: inferior lobule.

Postnatal day 4

On P4, a reactivation of ERK signaling in maturing Purkinje cells was detected with light to moderate levels of pERK immunostaining of scattered Purkinje cells (Fig. 26F; arrowheads).

Immunopositive granule cells were found in moderate numbers in the anterior lobe with fewer dispersed immunopositive granule cells in the posterior lobe (data not shown). Immunopositive maturing granule cell precursors remained scattered throughout the mitotic subdivision of the EGL. Proliferating Bergmann glia were heavily stained and organized into layers 2–3 cells deep (Fig. 26F).

In addition to morphological criteria, the identity of the pERK-IR cells at early postnatal times (P4) was established by double-immunofluorescent staining for pERK and glia-specific GFAP or neuron-specific β-tubulin. On P4, these double-labeling studies confirmed that pERK was present in GFAP-positive Bergmann glia (Fig. 27A; inset white arrow) and in the large GFAP-negative (Fig. 27A; inset white arrowhead) β-tubulin expressing Purkinje cells (Fig. 2B; inset white arrowhead) and in the smaller granule cell neurons (Fig. 27B).

Postnatal days 5-8

Between P5 and 8, the density of immunopositive granule cells remained low (Fig. 28A). In contrast, the numeric density of immunopositive Purkinje cells was highest and the intensity of immunostaining was increased during this period (Figs. 27C–E and 28B). Compared to P4, immunostaining was less intense in proliferating Bergmann glia on P5 and P6; however, an increase in the density of immunopositive Bergmann glia clusters was observed on P6 (Fig. 28C). This increase in immunopositive Bergmann glia clusters was transient with decreasing densities of pERK immunopositive cell clusters detected from P8 until P22 (Fig. 28C).

Postnatal day 10

On P10, the density of immunopositive Purkinje cells was similar to that observed on P6 (Figs. 28B and 29A); however, a decreasing trend was detected. Similarly, a

consistently notable decrease in the intensity of staining was observed. The intracellular localization of pERK-IR was variable, with immunoreactivity in individual cells dispersed throughout the entire cytoplasm, confined to the apical portion of the cytoplasm in some cells, or restricted to the nucleus in others (Fig. 29A, A1). Co-expression of GFAP and pERK was evident in astrocytes in the deep IGL and corpus medullare (Fig. 29A, A2). On P10, the density of immunopositive granule cells increased (Fig. 28A).

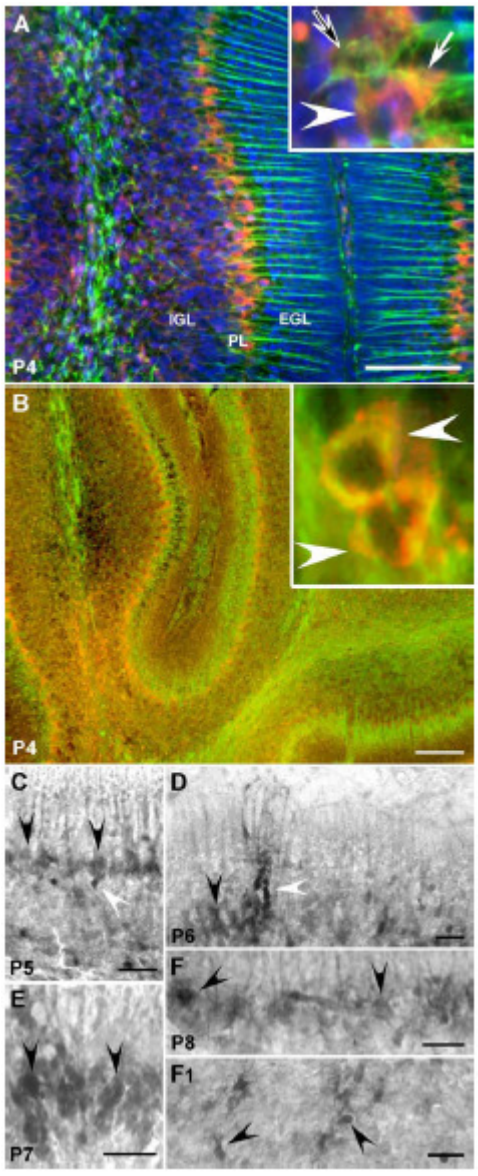

Figure 27. Immunolocalization of pERK in the developing cerebellum between P4 and P8. (**A**) At P4, numerous Bergmann glial cells were double-labeled for phospho-ERK (red) and glial fibrillary acidic protein (GFAP; green); cells immunopositive for both pERK and GFAP appear orange/yellow in the presented overlay of the individual red and green channels. Phospho-ERK-immunoreactivity (IR) was more intense in the Purkinje cell layer (PL) than in the internal granular layer (IGL), pERK-IR was not detected in mitotic granule cell precursors in the external germinal layer (EGL). Inset: black arrow-single labeled GFAP-IR Bergmann glial cell; white arrow—a Bergmann glial cell immunoreactive for pERK and GFAP; white arrowhead—a pERK-IR Purkinje cell. Cell nuclei were visualized with DAPI (blue). (**B**) Double labeling for pERK (red) and the neuronal marker β-tubulin (green) revealed that at P4, the vast majority of pERK-IR cells were neurons (yellow/orange). Inset: white arrowhead-double labeled Purkinje cell. (**C**) By P5, the number of pERK-IR Purkinje cells increased (black arrowheads). A row of scattered pERK-IR Bergmann glial cells was observed just beneath the PL (white arrowhead). (**D**) By P6, pERK-IR became more intense in Purkinje cells (black arrowhead). White arrowhead points to a pERK-IR Bergmann glia cluster. (**E**) At P7, Purkinje cell staining was substantially more intense (black arrowheads). (**F**) At P8, the number of immunoreactive Purkinje cells decreased, and the staining intensity in Purkinje cells fell to moderate levels (black arrowheads). Immunoreactive granule cells were scattered and mainly located in the IGL of the posterior lobe (**F**1, black arrowheads). Scale bars: (**A**–**B**) 100 μm; (**C**–**F**) 25 μm.

Immunostaining of granule cells at this time was characterized by a significant increase in moderate levels of homogeneous staining in the internal granular layer (IGL; Figs. 28A, 29A and 30A1) along with the appearance of scattered conglomerates of 5–10 intensely immunoreactive granule cells in the IGL (Fig. 30A and A1 inset). Clustered

rows of immunostained Bergmann glia, with pERK localized to the soma, were positioned between intervening Purkinje cells in groups of approximately 8–20 cells (data not shown).

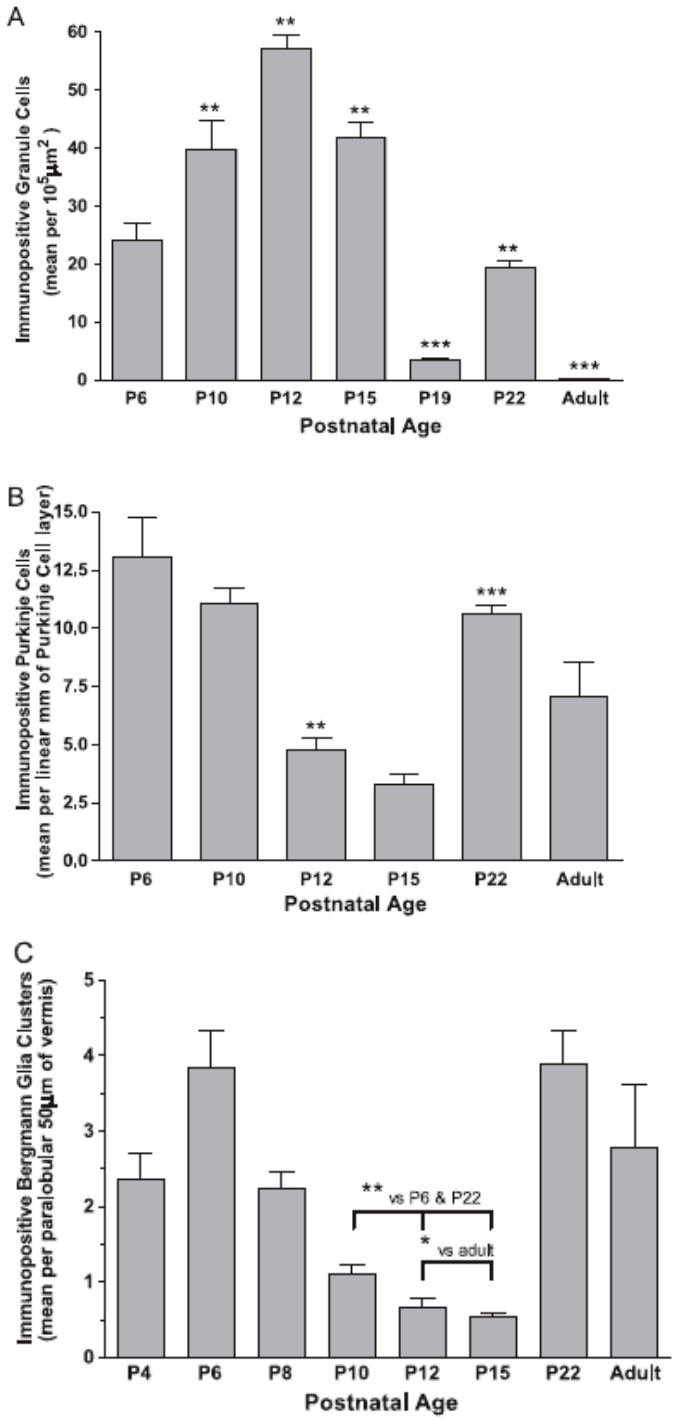

Figure 28. Quantitative immunohistochemical analysis of pERK during postnatal cerebellar development. Numerical values of immunopositive cell densities from the developing and mature cerebellum are graphically represented for (**A**) granule cells, (**B**) Purkinje cells, and (**C**) Bergmann glia clusters at indicated postnatal ages. Values presented are means ± S.E.M. from six different animals. For granule and Purkinje cells, the levels of significance for differences between values obtained for an age group and the preceding age group are indicated. For Bergmann glia cell clusters, levels of significance between paired groups are indicated above the bars. The level of statistical significance between groups is indicated as follows: *$p < 0.05$; **$p < 0.01$; ***$p < 0.001$.

Postnatal day 12

At P12, the density of pERK-IR Purkinje cells decreased further (Fig. 28B), and the intensity of staining became moderate to light. In contrast, the density of immunoreactive granule cells increased further, reaching the highest density observed (Fig. 28A). Intensely stained granule cells were located close to the corpus medullare with a gradient of decreased staining intensities in granule cells located closer to the Purkinje cell layer (Fig. 30B, B1). Nuclear pERK-IR was found in scattered Bergmann glia (Fig. 30D).

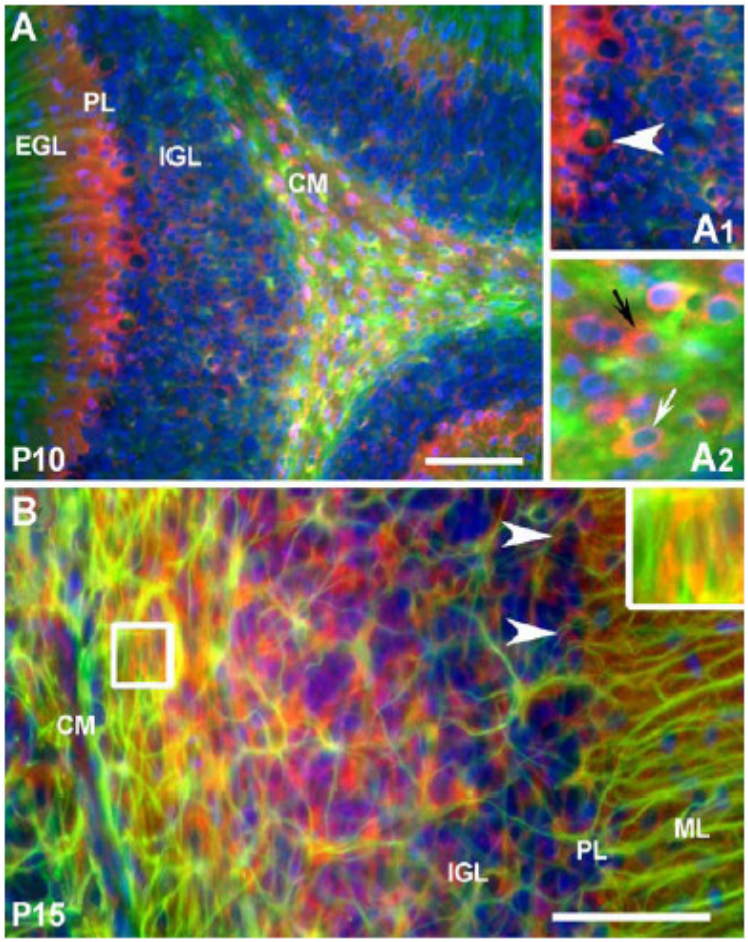

Figure 29. Cellular localization of pERK in the cerebellum at P10 and P15. (**A**) Double immunofluorescent labeling for pERK (red) and glial fibrillary acidic protein (green) in P10 cerebella: along with Purkinje cells (**A**1, white arrowhead) and neurons of the internal granular layer (IGL), numerous GFAP-immunoreactive (IR) astrocytes in the corpus medullare (CM), were pERK-IR (**A**2, white arrow), Numerous GFAP-negative, pERK-IR cells were also detected (**A**2, black arrow). Cell nuclei were stained with DAPI (blue). (**B**) Phospho-ERK-IR (red) was detected in GFAP-IR (green) astrocytes at P15 (inset; yellow/orange). At this time, the intensity of pERK-IR in Purkinje cells was decreased to just above background (white arrowheads); whereas in the IGL, both the number of pERK-IR cells and the intensity of their staining remained high. Scale bars represent 100 µm. PL: Purkinje cell layer; EGL: external germinal layer.

Postnatal day 15

In scattered Purkinje cells at P14–15, the basal portion of the cytoplasm was lightly stained. Immunoreactive Purkinje cell density was lowest among the age groups examined (Fig. 28B). The intensity of granule cell staining in the deep IGL was slightly decreased (Fig. 30C) and the density of pERK-IR granule cells at P15 decreased

significantly compared to P12 (Fig. 28A). By P16, only light to background levels of immunoreactivity was seen in the bulk of granule cell neurons; however, immunopositive granule cell conglomerates remained (Fig. 30D; arrowheads). As in other cell types at P15, pERK-IR astrocytes became less numerous (Fig. 28C) with moderate levels of pERK staining in most Bergmann glial cells, however, intense immunoreactivity was observed in both the somata and radial processes of Bergmann glial cell clusters (Fig. 30D, arrow). The density of Bergmann glia clusters was the lowest among all age groups examined (Fig. 28C).

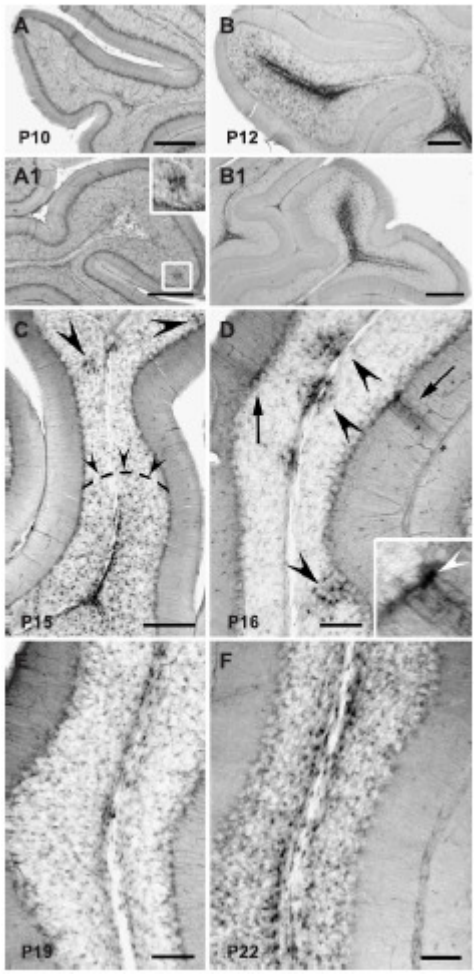

Figure 30. Distribution of pERK-immunoreactive (IR) cerebellar cells between P10 and P22. (**A**) At P10, only scattered pERK-IR cells were detected in the anterior lobe of the cerebellum. Immunoreactive granule cells were more numerous in the posterior lobe (**A**1); however, general staining intensity was low, with intense staining levels localized to granule cell conglomerates (**A**1, inset). (**B**) At P12, immunoreactive granule cells were homogenously distributed in the internal granular layer of the anterior (**B**) and posterior lobes (**B**1), as well as the central- and inferior lobes. A gradient of staining intensity was evident; cells located closer to the white matter were more intensely stained, with a progressive decrease in staining intensity in cells closer to the Purkinje cell layer. (**C**) Phospho-ERK-IR withdrew from the apical portion towards the stem of the foliae at P15 (small arrowheads), conglomerates of pERK-IR granule cells remained (large arrowheads). (**D**) By P16, granule cell pERK-IR was confined to cell conglomerates (arrowheads) and Bergmann glial cell clusters (arrow). Nuclear localized immunoreactivity was frequently detected in the Bergmann glia (inset, white arrowhead). (**E**) At P19, only scattered pERK-IR granule cells were detected in the internal granular layer. (**F**) At P22, a transient rise in the number of pERK-IR granule cells was observed. Scale bars: (**A**–**B**) 100 μm; (**C**–**F**) 200 μm.

Postnatal day 19

At P19, moderate pERK-IR was detected along the perikaryal plasma membrane and the basal portion of the cytoplasm in immunostained Purkinje cell groups (Fig. 30E). Within the IGL, only very light background staining was observed in homogeneously distributed granule cells (Fig. 30E). Overall, the immunopositive cell density was very

low (Fig. 28A) with infrequent scattered granule cell conglomerates showing more intense staining (not shown). In the radial processes of scattered solitarily immunopositive Bergmann glial cells that were positioned between Purkinje cells, the intensity of immunostaining was also decreased.

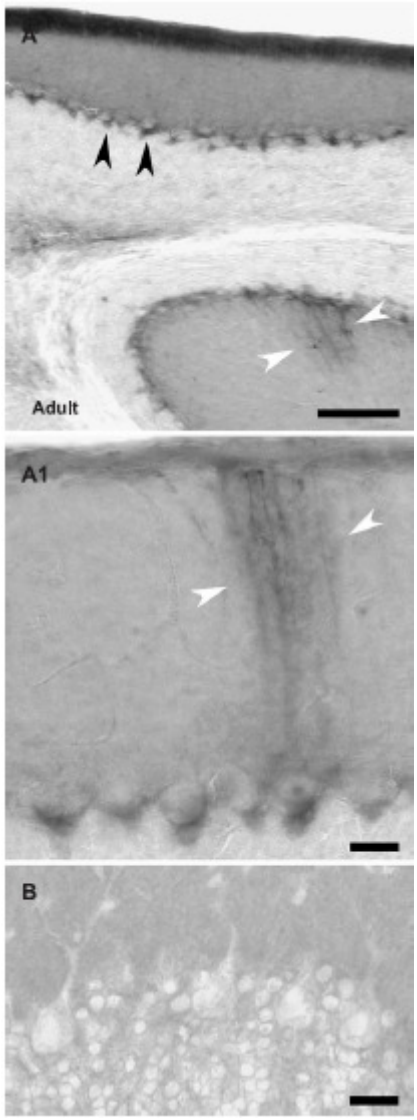

Figure 31. Immunolocalization of pERK in the mature cerebellum. As shown in representative low- (**A**) and high- (**A**1) magnification images of the cerebellum of adult rats, pERK-immunoreactivity was confined to the ventrolateral portion of the soma and the axon hillock area of Purkinje cells (black arrowheads) and the radial processes of scattered Bergmann glial clusters (white arrowheads). (**B**) Immunodepletion of primary antiserum with immunogenic phospho-ERK2 results in no specific immunostaining. Scale bars: (**A**) 100 µm; (**A**1, **B**) 20 µm.

Postnatal day 22-adult

On P22, pERK-IR granule cell density was significantly increased compared to the very low levels observed on P19 (Figs. 28A and 30F). Phospho-ERK immunostaining of granule cells was not detected in the mature cerebellum (Figs. 28A and 31). In Purkinje cells at P22 and in adults, pERK-IR was moderate in the apical regions of the cerebellar

foliae and confined to the basal portion of the cytoplasm and the neighboring axon hillock of immunopositive cells. Immunostaining was also detected in the soma and radial processes of Bergmann glia clusters. As observed for granule cells, a dramatic and significant increase in the density of immunopositive Purkinje cells and Bergmann glia clusters was observed at P22 (Fig. 28B-C). In the cerebella of adults, the staining pattern for Bergmann glia was comparable to that on P19, with moderate staining confined to the radial processes of scattered cell clusters (Fig. 31).

3c. *Identification of direct in vivo estrogen effects on the activation of cerebellar ERK1/2-activation: analysis of dose- and age-dependency.*

To determine whether E_2 could rapidly regulate ERK-signaling *in vivo*, a wide range of physiological and pharmacological concentrations of E_2 were directly injected into the cerebella of neonatal (P4 to P12) and adult rats. Following a brief exposure, the effects the treatment had on pERK-IR were determined by immunolocalization of activated ERK-IR and comparison of age-matched controls. In general, the individual variability of pERK-IR in cerebella of the untreated, mock and vehicle-injected control groups was greater than observed in cerebella treated with any concentration of E_2. On P4 and P6, E_2 exposure did not influence the observed normal pattern of pERK expression. On P8, the injection of 10^{-11} and 10^{-7} M E_2 resulted in increased pERK immunostaining in the IGL of the posterior cerebellar lobe that was most pronounced in folium IX (Fig. 32). Reminiscent of previous *in vitro* dose response studies (**22**), E_2 concentrations intermediate to 10^{-11} M and 10^{-7} M were less efficacious in stimulating ERK signaling, differing only slightly from vehicle-injected controls (e.g. Fig. 32C).

At P10, E_2 stimulated ERK1/2-phosphorylation in granule cells located in the IGL in all cerebellar lobes (Fig. 33). A bi-modal dose-response to E_2 was again observed, however, a reproducible decrease in potency was evident. At P10, 10^{-10} M and 10^{-6} M E_2 were the most efficacious in increasing the number of pERK-IR cells. In cerebella exposed to intermediate doses of E_2 (e.g. 10^{-9} M) the pattern and intensity of pERK immunostaining was comparable to vehicle-injected and un-injected controls. On P12, rather than stimulating ERK-signaling, E_2 decreased the number of pERK-IR cells in a bi-modal dose-specific fashion (Fig. 34). The decrease in pERK-IR was most apparent following injection of 10^{-6} M E_2.

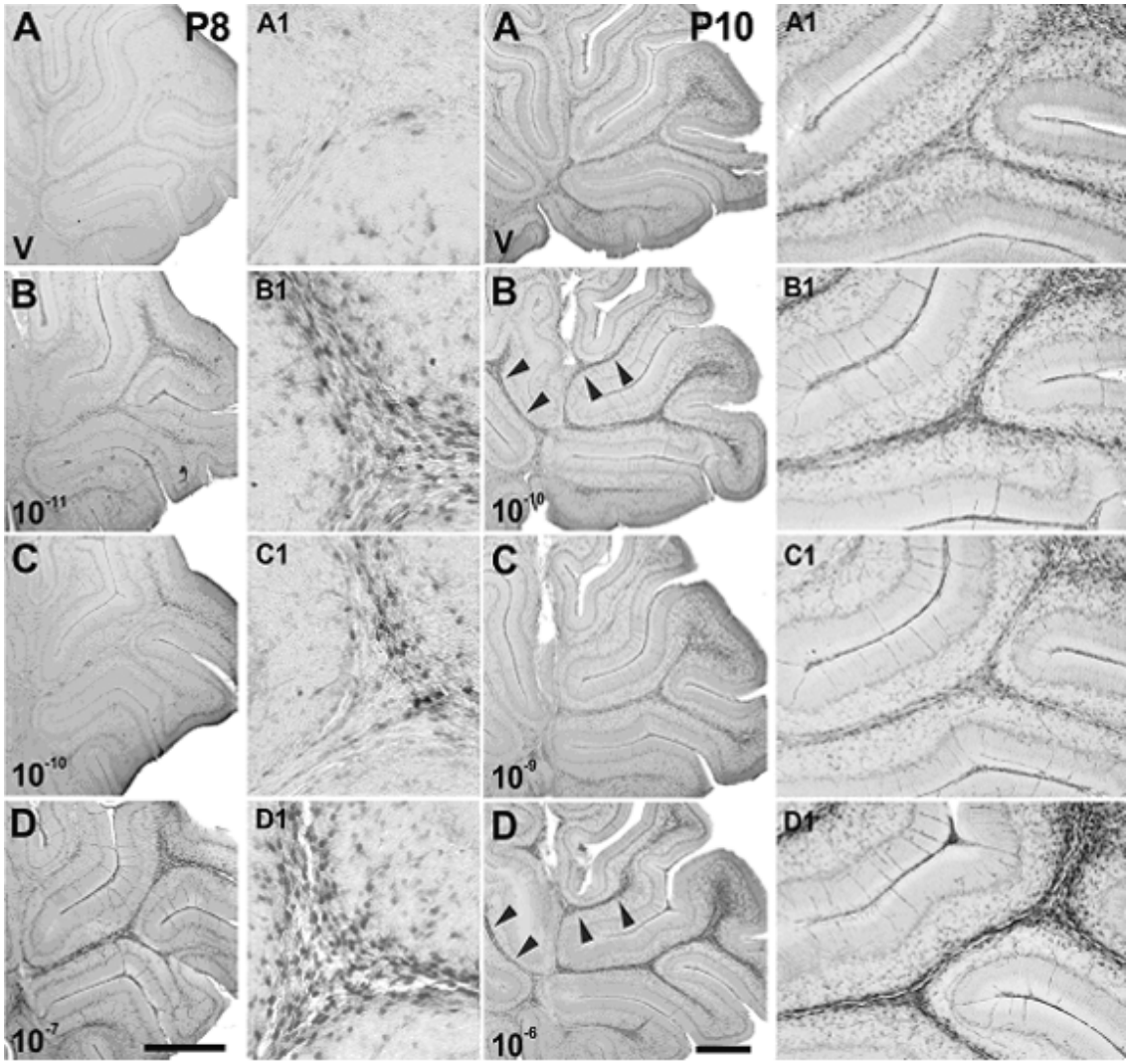

Figure 32. Dose-dependency of increased pERK-IR following estradiol injection on P8. Intracerebellar injection of 10^{-11}- **(B)** and 10^{-7} **(D)** M E_2 resulted a considerable increase in the number of pERK-IR cells compared to vehicle- (V) injected controls **(A)**; The increase in the number of immunoreactive cells occurred in both the internal granular layer and the corpus medullare of the posterior lobe. Lowest levels of pERK-IR were observed at 10^{-10} M E_2 **(C)**.

Figure 33. Dose-dependency of increased pERK-IR following estradiol injection on P10. Intracerebellar injection of 10^{-10}- **(B)** and 10^{-6} M **(D)** E_2 resulted in a robust increase in the number of pERK-IR cells. Cerebella injected with 10^{-9} M E_2 **(C)** did not differ noticeably from the vehicle injected controls **(A)**. The stimulatory effects of E_2 on ERK-phosphorylation were also seen in the proximal portion of the central and anterior lobes (arrowheads). It is of note that on P10 E_2 stimulated ERK-phosphorylation effects were right-shifted by an order of magnitude compared to P8, indicating a decrease in the sensitivity of cerebellar cells to E_2.

In contrast, 10^{-9} M E_2 was without effect as indicated by immunostaining patterns being similar to un-injected and vehicle-injected controls. However, as can be seen for 10^{-12} M E_2, exposure to lower concentration of E_2 also resulted in a marked decrease in the number of pERK-immunopositive cell numbers. In contrast to the overall reduction in the number of pERK-immunopositive cells, in scattered Golgi-like neurons at P12 E_2

stimulated ERK-signaling. In most of these Golgi-like neurons, nuclear pERK-IR was observed.

In adults, E_2-effects were limited to the injected folium. Exposure to 10^{-6} M (Fig. 35) and 10^{-10} M E_2 induced ERK-phosphorylation with highest potency in Golgi-like interneurons stellate-, basket- and Lugaro cells, in granule neurons, and in cells whose morphology and localization showed resemblance to the “globular” cells described by Laine and Axelrad (2002) (**52**), as well as in some granule cells. In most of the animals, E_2-injection eliminated pERK-IR from the 'ventrolateral' perikaryal region of Purkinje cells and their axon hillock in the vicinity of the injection site. Intermediate concentrations of E_2 (10^{-8}, 10^{-9} M) did not induce considerable ERK-activation.

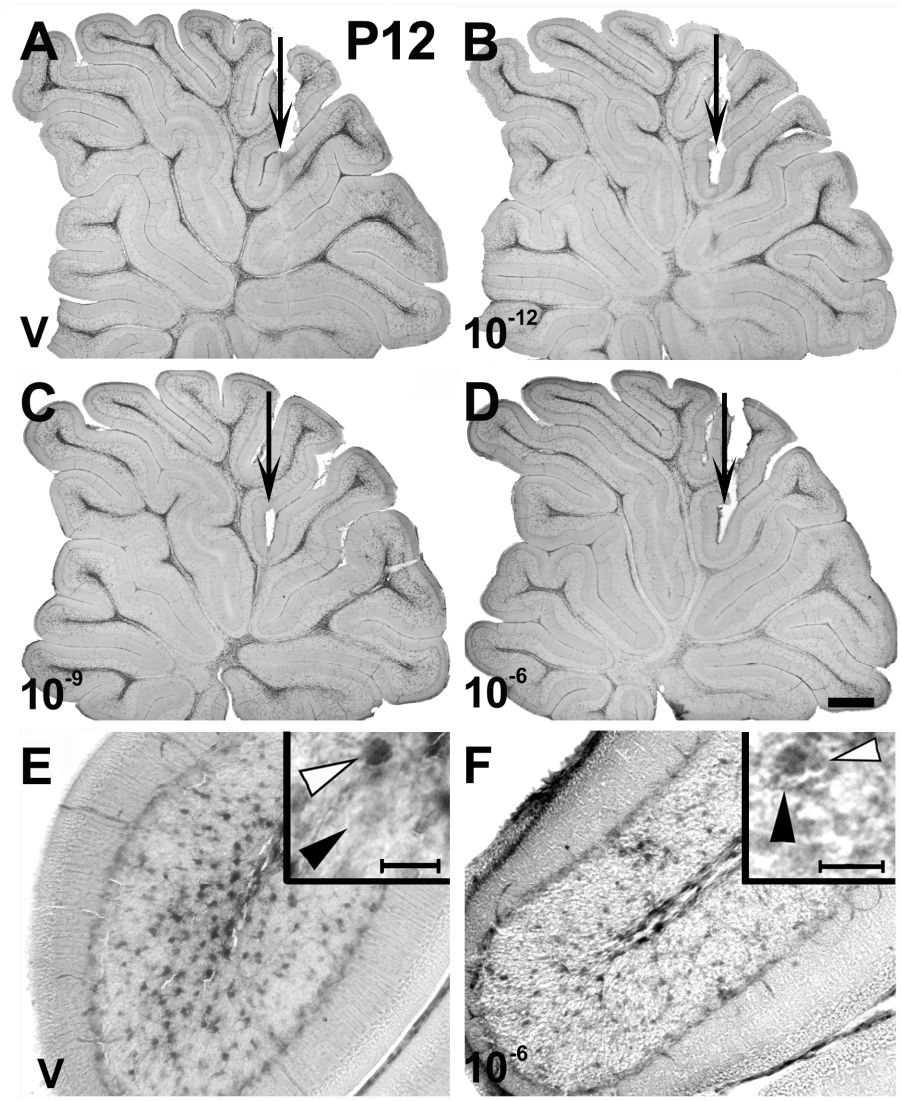

Figure 34. Effects of estradiol on cerebellar phospho-ERK1/2-immunoreactivity at P12. At P12, estradiol decreased the number of phospho-ERK1/2-immunoreactive (pERK1/2-IR) cells in all lobes of the cerebellum, in a dose-dependent fashion (A-D): while 10^{-12}- (B) and 10^{-6} M estradiol (D) substantially reduced the number of pERK1/2-IR cells, 10^{-9} M (C) did not have a noticeable effect, compared to the vehicle injected (V) controls (A). Arrows indicate the site of injection. Scale bar on panel D represents 500 µm. In the cerebella of control animals (E) phospho-ERK1/2-IR was detected in granule cells (inset, white arrowhead), but not in Golgi-like neurons (inset, black arrowhead). Injection of estradiol resulted in a decrease in the overall number of pERK1/2-IR cells (F), however, nuclear-localized phospho-ERK1/2-IR was detected in scattered granule cells (inset, white arrowhead), as well as Golgi-like neurons (inset, black arrowhead). Scale bars in insets represent 20 µm.

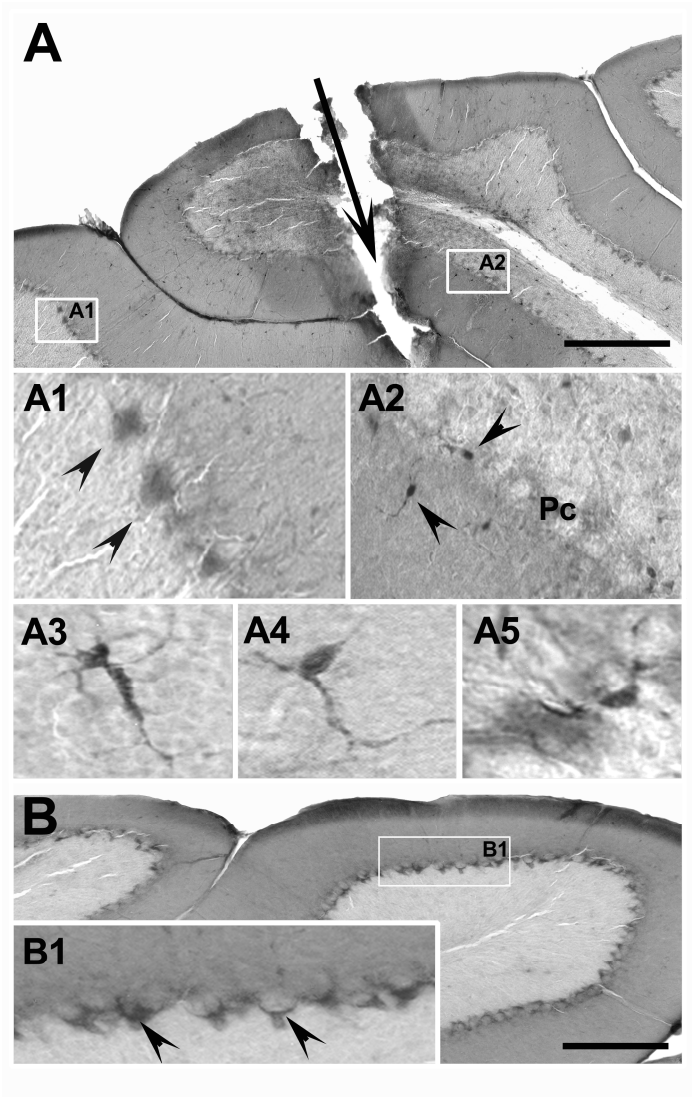

Figure 35. Effects of estradiol on ERK-phosphorylation in the mature cerebellum (**A**, **B**). In foliae not injected with E_2, as well in cerebella of control animals (**B**), phospho-ERK1/2-immunoreactivity was localized to the ventral portion of Purkinje cells (**A**1, **B**1, arrowheads). High (**A**) and low (10^{-10} M, not shown) concentrations of estradiol induced ERK-activation in various cell types (**A**2, arrowheads), including granule neurons, basket cells (**A**3), stellate cells (**A**4) and Lugaro cells (**A**5). Phospho-ERK1/2-IR in cerebella injected with 10^{-9} or 10^{-8} M estradiol did not considerably differ from controls (not shown).

Summary of results

In identifying the neurons of the neuroendocrine hypothalamus expressing various ionotropic AMPA-type glutamate receptors, we determined that there are two main neuronal populations in the arcuate nucleus: one under the direct influence of excitatory amino acid neurotransmission, and another one, a dopaminergig cell population that does not express such AMPA receptors.

We have demonstrated that E_2 induces a well-defined, characteristic pattern of changes in the synaptology of the neuroendocrine hypothalamus, and determined that it is a subset of the hypothalamic GABAergic neurons that undergoes EISP during the gonadotropin feedback.

In studying the molecular mechanisms that underlie the rapid cellular changes during the positive gonadotropin feedback, we provided evidence that the ERK1/2 MAPK signaling pathway is a likely candidate to mediate the rapid, non-genomic effects of estrogen. To exclude the masking effects of the 'de novo' estrogen synthesis, we gathered evidence in a non-neuroendocrine part of the brain, the cerebellum (the cerebellum does not express aromatase), and demonstrated that E_2 can rapidly modulate the activation of the ERK1/2 pathway. We have clearly distinguished rapid, non-genomic, and slow, ER-mediated cellular effects of E_2 in vitro; and demonstrated in vivo that E_2 rapidly modulates ERK-activation in a non-neuroendocrine part of the brain, where E_2-induced modulation of the ERK-pathway coincided in time with the time of synaptogenesis and synaptic maturation in the developing cerebellum. In the mature cerebellum E_2, by influencing the activation of the ERK-pathway, seems to directly affect the function of intrinsic cerebellar circuits and the regulation of the information-flow along these neuronal circuits.

DISCUSSION

1. *Identification and biochemical characterization of MBH neurons that are regulated by excitatory amino acid (EAA) neurotransmission.*

Anatomical background and functional considerations

Beta-endorphin (beta-END) neurons of the AN are known to be synaptic targets of the cell types that were subjects of the present investigation (**53, 54**), as well as of those acting through GABA neurotransmission (**55, 56**). The anatomical and functional integrity of these neuron populations form a complex circuit, regulating the biphasic GnRH secretion/release of normal cycling female rats via direct inhibitory action of beta-END cells on MPO GnRH neurons. The lack of E_2 and AMPA receptors within GnRH cells further reinforces the importance of this circuit. The role of AN GAL and NPY neurons in the regulation of GnRH release is well described. Intracerebroventricular application of GAL or NPY readily augmented LH release in ovariectomized, E_2-primed rats (**57**). In addition, Horvath et al., 1995 (**54**) demonstrated that GAL neurons located in the AN terminate on local beta-END cells and exhibit asymmetric membrane specializations. It is also known that NPY neurons of undefined origin – but suggested to be located, at least partially, within the AN – also terminate on beta-END cells (**53**), as well as on GAL- (**58**) and TH-IR (**59**) neurons. Since dopaminergic neurons establish inhibitory synapses on beta-END cells and a substantial number of NPY neurons are known to contain GABA, NPY cells are suggested to have both excitatory and inhibitory effects on beta-END neurons of the AN.

The widespread distribution of aspartate/glutamatergic axon terminals, together with the fact that they terminate on dendrites and cell bodies of AN neurons (**60**), strongly implies that the EAA innervation of the AN is involved in the regulation of pituitary Gn release. This has been further supported by the physiological finding that glutamate injection into the third ventricle readily increases the plasma LH level, but does not affect the FSH level (**61**), indicating that the site of glutamate action is outside the pituitary.

AMPA receptor content of GAL and NPY neurons

We consider the AMPA receptor content of a cell to be an indicator of aspartate/glutamatergic innervation. GAL and NPY neurons of the AN form excitatory synapses on beta-END neurons, thus facilitating their direct inhibitory effect on MPO GnRH-producing neurons. However, this thinking would lead to the conclusion that since these (GAL, NPY) neurons contain AMPA receptors, their EAA innervation would further strengthen the inhibition of GnRH secretion. This speculation is in contradiction to the finding by Olney et al., 1976 (**61**) that glutamate effectively increases LH when injected into the third ventricle. The anatomical pattern of connectivity between beta-END neurons and GAL, NPY, GABA and dopaminergic cells, as well as the extent of the AMPA receptor content of these neurons, may help explain this paradox. As mentioned above, NPY neurons innervate not only beta-END cells (either directly or indirectly), but they also terminate on dopaminergic neurons that have inhibitory nerve terminals on beta-END cells. In addition, our previous work demonstrated that approximately one-third of the AN NPY neurons are GABAergic (**62**). This versatility on the part of the NPY neurons could be of great significance since it not only helps to understand the contradictory effects of NPY cells, but implicates that they can both excite and inhibit beta-END neurons and, hence, GnRH release. Our present results showing that the vast majority of AN NPY neurons contain AMPA receptors indicate that a uniform EAA system may up-regulate the influence of the examined cell populations on beta-END cells, as well as the function of beta-END cells, themselves, since they also contain AMPA receptors.

A look at the mechanism by which AMPA receptor containing neurons respond to incoming stimuli has placed further significance on our present findings. Activation of such ionotropic receptors leads directly to the opening of ion channels that are typified by their different permeability to Na, K and Ca ions. GluR1 and -3 are known to open calcium (Ca) channels, allowing an influx of Ca into the cell, whereas GluR2 blocks the Ca-permeability of the neuronal plasma membrane. Thus, AMPA receptors substantially affect the dynamic changes of the cytosolic Ca-concentration. However, to the best of our knowledge, there are no data regarding the relationship between cytosolic Ca events of AN neuropeptide-containing cells and GnRH regulation. In the absence of such information, the findings of Garthwaite et al., 1992 (**63**) could shed

some light on the topic. They demonstrated that different cell types of surviving brain slices incubated in Ca-free medium generated whorl-like cytoplasmic inclusion bodies from their rough endoplasmic reticulum, as a response to Ca deprivation, and these inclusions disappeared when Ca was replenished to the incubation medium. These whorl bodies looked similar to those developing in ovariectomized rat and primate AN (**64, 65**). The in vitro study of Rizzuto et al., 1998 (**66**) demonstrated that changes in cytosolic Ca-concentration are strongly related to morphological alterations of endoplasmic reticulum, thus confirming the causal connection between intracellular Ca events and the generation of whorl-like inclusion bodies. Along this line, it can be speculated that if the appearance of whorl bodies is based on the lack of cytosolic Ca, then a prolonged lack of AMPA receptor activation might be the cause of the development of hypothalamic whorl bodies. Because the examined AMPA receptor-containing cell types [beta-END (unpublished), GAL and NPY] are known to be E_2-responsive and E_2 has been demonstrated to have a stimulatory effect on hypothalamic AMPA expression (**67**), it is possible that the absence of constant levels of E_2 decreases or, for shorter time periods, abolishes the activity of AMPA receptors within these cells. In the present experiment, we did not observe a co-localization of TH with AMPA receptors. This indicates that the dopaminergic cell population of the AN is not directly influenced by the glutamatergic system. The exact mechanism by which the aspartate/glutamatergic system affects the AN circuit is not known. The presence of AMPA receptors in both inhibitory and excitatory neurons that are E_2-responsive, in conjunction with the idea that E_2 increases AMPA-expression, raises the question of whether the aspartate/glutamatergic axon terminals that target AN cells are, in some way, responsible for the negative feedback-controlled baseline regulation of Gn secretion. On the other hand, the lack of AMPA receptors in dopaminergic AN neurons that (unlike the EAA terminals) are known to make symmetric type contacts with their target cells (for example beta-END cells) suggests that these TH-IR neurons may act in direct contrast to the EAA system; thus, they might be involved in the positive feedback-based preovulatory LH surge.

Taken together, the present study provides evidence for the previous proposal that the EAA neurotransmission, at the level of the AN, is highly involved in the complex regulation of GnRH. Our results also show that there are at least two populations of neurons within the AN, one of which (most of the neuropeptide-containing neurons) is

under an aspartate/glutamatergic "supervision," while the other (dopaminergic neurons) is not.

2. *Determination and analysis of estrogen-induced synaptic plasticity (EISP) in the primate and rat arcuate nucleus (AN).*

2a. *Identification of neurons undergoing EISP*

The median eminence is one of the areas of the CNS which has fenestrated capillaries, i.e. disrupted blood–brain barrier. This makes possible the bidirectional movement of polar molecules between the hemal and neural milieu. Therefore, the intraperitoneally applied FG is taken up by the axon terminals in the median eminence and results in the retrograde labeling of neurons projecting to this area. In such a way, we are able to label selectively a well-defined population of arcuate neurons and our results demonstrate that retrogradely labeled cells are distributed throughout the entire nucleus as shown previously (**68**). It was intriguing to find that E_2-induced synaptic reorganization was present on these neuroendocrine cells, suggesting a role for EISP in the regulation of anterior pituitary hormone secretion.

It is generally accepted that gonadal hormones have both organizational and activational effects on the nervous system (**69**). At certain well-defined time points during the fetal–neonatal period, the hormonal milieu determines the direction of the differentiation of neuronal networks, which, in turn, leads to structural sexual dimorphism (**70, 71**). This dimorphism exists at many morphological levels, such as the volume of different nuclei, neuron number, dendritic length and structure, synapse number and neuronal membrane organization (**72-75**).

Recent studies have shown that the effect of gonadal steroids is not limited to early developmental stages. Several authors report on neuro-glial plastic changes and synaptic remodeling that is linked to the hormonal variations during the ovarian cycle (**76**). Experiments on ovariectomized and hormone-treated animals indicate that E_2 plays a key role in these plastic processes. It has been demonstrated that E_2 is involved in determining dendrite- and axon length and their branching patterns in specific areas of the CNS. In the ventromedial hypothalamic nucleus and in hippocampal pyramidal cells, E_2 increases the dendritic spine density (**77, 78**). In the magnocellular nuclei, the

activity-induced changes in synaptic connectivity are connected to the astrocytic changes, indicating that both components are involved in the phenomenon (**79**). Concerning hormone-induced synaptic remodeling, one of the best-studied systems is the arcuate nucleus. Data obtained thus far clearly indicate that there is an E_2-dependent cyclic change in the number of axo-somatic synapses and it has also been demonstrated that the GABAergic nerve terminals are involved (**80**). Additionally, solid information has been gathered on the cellular and molecular mechanisms of the effect of E_2 and the physiological importance of the phenomenon (**81**).

The retrograde labeling used in the present experiments identifies those neurons that terminate on portal capillaries of the median eminence. Concerning the neurochemical nature of this subpopulation, we do not have any direct evidence, only the anatomical localization may provide some information. As mentioned earlier, the ventrolateral part of the nucleus was excluded from the measurements, because of the low number of FG-containing neurons. The selected area is rich in non-neuroendocrine NPY neurons, but earlier studies have also shown the presence of DAergic cells. With the application of the combined pre- and postembedding immunostaining by using different antisera will certainly provide more information on the neurons which are involved in EISP.

On the basis of the present data, we conclude that the synaptic connectivity of these "hypophysiotropic neurons" is different from the other, non-labeled population, and their response to estradiol is not uniform. Neurons that project to the median eminence receive less axo-somatic input than neurons which have no connections with this area. On the other hand, the results of the present study clearly indicate that the effect of E_2 is specific, i.e., not all arcuate neurons are affected by the structural synaptic remodeling, but only those that are FG labeled. Worthy of note is that E_2 induces an opposite effect (increase) on the number of axodendritic synapses (**82**). These observations together with the electrophysiological data support the notion that the hormonally induced plastic changes may serve as the morphological basis for the cyclic regulation of the anterior pituitary.

2b. *Determination of the number of synaptic connections on gonadotrop hormone-releasing hormone- (GnRH) and other neurons in the AN of ovariectomized versus ovariectomized plus estrogen-treated monkeys.*

A previous study reported that estradiol valerate treatment resulted in a 61% decrease in the number of axosomatic synapses within the arcuate nucleus of the African green monkey (**12**). That finding was somewhat surprising considering the former description of Witkin et al., 1991 (**44**), who found that E_2-replacement in OVX rhesus monkeys leads to an increase of synaptic inputs on arcuate nucleus GnRH neurones. Due to the very different experimental conditions applied in those studies, it is difficult to draw a correlation between the two reports. In the present experiment, we attempted to determine the E_2-regulated temporal pattern of changes in inhibitory/excitatory synaptic inputs on GnRH cells of the primate arcuate nucleus. In addition, we also characterized the synaptic events on non-GnRH neurons located in close proximity to the GnRH cells.

That we were unable to find axosomatic synapses of any kind on GnRH neurons in OVX monkeys, together with the observation that they were massively surrounded by glial processes, corresponds well with Witkin's description. Our finding that estradiol benzoate day 1 monkeys exhibit a high number of synaptic contacts on GnRH cells further supports their results. However, we also found that synaptic counts on non-GnRH neurons substantially decrease within 24 h, in response to E_2-treatment. In further support of earlier finding (**12**), averaged synaptic numbers of estradiol benzoate-treated monkeys showed a decrease of 43.3% between days 1 and 8 after estradiol benzoate-treatment.

The temporal changes in the synaptic status of GnRH- and non-GnRH cells show an opposite tendency in their fluctuation. This suggests that non-GnRH neurons in close proximity to GnRH cells may be involved in the regulation of synaptic events on the latter and, thus, on GnRH-release. However, it is also possible that an E_2-responsive neuronal system other than the one studied here may differentially affect synaptic plasticity on arcuate nucleus GnRH-and non-GnRH cells.

The differential synaptic assessment revealed that from the start of the E_2 surge until the restoration of baseline concentrations of plasma E_2, both GnRH- and non-GnRH neurons are under the dominance of an inhibitory afferentation. However, in estradiol benzoate day 8 monkeys, in which blood E_2 returned to physiological baseline

concentrations, the inhibitory and excitatory synaptic numbers on non-GnRH cells became well balanced, while the inputs on GnRH cells remained predominantly inhibitory. Although we do not know the reason for this, it seems to be in agreement with the literature. For example, on the basis of both in vitro and in vivo studies, it is believed that GnRH cells of rodents are capable of a pulsatile GnRH secretion/release on their own (**83-86**), and the same is true in primates (**87-89**). High concentrations of blood LH, in the absence of measurable amounts of E_2, underlies this idea. It is worthy of note that under in vitro conditions (cell culture of purified GnRH neurons), GnRH neurons lack non-GnRH-derived synaptic input, which makes their synaptological status analogous to that of the OVX animals. In turn, it is also known that under physiological conditions - when a certain baseline plasma E_2 concentration is always detectable - the pulsatile GnRH release appears to be concealed/suppressed by an E_2-dependent negative feedback regulation (**90-94**). This is in agreement with the finding that GnRH cells of estradiol benzoate day 8 monkeys are under a predominantly inhibitory innervation.

Although our present results reveal temporal events of E_2-regulated synaptic plasticity from 24 h to 8 days after E_2-treatment, our assessments do not cover the synaptic changes of the first 24 h of the treatment, which coincides in time with the major hypothalamic events of the positive feedback-regulated GnRH surge. Therefore, from the synaptic values of OVX and estradiol benzoate day 1 monkeys, we can only infer that the rapid elevation of blood E_2 concentration from its previously un-measurable level evokes a drastic increase in the innervation of GnRH cells. Our finding that the synaptic events throughout the examined period of time display a continuous dominance of inhibitory innervation raises the need for further immunohistochemical characterization of the inhibitory afferentation of GnRH-and other neurons of the arcuate nucleus.

2c. *Determination of the number of synaptic connections on glutamic-acid-decarboxylase-immunoreactive (GAD-IR) inhibitory GABAergic neurons in the AN of monkeys.*

In the present study, we hypothesized that E_2 regulates GnRH-biosynthesis/release via the modulation of synaptic input/balance directly on GnRH neurons and probably on arcuate putative GABA (P-GABA) cells, as well.

As a main goal of our study, we wanted to know how blood E_2 concentrations correlate with the present synaptic counts and, in turn, how they relate to LH levels. On the one hand, we found that in general, synaptic counts on GnRH neurons follow the changes in blood E_2 levels. On the other hand, a similarity between the time-dependent changes in synaptic counts on P-GABA cells and those in blood LH levels could be observed. These findings imply that E_2 regulates the synaptic pattern on the examined cell types. However, such correlations (between synapse numbers on P-GABA cells and blood LH on one hand; between those on GnRH cells and blood E_2 on the other hand) make our data unconventional and conflicting. It has been previously described that the majority of mediobasal hypothalamic GABAergic neurons possess estrogen receptors (**95**), and that the vast majority of hypothalamic GABAergic axon terminals are of local (AN) origin (**45**). Therefore, it is likely that the parent neurons of the GAD-IR terminals that synapse with the GnRH cells are E_2-responsive, local GABAergic cells. The highly E_2-responsive reaction of GAD-IR axon terminals on GnRH neurons underlies the idea that they play an important role in the synaptic regulation of the latter. However, the comparison of pure values of synaptic counts does not seem to explain the mechanism by which this regulation is manifested. It is generally believed that the synaptic activity of a neuron depends upon the actual balance of its inhibitory and excitatory afferentation. Therefore, we sought to determine the synaptic status of examined neurons by establishing the concept of the "synaptic balance" value (ratio of inhibitory/excitatory synapses on examined cells). The comparison of these values revealed that the synaptic balance values of P-GABA neurons follow the changes seen in blood E_2-levels, while the temporal changes in the synaptic balance values of GnRH cells is more closely associated with the pattern shown by blood LH. This approach better explains the functional relationship between the E_2-levels and the synaptological status of AN P-GABA neurons, as it does between the synaptic balance values of GnRH

cells and the blood LH concentrations. Therefore, the present results suggest that circulating blood E_2 regulates the synaptic status of AN GABAergic cells and also, in some way, that of GnRH neurons which, in turn, controls the actual concentration of blood LH.

Due to the scope of the present experiment, the anatomical relationship between the examined P-GABA and GnRH cells remains unknown. However, the comparison of synaptic status (synaptic balance values) of these two cell types ([P-GABA inhibitory/excitatory]/[GnRH inhibitory/excitatory]) may indicate a possible functional relationship between them that may represent one link in the regulation of blood LH concentrations. While we understand that these values have their limitation in that we can only imply a possible functional and/or morphological relationship between the GnRH and P-GABA cells, their temporal changes resemble those seen in blood E_2-levels, and therefore, suggests that at least a portion of the P-GABA cells of the AN (while being under an E_2-regulated innervation) may be directly involved in the synaptic control of GnRH neurons of the same area.

Taken together, our present results show that E_2 induces synaptic plasticity on both GnRH- and P-GABA neurons within the AN of the female monkey and suggests that GABA cells of the AN, at least in part, are directly involved in the E_2-dependent synaptic control of GnRH neurons.

3. *Identification and characterization of rapid, non-genomic estrogen effects on non-neuroendocrine neurons: estrogen-induced rapid modulation of the extracellularly regulated kinases 1 and 2 (ERK1/2) MAPK- (mitogen-activated protein kinase) pathway in the cerebellum.*

3a. *Determination of rapid estrogen effects in primary neuronal cell cultures.*

The present study provides data indicating that 17β-E_2, 17α-E_2, and the ER antagonist ICI182,780 activate ERK1/2 MAPK signaling in developing and mature cerebellar neurons. The dose–response characteristics for each estrogen-like compound were hormetic (**96**), as indicated by an inverted U-shaped dose–response curve with low-concentration agonist effects and antagonist-like or no effects at higher concentrations. For 17β-E_2, ERK1/2 phosphorylation was increased significantly at low physiological

concentrations; this stimulation was lost between 1 and 10 nM and observed again at pharmacological concentrations.

The bimodal nature of the effects observed at physiological and again at supraphysiological E_2 concentrations may be mediated via different mechanisms. At 10^{-8} M 17β-E_2, a concentration often considered experimentally physiological, no significant stimulation of ERK1/2 signaling was observed as a result of a high frequency in failure to respond. This increased variability likely resulted from 10^{-8} M E_2 inducing effects intermediate to physiological dose inhibition and supraphysiological dose activation. The most efficacious concentrations (10^{-11} to 10^{-10} M) correspond closely with the bioavailable concentration of free E_2 in the neonatal rat brain (**97**). Thus in regions of the neonatal rat brain not expressing aromatase (**98**), 10^{-11} M may reflect the physiological concentration of free estradiol.

Temporal analysis indicated that E_2 activates ERK1/2 in a rapid and transient manner reminiscent of EGF-mediated ERK1/2 signaling in PC12 cells (**99**). As in PC12 cells this transient increase in ERK phosphorylation may arise from formation of the short-lived scaffolding protein complexes necessary for MAPK activation (**100**). Alternatively, transient activation may result from PKA-mediated negative feedback regulation of Raf activity (**101**). Although further investigation into the mechanism of rapid E_2-induced ERK signaling is necessary, it is clear that, in studies lacking a well characterized dose–response curve and/or time course analyses, the potential for misinterpretation of false-negative results is high.

The ability of E_2 to increase ERK signaling in cerebellar neurons contrasts with previous studies reporting that 10 nM E_2 could not stimulate ERK1/2 phosphorylation in organotypic cerebellar cultures (**102-103**). These differences may have resulted from differences in the steroid and neurotrophic stimulation received during culture. Alternatively, a failure to respond to 10 nM E_2 is consistent with our observed variable responsiveness at this concentration. Because of the rapid and transient nature of the response, slow or unequal exposure of cells may be especially problematic in organotypic cultures in which close cell–cell interactions may induce barriers to rapid diffusion.

The estrogen receptor antagonist ICI182,780 is a 7α-alkylamide analog of 17β-E_2, consisting of a central estradiol moiety with a long side chain extending from C7 (**104-**

106). With binding in the ligand-binding domain, the 7α side chain of ICI182,780 influences the conformation of helix 12 to block AF2 function (**107-109**). Micromolar concentrations of this transactivational antagonist often have been used to discriminate whether or not rapid estrogen actions are mediated via a classical ER. However, if rapid effects are ER-mediated, the conformational changes required to stimulate ERK signaling may differ from those involved with AF2 transactivation. The effects of ICI182,780 binding at a distinct class of ERs that mediate rapid E_2 actions are not known. In either case there is no a priori reason for ICI182,780 binding to induce conformational effects that block rapid signaling mechanisms.

The finding that ICI182,780 is a highly efficacious agonist of ERK1/2 phosphorylation in cerebellar neurons is especially significant. Because dose-dependent hormetic inhibition was observed at the high concentrations of ICI182,780 used experimentally, the ability of ICI182,780 to block rapid E_2 effects may only mimic true ER antagonism. Further, ICI182,780 blockade often is assessed after a pretreatment period; this pre-exposure could result in the examination of endpoints at times long after a transient response. Thus hormetic high-dose inhibition and/or desensitization after pretreatment, rather than competitive inhibition, may explain the variable ability of ICI182,780 to block rapid E_2 actions in other experimental systems (**110-112**).

Depending on the duration of exposure, E_2 can impose contrasting effects on mitogenesis and viability in granule cell neuroblasts. Chronic exposure to E_2 was anti-mitotic, yet an increase in viable granule cell number was observed. Those results suggest that chronic E_2 exposure can induce neuroprotective mechanisms that compensate for the anti-mitotic effects. In contrast, pulsed E_2 treatments significantly increased mitogenesis but caused a decrease in viable granule cell numbers. These results suggest that pulsed E_2 exposure increases granule cell death but increases mitogenesis in granule cell neuroblasts that are refractory to E_2 toxicity. The neuroprotective or neurotoxic effects resulting from chronic or pulsed estrogen treatment differed in ERK1/2 dependency. Decreased granule cell viability after pulsed E_2 treatments was MAPK-dependent, whereas the neuroprotective effects of chronic E_2 exposure were MAPK-independent. Interestingly, in this one model system the same concentration of E_2 can induce either neuroprotection or neurotoxicity, depending only on the duration of exposure. These opposing effects may underlie fundamental

differences between the mechanisms that control longer-term ER-mediated transcriptional effects and those that are involved in rapid intracellular signaling. These differences may have important relevance to the normal fluctuations in hormone concentrations that occur in vivo during development and in adults.

The neuroprotective actions of E_2 that have been observed here likely involve ER-mediated transactivation, as suggested by these effects being MAPK-independent and requiring longer exposure periods. The longer times necessary for the implementation of these protective effects suggest that ER-mediated expression of E_2-responsive genes may be required. In contrast, the neurotoxicity of pulsed E_2 exposures may not rely on ER transcriptional activities. The pulsed treatment constitutes a very short exposure time, a treatment protocol designed to elicit primarily E_2-induced rapid effects. Consistent with a central role for E_2-stimulated ERK1/2 signaling in these effects was the finding that a blockade of MEK–ERK signaling inhibited E_2 neurotoxicity. Because ICI182,780 inhibits ER-mediated transactivation, the fact that ICI182,780 treatment mimicked E_2 neurotoxicity suggests further that a mechanism independent of ER transactivation is involved. Because viability and cellular permeability of mature granule cells was not impacted by pulsed or continuous exposure to any concentration of E_2 that was tested, it appears that only immature granule cells are sensitive to the mitogenic and neurotoxic actions of estradiol.

Because the neuroprotective actions of E_2 are well documented (**113-118**), we chose to focus our studies on understanding in more detail the mechanisms of low-dose E_2 neurotoxicity. During cerebellar development, granule cell death occurs as a fundamental biological process to eliminate excess cells. On the basis of morphological and biochemical characteristics, cell death mechanisms can be divided into two major types: oncosis/necrosis and apoptosis (**49, 119**). The loss of plasma membrane integrity is a hallmark of oncotic cell death; permeability of PI and LDH release are sensitive indicators of compromised plasma membrane integrity. Increased numbers of PI-stained cells were observed 3–24 hr after pulsed E_2 exposure, and LDH release was increased 24 hr after treatment. However, increased granule cell permeability was not detected at 48–72 hr after treatment, a time that coincides with significant increases in granule cell numbers and mitogenesis. Similar to direct cell-counting results, LDH release was dependent on ERK1/2 signaling, but was not blocked by ICI182,780, suggesting that

classical E_2-responsive gene expression was not involved. Brief exposures to ICI182,780 alone increased LDH release, suggesting that ICI182,780-induced activation of MAPK results in E_2-like neurotoxicity. Because E_2 exposures did not increase caspase-3 activity significantly and inhibition of caspase activity did not block E_2-induced effects, E_2 neurotoxicity in immature granule cells was not classically apoptotic. These results are consistent with our Western blotting studies, which indicate that E_2 treatment does not influence pro-apoptotic JNK1/2 or p38 MAPK signaling. A summary of potential E_2-induced rapid mechanisms is presented in figure 36.

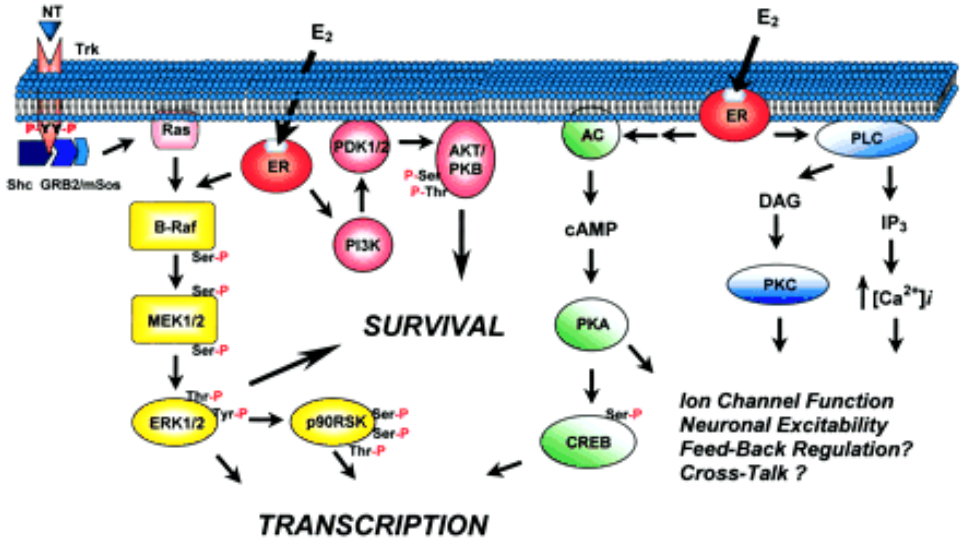

Figure 36. Schematic representation of the rapid mechanisms activated by estrogen in the brain. E_2 acts at estrogen receptor ER binding sites either near or associated with the plasma membrane to modulate the activity of multiple signal transduction cascades. The MAPK pathway, which is normally activated by binding of neurotrophins (NT) at their cognate receptor tyrosine kinases (Trk), can also be activated by E_2, resulting in the subsequent phosphorylation and activation of the MAPK kinase kinase B-Raf, the MAPK kinase MEK1/2, and the ERK1/2. Activated ERK1/2 can alter gene expression by phosphorylation of a specific set of transcription factors or by the phosphorylation of the 90-kDa ribosomal S6 kinase (p90RSK). E_2 also modulates the Akt/protein kinase B (AKT/PKB) pathway through activation of phosphatidylinositol-3 kinase (PI3K) that converts phosphatidylinositol 4,5-bisphosphate [PtdIns(4,5)P_2] to PtdIns(3,4,5)P_3 leading to activation of the phosphoinositide-dependent kinase (PDK1/2) that subsequently activates AKT/PKB, which results in increased cell survival. Additionally, E_2 can activate phospholipase C (PLC), which hydrolyzes PtdIns(4,5)P_2 to generate Ins(1,4,5)P_3 (IP_3) and diacylglycerol, leading to the release of Ca^{2+} from intracellular stores and the activation of protein kinase C (PKC). The ER mediates activation of adenylate cyclase (AC) and results in the cAMP-dependent activation of PKA, leading to phosphorylation and activation of the CREB, which then alters gene expression by binding at CRE. The AC and PLC pathways can also alter neuronal excitability by PKA or PKC phosphorylating specific ion channels to modulate their function. The actions of these pathways are also likely to interact with, and modulate other rapid E_2-activated signaling pathways. AKT, cellular homolog of the *v-akt* oncogene; GRB2, growth factor receptor-bound protein 2; Shc, SH_2-containing collagen-related proteins; mSos, mammalian homolog of Son of sevenless guanine nucleotide exchange factor.

Increased calpain activity and a lack of increased caspase activity during cell death are other distinguishing features of oncotic/necrotic cell death. Calpains are Ca^{2+}-dependent neutral proteases that participate in essential and pathological cellular functions (**120-121**). The blockade of E_2-induced LDH release by the calpain inhibitor PD150606 suggests that oncotic cell death is induced in a subset of developing cerebellar neurons. Although calpain inhibitors are cytoprotective (**122**) and calpains act to weaken the cytoskeleton before cell lysis (**120**), the mechanism of E_2-mediated ERK activation of calpains is unknown. In other systems EGF receptor activation of ERK1/2 results in increased intracellular calcium concentrations as a prerequisite for calpain activation (**123, 124**), whereas ERK1/2 activity also has been proposed to enhance calpain activity via a PKA-dependent mechanism (**125**). Although the mechanism through which E_2-stimulated ERK signaling induces calpain-dependent oncotic granule cell death is unknown, these mechanisms normally may function to regulate mature cerebellar neuron numbers and may have important implications in understanding the action of xenoestrogens and phytoestrogens in the developing brain.

The results presented here may lend insight to the role of E_2 in the developing cerebellum and potentially other brain regions. Developing neurons may respond to changing E_2 levels via rapid mechanisms to regulate the numbers of neurons by removing those neuroblasts that remain sensitive because of improper synaptic connections or that have not received appropriate biochemical signals. The subpopulations of neuroblasts refractory to the estrogenic insult may undergo further mitogenesis and subsequently continue along their developmental pathways. In more mature cells, E_2 exposure then may become neuroprotective and aid cellular survival during the developmental progression. Thus E_2 may play numerous and sometimes opposing roles in developing and mature neurons that could be a direct consequence of the ability of this steroid hormone to elicit ER-mediated changes in gene expression and to alter intracellular signaling rapidly. The pure antagonist of ER transactivation ICI182,780 might prove to be a useful pharmacological tool for experimentally separating rapid effects from the combined rapid and “classic” transcriptional effects of estrogen.

3b. *Determination of the spatiotemporal distribution of activated, dually phosphorylated ERK1/2 (pERK) in the rat cerebellum.*

In the rat, the majority of histomorphological changes that occur during cerebellar development take place between embryonic day 13 and the end of the third postnatal week (**126**). However, formation and resolution of the fine synaptic structures of the cerebellum continue for sometime after the third postnatal week. At birth, the rat cerebellum is primarily composed of immature precursor cells whose paths to their final mature form depend on the appropriate combinations of numerous developmental, biochemical, and functional cues. The complex events that occur during this protracted period of postnatal cerebellar development are orchestrated by a wide array of extracellular signals that specifically influence numerous intracellular signaling mechanisms, including the ERK MAPK pathway.

Previous studies indicate that transcripts encoding ERK1 and ERK2 (**127**), and ERK2 protein are expressed in the adult rat cerebellum. Because ERK activity is dependent on phosphorylation by an upstream MAPK kinase (**128, 129**) and because much of the expressed ERK-protein is normally unphosphorylated, and therefore quiescent, a clear picture of the importance of ERK-expression in cerebellar cells necessitates identification of the activated fraction of the total expressed ERK-proteins. In the present study, we elucidated the spatiotemporal and cell type distribution of activated ERK-IR during postnatal development in the cerebellum. A high degree of developmental plasticity in the cellular distribution and intracellular localization of active ERK was found. The coincidence of the onset of ERK-activation with specific developmental events suggests that intracellular signaling via the ERK-pathway may play an important role in regulating cell migration, proliferation, and synaptic maturation in the developing cerebellum. The cellular and intracellular patterns of pERK-IR in the cerebella of adults suggest that the ERK-signaling may mediate post-synaptic information processing in the mature cerebellum.

Expression of activated ERK-IR in Purkinje cells

During the first postnatal week, pERK-IR was detected in post-mitotic Purkinje cells within the cerebellar matrix and in increasing numbers of immature Purkinje cells

positioned in the forming Purkinje cell layer. Between P2 and 5, immunoreactive Purkinje cells were less abundant and the intensity of staining was decreased. Interestingly on P3–P4 there is a general slowing of Purkinje cell migration and the vast majority of Purkinje cells begin to align into the future Purkinje cell monolayer. Thus, the decreased level of pERK-IR on P3–P4 in Purkinje cells coincides with the cessation of postnatal migration and beginning of cell settling. These observations suggest that activation of the ERK-pathway may be associated with Purkinje cell migration.

Between P5 and 7, the number of pERK-immunopositive Purkinje cells and the intensity of their staining appeared to increase gradually. The observed peak in immunostaining for active ERK at P6–7 coincides with the initiation of Purkinje cell dendritic sprouting from the apical swelling of maturing Purkinje cells. Because it is well established that the ERK-pathway mediates neurite outgrowth (**130, 131**), it is likely that ERK-activation during this period is associated with the morphogenesis of Purkinje cell dendrites. Following peak pERK-immunostaining on P6–7, the levels of pERK in Purkinje cells was reduced suggesting that once initiated the elaboration of Purkinje cell dendrites, a morphogenetic phase that is only completed around P21, is not dependent on high levels of sustained ERK signaling. The initiation of the Purkinje cell's morphogenetic phase is paralleled by the formation of transient immature parallel fiber-Purkinje cell synapses, and climbing fiber-Purkinje cell synapses. The translocation of existing synapses from the Purkinje cell soma to the apical swelling and the initial branches of the growing dendrites also form at this time. Because glutamate can induce activation of the ERK pathway in cultured cerebellar cells (**132-134**), it is possible that the initiation of glutamatergic neurotransmission at these excitatory synapses is responsible in part for the activation of ERK-signaling in these maturing Purkinje cells.

At P10, pERK-IR in Purkinje cells was generally, although not significantly decreased, and more variability in the intensity and intracellular localization of staining was observed. This postnatal period represents an important milestone in the formation of the permanent pattern of the cerebellar circuitry. Beginning around P8, the first migrating granule cells settle into the IGL, and begin to establish immature synaptic contacts with their extracerebellar afferents, the mossy fibers (**126**). In maturing Purkinje cells, the first permanent dendrites with their climbing fiber synapses are

formed on P10, thus the variations seen in Purkinje cell staining pattern may be associated with increased synaptic activity and/or the adjustment of Purkinje cell function to changes in the synaptology of intra- and extra-cerebellar Purkinje cell afferents.

By P12, pERK staining intensity in Purkinje cells was diminished and remained low from P14 to 19. During this later period of cerebellar maturation, intracellular staining was confined to the basal portions of the Purkinje cell cytoplasm, and included the axon hillock region in the adult. Immunostaining for total ERK2 suggests homogeneous localization of ERK proteins within Purkinje cells of the mature cerebellum (**135**). Therefore, our finding that the activated ERK-IR is localized to the ventral part of Purkinje cells indicates that ERK-signaling is either inhibited at the apical portion of the cytoplasm, or activated in locally restricted subcellular domains in the basal aspect of Purkinje cells. The topographical organization of Purkinje cell afferent synapses shows a well-defined pattern: excitatory climbing fiber and parallel fiber afferents terminate on the dendritic arbors; the inhibitory stellate cell afferents occupy the stem of the dendritic branches; and the basket cell afferents are localized to ventrolateral regions of the Purkinje cell soma (**126**). The observed intracellular localization of activated pERK was associated with the major target area of the inhibitory interneuronal axon terminals. This localization pattern suggests that ERK-activation in mature Purkinje cells is most closely associated with inhibitory synaptic neurotransmission. Association of ERK activity with inhibitory synaptic activity seems to contradict the findings that have shown that glutamate-induced depolarization of Purkinje cells induces ERK-activation (**132**). However, prolonged exposure of Purkinje cells to glutamate or other depolarizing agents has also been shown to induce cerebellar long-term depression (**136, 137**). This type of persistent reduction in the strength of excitatory synaptic transmission in Purkinje cells may be reflected by reduced ERK-phosphorylation in the apical regions of Purkinje cells, whereas the continued inhibitory input in ventrolateral perikayal regions may reflect increased levels of ERK-signaling.

Most notable was a dramatic increase of pERK-IR in all cerebellar cell types analyzed at P22. The observed increase in immunoreactive cell numbers and the increased intensity of staining compared to early times is associated with the weaning of pups on P21. The observed increase in pERK-IR coincident with weaning and maternal

separation may result from increased motor activity associated with exploratory behaviors or other factors associated with new environmental influences such as change in diet.

Expression of activated ERK-IR in granule cells

In granule cells, pERK immunostaining was first detected in scattered cells in the mitotic subdivision of the EGL on P1. Based on their location and morphology, these immunopositive cells are most likely perimitotic granule cell precursors. In general, there were increases in the number of pERK-IR granule cells within the IGL during postnatal development of the cerebellum. Immunopositive granule cells were detected in all foliae between P6 and 10, and were consistently most concentrated in the anterior lobe between P12 and 22. From peak densities at P12 to P19, the density of immunoreactive granule cells decreased, was transiently increased on P22, and was absent in the mature cerebellum.

Early increased levels of pERK-immunostaining in granule cells coincide with initiation of granule cell differentiation, synaptogenesis and synaptic maturation in granule cells and intermediate neurons within the IGL, suggesting a role for ERK-activation during synaptogenesis (**126**). The involvement of the ERK-pathway in cerebellar excitatory synaptic function is well established (**133, 134, 138**) with numerous studies describing the involvement of ERK-signaling in the interplay between glutamatergic neurotransmission and modifications in post-synaptic cytoskeletal elements (**130, 133, 135, 139-141**). Between P8 and 10 when higher levels of ERK-activation are detected in granule cells, nearly all of the afferent synapses on granule cells are excitatory mossy fiber synapses (**126**). It is only at later developmental times when decreases in pERK are observed do considerable numbers of inhibitory contacts form and take on their full functionality. The likely consequence of this increase in inhibitory function would be decreased excitatory neurotransmission and an associated decrease in ERK activity.

Expression of activated ERK-IR in cerebellar glia

During early stages of Bergmann glia differentiation (P1–7), a homogeneous pERK-IR staining pattern was observed throughout the cytoplasm of immunopositive Bergmann

glial cells. Between P2 and 5, the vast majority of immunoreactive cells formed a 2–6 cell-deep layer under the Purkinje cell layer, and possessed the histological characteristics of proliferating and maturing Bergmann glial cells (**126**). A similar pERK-staining pattern was detected in maturing Bergmann glial cells that were identifiable by radial processes that had reached the pial surface, but were thicker and less ramificated than those of mature cells. Studies of Das et al., 1974 (**142**) have indicated that a second wave of Bergmann glia proliferation occurs during the second postnatal week. During this time, we did not observe increased ERK-activation in mass amounts of Bergmann glial cells. This observation suggests that ERK-activation is either associated with only the initial round of Bergmann glia proliferation, or transiently or asynchronously increased in association with the secondary initiation of Bergmann glia proliferation.

As Bergmann glia maturation progressed, the number of pERK-IR cells decreased and became associated with scattered clusters of immunopositive cells. Coincident with the appearance of the first permanent Purkinje cell glutamatergic synapses at P10, pERK immunostaining became restricted to the somata of Bergmann glia positioned between Purkinje cells. The radial processes of immunopositive cells in these clusters remained intensely stained. In light of glutamate's ability to induce ERK2 activation in Bergmann glia, and the functional interactions between Bergmann glia and Purkinje cell excitatory synaptic function (**143-148**), it is likely that ERK activity in Bergmann glia is responsive to the changing nature of synaptic function during Purkinje cell maturation. An interaction between ERK signaling in Bergmann glia and Purkinje cells is supported by the similarity in age-related changes in density of pERK-IR Bergmann glia clusters and Purkinje cells.

The intracellular pattern of pERK staining in Bergmann glial cells continued to undergo further, age-related changes, with pERK-IR becoming localized to the nucleus at P12 and then distributed throughout the cytoplasm between P14 and 22. Immunostaining in adults was confined to the radial processes of scattered Bergmann glial clusters. This changing pattern of the cellular and subcellular localization of activated ERK in the maturing cerebellum likely reflects further the changeable nature of the interactions between Bergmann glial processes and Purkinje cells dendrites. The activity of ERK

may continue to play a role in the plastic interaction between Bergmann glia and Purkinje cells even after the cerebellum has matured.

Double labeling for GFAP and pERK at P10 revealed pERK-IR in numerous astrocytes located in or close to the corpus medullare. The number of pERK-IR astrocytes was decreased by P15. In cerebella of P10 and older animals, pERK immunostaining was also noted in cells whose location and morphology resembled that of oligodendrocytes. The changing levels of pERK-IR in developing cerebellar glia during development are consistent with previous studies that demonstrate ERK1/2 mRNA (**127**) and p42 MAPK protein (**135**) expression in cerebellar astroglia and oligodendrocytes. Additionally, ERK-activation has been previously described in cultured rat cerebellar astrocytes (**149**) and numerous studies have highlighted the important role of the ERK signal transduction as a mediator of cellular events that regulate apoptosis and cell survival in astrocytes (**150-152**).

In summary, our present results suggest that the ERK-pathway may play a role in cell migration, proliferation and differentiation of both neurons and glia in the developing rat cerebellum. The observation that ERK-activation in the developing cerebellum coincided with the initiation, but not the entire time-course of Purkinje cell dendritic sprouting and synaptic organization, and with the initial phase of Bergmann glia proliferation suggests that transient activation of the ERK signaling cascade, and the resulting changes in gene expression, are intimately involved with initial events of these developmental processes. The changeable spatiotemporal staining pattern within specific cell types during cerebellar development, also suggests that ERK-activation is likely associated with plastic aspects of cellular maturation and function and likely plays a role in the interactions between neurons and glia, an interaction that appears to remain present into adulthood.

3c. *Identification of direct in vivo estrogen effects on the activation of cerebellar ERK1/2-activation: analysis of dose- and age-dependency.*

In the present study we found that a single, intracerebellar injection of E_2 can influence the rapid activation of the ERK-pathway at ages P8 and older, whereas in P4-6 animals E_2 had no apparent effect on pERK-IR. These results indicate that E_2 has a rapid (within

minutes), dose-specific modulatory effect on ERK-activation in the developing cerebellar tissue, most likely affecting cerebellar development, as well as neurotransmission in the cerebellum of adult animals.

Previous studies have reported that the activation of the ERK-pathway is necessary for certain aspects of neurodevelopment (**131, 153-156**), and simultaneous *in vitro* studies of our laboratory also indicate that E_2-activation of the ERK-pathway plays a role in granule cell proliferation and probably regulates cell pruning as well (**22**).

Cell proliferation in the developing cerebellum begins in embryonic life (like in all other regions of the central nervous system), then gradually slows down and ends by the end of the third postnatal week. The parallel fibers start invading the molecular layer on P2 and continue to grow and mature until the end of the third postnatal week. A number of studies have reported the role of E_2 in the regulation of axon outgrowth (for example see **34, 157-161**), and some also suggested that axon growth is regulated via the ERK-signaling pathway (**131, 156**). Thus, it is possible that E_2 influences cell proliferation and axonal growth in the developing cerebellum by the modulation of the ERK-pathway. However, the present findings show that estrogenic modulation of ERK-phosphorylation is bound to the age of P8 and older, which substantially narrows the time during which cell proliferation/axon growth, and the observed E_2-modulated ERK-activation overlap. Furthermore, double labeling for pERK and the synaptic marker synaptophysin in P10 animals (data not shown) suggested that pERK-IR is more intense in neurons that receive massive synaptic input than less-innervated neurons, while cells located in the external germinal layer were not immunoreactive for synaptophysin or pERK. This observation may suggest that *in vivo*, synaptic contact is required in the developing cerebellum for ERK-phosphorylation in the post-synaptic cell. Therefore, while it remains possible that E_2, via the modulation of ERK-activation, influences the above mentioned developmental processes *in vivo* after P7, it is more likely that such E_2-effects are involved in other aspects of the cerebellar development.

We have found an E_2-induced increase in the number of pERK-IR cells at P8 that was confined to the posterior lobe of the cerebellum. This observation may be due to the developmental stage of the cerebellum at P8: this age is marked by the settlement of post-migratory granule neurons. According to Altman and Bayer, 1997 (**126**), granule cell migration is first completed in the posterior foliae. Because the settlement of

granule cells is immediately followed by the generation of their afferent innervation from the mossy fibers, it is possible that the E_2-induced increase in pERK-IR is associated with concurrent synaptogenesis. A number of studies described the involvement of the ERK-pathway in the interplay between glutamatergic neurotransmission and the cytoskeleton of the post-synaptic element (**130, 133, 135, 140, 141**), which is necessary for synaptic assembly and -function as well. In addition, E_2 reportedly increases the number of synapses in different parts of the nervous system (**2, 162-168**). Those studies support the idea that E_2-induced ERK-activation may play a role in synaptogenesis. However, the observation that in P12 (and adult) animals E_2 did not induce ERK-activation in granule cells suggests that if ERK-activation at P8- and P10 is associated with synaptogenesis, it is limited to that occurring only on granule cells. This idea is supported by previous reports on the involvement of the ERK-pathway in cerebellar excitatory synaptic function (**134, 138**). According to Altman and Bayer, 1997 (**126**), mossy fiber synapses on granule neurons undergo further maturation before they become fully functional by P12, and Golgi neurons that are the main inhibitors of the postmigratory granule cells, do not establish their efferent connections before P11. Therefore, the neural connectivity of granule cells at P8-10 consists of immature excitatory synapses. In this context, the findings of Marie et al., 2002 (**169**) that Ajuba (a scaffolding protein) activates ERKs within minutes, to allow GLT-1 glutamate transporter to regulate intracellular signaling or interact with the cytoskeleton, may be of particular interest, and would also suggest that E_2-induced ERK-phosphorylation plays a role in excitatory synaptic activity during the maturation of mossy fiber synapses on granule cells. In the light of these data, our present findings suggest that at P8-10, E_2-induced ERK-activation may be involved in the modulation of the maturation and/or the activity of immature excitatory synapses.

Injection of E_2 into the P12 cerebellum resulted in a decrease in the number of pERK-IR cells. One possible explanation for this observation is that at- or around P12, there is a switch in the mechanism of the intracellular machinery that couples the E_2-cell interface to the ERK-pathway, thereby turning the (previously) stimulatory E_2-effect into an inhibitory influence. However, a second scenario may also be possible: The age of P12 is marked by the completion of the maturation of granule cell excitatory afferents, and by the appearance of abundant inhibitory Golgi-terminals on granule neurons, as well as on Golgi cells themselves. Thus, the initiation of the intrinsic

inhibitory network coincides in time with a switch in the effect (from increase to decrease) of E_2 on granule cell ERK-phosphorylation and with E_2-induced ERK-phosphorylation in inhibitory neurons. Our observation that in the P12 cerebellum E_2 induced ERK-activation in Golgi-like cells, and in the mature cerebellum E_2 induced ERK-phosphorylation in inhibitory interneurons (stellate-, basket-, Lugaro- and Golgi-like neurons), suggests that E_2's role in the mature cerebellum is distinct from that in the developing cerebellum. Consistently, we found that besides the overall decrease in the numbers of pERK-IR cells seen in E_2-treated P12 animals, there was some degree of increase in the number of pERK-IR Golgi-like inhibitory cells, which being activated could, in turn, reduce ERK-dependent neuronal activity in mass amounts of granule neurons by synaptic inhibition. In support of the possibility that at- or around P12 the inhibitory cerebellar circuit becomes E_2's target (with regard to ERK-activation), is the finding that shortly after the formation of the cerebellar inhibitory circuit, from the age of P11-12, pERK-IR of IGL granule neurons gradually withdraws from the apical regions towards the stem of the cerebellar foliae, leaving behind glomerulus-associated clusters of pERK-IR cells that also lose their immunoreactivity by P19.

In adult rat, E_2 activated the ERK-pathway not only in granule cells, but mostly in inhibitory interneurons, including Golgi-like cells, stellate-, Lugaro- and basket neurons, all of which are responsible for the final shaping of Purkinje cell function. Stellate cells form inhibitory synapses on the stem of Purkinje cell dendritic branches, thus being able to selectively isolate dendritic branch-excitation from the soma of Purkinje cells, while basket neurons block Purkinje cell output at the 'ventrolateral' soma and adjacent axon hillock area of Purkinje cells. Lugaro cells terminate on stellate-, basket-, and probably on Golgi neurons as well. In order to synchronize their function, these three types of inhibitory neurons synapse with each other, forming an intrinsic inhibitory network. Therefore, the finding that E_2 activated the ERK-pathway in these inhibitory interneurons, but eliminated pERK-IR from the axon hillock area of Purkinje cells, suggests that E_2-activation of the above mentioned inhibitory network could result in the disinhibition of Purkinje cells. This idea is well supported by the findings of Smith et al. (**170, 171**), that locally applied E_2 rapidly (within minutes) potentiated glutamate-evoked excitation of cerebellar Purkinje cells.

In the present study, we found that E_2 exerted a bi-phasic, dose-dependent influence on ERK-phosphorylation in the developing and mature cerebellum. This is consistent with previous studies that have reported the bi-phasic dose-specificity of E_2 and estrogenic compounds in several biological contexts, such as plasminogen activation, oxytocin secretion, angiogenesis, cell proliferation, bone growth, monocyte chemotaxis, etc., (topic reviewed by Calabrese, 2001 [**172**]; Calabrese and Baldwin, 2003 [**96**]). Since, according to these authors, opposite estrogenic effects can be evoked by high (inhibition) and low (stimulation) concentrations of E_2 and estrogenic substances, this dose-response phenomenon (named the Hormesis concept) has recently received special attention because its potential to revolutionize certain aspects of toxicology and related disciplines. The Hormesis concept holds that the effects of high and low concentrations of E_2 (in this context) stand on the two opposite sides of the experimental control values and thus, form two distinct endpoints in the nature of the biological effect. In contrast, our dose-response-observations in the *in vivo* developing cerebellum suggest that at a given developmental stage, E_2 can only increase (at P8-10) or only decrease (at P12) ERK-phosphorylation when injected at high- and low concentrations, whereas mid-dilutions of E_2 have no substantial effect on ERK-activation. Opposite E_2-effects on ERK-phosphorylation, instead of having been evoked by different E_2-concentrations at a given age, were only brought seen at different developmental stages of the cerebellum, i.e., the increase in ERK-activation by E_2 on P8-10 turned into a decrease at P12, nevertheless, as mentioned above, this phenomenon may have resulted from an E_2-modulated neuron-neuron interaction instead of a reversion of direct E_2-effects on ERK-phosphorylation. It has to be noted that in Calabrese's reviews E_2's hormetic effects were discussed in the context of biological effects influenced/regulated by high or low concentrations of E_2, while our study examined E_2's influence on an intracellular signaling pathway, without identifying its biological outcome. Therefore, it is difficult to determine whether the bi-phasic dose-dependent influence of E_2 on cerebellar ERK-activation is hormetic. Nevertheless, the dose-specificity of E_2-effects observed in this study is well consistent with recent in vitro dose-response studies of our laboratory: In granule cell cultures exposed to various concentrations of E_2 for 10 minutes, ERK-activation followed a biphasic dose response curve with significant increases in ERK-phosphorylation observed with 10^{-11}-10^{-10} M and 10^{-7}-10^{-6} M E_2, and with highly variable and insignificant responsiveness at the 10^{-8} M concentration (**22**).

The mechanism underlying E_2's dose-specific effects is not known. Our study demonstrates that in the cerebellum, there is a developmental switch in the platform of estrogenic modulation of ERK-activation, from the excitatory granule neurons at P8-10, to the inhibitory interneurons in P12- and older animals. Although it has not been examined, it is unlikely that both mentioned neuronal populations are equally responsive to E_2. Therefore, it is possible that the high- and low concentrations of E_2 that were found to be the most potent in modulating ERK-activation, represent the E_2-concentrations adequate to stimulate ERK-phosphorylation in excitatory and inhibitory cell populations. However, cell-cell interactions in the *in vivo* system and the likely contribution of synaptic neurotransmission to activate the ERK-pathway may mask E_2's possible separate effects on excitatory and inhibitory neurons, thus complicating the evaluation of overall E_2 effects. Therefore, further studies are needed to determine the role of E_2-modulated ERK-activation in cerebellar neurotransmission.

Summary of discussion

In summarizing the outcome of our studies, as a conclusion, we describe a proposed neuronal and cellular mechanism of the regulation of the pituitary LH-surge that leads to subsequent ovulation. We present here a scenario best supported by our present results, considering the preliminary results of some of our pilot studies and the corresponding literature.

For the most part of the estrous cycle, the hypothalamic GnRH- (and pituitary LH) release is regulated by an E_2-sensitive neuronal circuit through a negative feedback-based mechanism. At the time of the midcycle E_2-surge during late proestrus, rapid events take place, starting with a sharp rise of the blood E_2 concentration. Our studies in the neurons of the cerebellum indicate that the direct effects of E_2 on neurons are both time- and concentration-dependent; moreover, the early, rapid effects display a bi-modal dose-dependent pattern. Those studies sugest that the key E_2-induced effects turning the reciprocal feedback into the positive feedback shortly after the E_2 surge do manifest themselves in the rapid activation of intracellular signaling systems, such as the ERK1/2 MAPK pathway. The rapid, E_2-induced activation of the ERK-pathway also facilitates excitatory glutamatergic neurotransmission by several means, for example, by mediating the assembly of cytoskeletal structures that are functional elements of the post-synaptic machinery of excitatory synapses. Simultaneously, the quickly rising plasma E_2 level during this time also increases the expression levels of excitatory amio acid receptors (AMPA). Results indicate that the facilitation of glutamatergic neurotransmission (that is responsible for the initiation of the positive gonadotropin feedback) occurs in hypothalamic GABAergic cells (these neurons have been shown to contain AMPA receptors and to be the exclusive subjects of the EISP). However, as discussed above, it is another population of neurons, a group of dopaminergic (DAergic) cells that, terminating on hypothalamic beta-END cells with inhibitory membrane specializations, can hyper-polarize (inhibit) beta-END cells when they, themselves, are dis-inhibited. Therefore, from the known pattern of neuronal connectivity within the hypothalamus, it is suggested that as a result of the initial excitatory amino acid neurotransmission, some of the first GABA neurons to act, inhibit certain secondary GABA interneurons which, in turn, dis-inhibit the AMPA-non-expressing DAergic cells. As a result, these DAergic cells act to inhibit the AN beta-

END neurons, latter which dis-inhibit the GnRH cells in the MPO (rat) or in the AN (primates), resulting in a surge in GnRH-release, followed by the release of LH from the pituitary gonadotrops already having been sensitized by E_2. As a result of these rapid changes, and also as part of them, the overall number of synapses in the hypothalamus quickly increases during the positive feedback-phase.

Simultaneously, the plasma E_2 concentration further increases and E_2 binds to its cognate receptor ERα in AN neurons. As a transactivational effect of the E_2-ER complex, the initial rise in synapse numbers within the AN reverts, and continues as a steady decrease, while simultaneously the plasma E_2 level also starts to decline. This reversal in synaptic changes is preceded by the offset of rapid E_2 effects, and causes the positive feedback to convert into a negative feedback. The specific pattern of changes in synapse numbers during the negative gonadotropin feedback suggests that it is estrogen that primarily propels EISP on AN GABAergic neurons, while consequential changes in the synaptology of GnRH cells regulate the pituitary LH-release.

We also attempted to answer the intriguing question of how does E_2 selectively induce synaptic plasticity in only a subpopulation of ER-expressing AN neurons, while other neuronal cells, even though express ERs, remain unaffected in this respect and do not undergo EISP: Neurons involved in EISP must contain the adequate set of tools for both the rapid events of the positive feedback (rapid second messenger system) and the ER-mediated mechanism regulating the second phase of EISP (overall, a decline in synapse numbers) during the negative feedback.

Using membrane-impermeable BSA-conjugated E_2, we have provided in vitro evidence that the rapid activation of the ERK-pathway by E_2 is mediated by a plasmamembrane-associated form of ER, although the molecular structure and the identity of this receptor remained to be determined. Other studies also imply the existence of such membrane-incorporated ERs in the hypothalamus. Studies in our laboratory are underway to identify and locate those plasma membrane-associated ERs that are responsible for the initiation of the positive gonadotropin feedback and thus, the pituitary gonadotropin surge.

NEW SCIENTIFIC RESULTS

In the present series of experiments we

- identified those neurons of the arcuate nucleus that are targets of excitatory amino acid neurotransmission;
- identified those neurons of the arcuate nucleus that undergo EISP;
- determined the temporal changes in the synaptic status of arcuate nucleus neurons during the gonadotropin feedback;
- assessed the role of EISP in the regulation of gonadotropin-release;
- demonstrated that estrogen modulates the rapid activation of the ERK1/2 MAPK signaling pathway in neurons in vitro;
- determined the spatiotemporal pattern of cerebellar ERK1/2-activation;
- demonstrated that estrogen modulates the rapid activation of the ERK1/2 MAPK signaling pathway in neurons in vivo.

REFERENCES

1 Parducz A., Zsarnovszky A**,** Naftolin F., Horvath TL. (2003) Estradiol affects axo-somatic contacts of neuroendocrine cells in the arcuate nucleus of adult rats. Neuroscience 117: 791-794.

2 Zsarnovszky A, Horvath TL, Garcia-Segura LM, Horvath B, Naftolin F. (2001). Oestrogen-induced changes in the synaptology of the monkey (Cercopithecus aethiops) arcuate nucleus during gonadotropin feedback. J Neuroendocrinol 13: 22-28.

3 Zsarnovszky A, Horvath TL, Garcia-Segura LM, Horvath B, Naftolin F. (2000) Plasticity of the hypothalamic GABA system and its relationship to GnRH neurons during positive gonadotrophin feedback in non-human primates. Annual Meeting of the Endocrine Society.

4 Horvath TL, Garcia-Segura LM, Naftolin F. (1996) Control of gonadotropin feedback: the possible role of estrogen-induced hypothalamic plasticity. Gynecol Endocrinol 10: 1-5.

5 Matsumoto A, Arai Y. (1976) Effect of estrogen on early postnatal development of synaptic formation in the hypothalamic arcuate nucleus. Neurosci Lett 2: 79-82.

6 Arai Y, Matsumoto A, Nishizuka M. (1986) Synaptogenezis and neuronal plasticity to gonadal steroids: implication for the development of sexual dimorphism in the neuroendocrin brain. Curr Topics Neuroendocrinol 7: 291-307.

7 Naftolin F, Leranth C, Horvath TL, Garcia-Segura LM. (1996) Potential neuronal mechanisms of estrogen actions in synaptogenesis and synaptic plasticity. Cell Mol Neurobiol 16: 213-223.

8 Naftolin F, Garcia-Segura LM, Keefe D, Leranth C, MacLusky NJ, Brawer JR. (1990) Estrogen effects on the synaptology and neural membranes of the rat hypothalamic arcuate nucleus. Biol Reprod 42: 21-28.

9 Olmos G, Naftolin F, Tranque P, Garcia-Segura LM. (1989) Synaptic remodeling in the rat arcuate nucleus during the estrus cycle. Neuroscience 32: 663-667.

10 Garcia-Segura LM, Baetens D, Naftolin F. (1986) Synaptic remodelling in arcuate nucleus after injection of estradiol valerate in adult female rats. Brain Res 366: 131-136.

11 Naftolin F, Mor G, Horvath TL, Luquin S, Fajer AB, Kohen F, Garcia-Segura LM. (1996) Synaptic remodeling in the arcuate nucleus during the estrous cycle is induced by estrogen and precedes the preovulatory gonadotropin surge. Endocrinology 137: 5576-5580.

12 Naftolin F, Leranth C, Perez J, Garcia-Segura LM. (1993) Estrogen induces synaptic plasticity in adult primate neurons. Neuroendocrinology 57: 935-940.

13 Zsarnovszky A, Horvath TL, Naftolin F, Leranth L. (2000) AMPA-receptors colocalize with neuropeptide Y- and galanin-containing, but not with dopamine neurons of the female rat arcuate nucleus: a semiquantitative immunohistochemical colocalization study. Exp Brain Res 133: 532-537.

14 Garcia-Segura LM, Olmos G, Tranque P, Naftolin F. (1987) Rapid effects of gonadal steroids upon hypothalamic neuronal membrane ultrastructure. J Steroid Biochem 27: 615-623.

15 Olmos G, Aguilera P, Tranque P, Naftolin F, Garcia-Segura LM. (1987) Estrogen-induced synaptic remodelling in adult rat brain is accompanied by the reorganization of neuronal membranes. Brain Res 425: 57-64.

16 Garcia-Segura LM, Perez J, Tranque PA, Olmos G, Naftolin F. (1988) Neuronal membrane remodelling during the oestrus cycle: a freeze-fracture study in the arcuate nucleus of the rat hypothalamus. J Neurocytol 17: 377-383.

17 Kim JS, Kim HY, Kim JH, Shin HK, Lee SH, Lee YS, Son H. (2002) Enhancement of rat hippocampal long-term potentiation by 17 beta-estradiol involves mitogen-activated protein kinase-dependent and –independent components. Neurosci Lett 332: 65-69.

18 Smith SS, Waterhouse BD, Woodward DJ. (1987) Sex steroid effects on extrahypothalamic CNS. I. Estrogen augments neuronal responsiveness to iontophoretically applied glutamate in the cerebellum. Brain Res 422: 40-51.

19 Smith SS, Waterhouse BD, Woodward DJ. (1988) Locally applied estrogens potentiate glutamate-evoked excitation of cerebellar Purkinje cells. Brain Res 475: 272-282.

20 Belcher SM, Zsarnovszky A. (2001) Estrogenic actions in the brain: Estrogen, phytoestrogens and rapid intracellular signaling mechanisms. J Pharm Exp Ther 299: 408-414.

21 Toran-Allerand CD, Guan X, MacLusky NJ, Horvath TL, Diano S, Singh M, Connolly ES Jr, Nethrapalli IS, Tinnikov AA. (2002) ER-X: a novel, plasma membrane-associated, putative estrogen receptor that is regulated during development and after ischemic brain injury. J Neurosci 22: 8391-8401.

22 Wong JK, Le HH, Zsarnovszky A, Belcher SM. (2003) Estrogens and ICI182,780 (Faslodex) modulate mitosis and cell death in immature cerebellar neurons via rapid activation of p44/p42 mitogen-activated protein kinase. J Neurosci 23: 4984-4995.

23 Kirby M, Zsarnovszky A, Belcher SM. (2004) Estrogen receptor expression in a human primitive neuroectodermal tumor cell line from the cerebral cortex: estrogen stimulates rapid ERK1/2 activation and receptor-dependent cellular migration. Biochem Biophys Res Com 319: 753-758.

24 Zsarnovszky A, Belcher SM. (2003) Estrogen rapidly modulates the phosphorylation of ERK1/2 in the rat cerebellum in vivo. 33rd Annual Meeting of the Society for Neuroscience.

25 Zsarnovszky A, Le H. H, Wang H-S, Belcher S. M. (2005) Ontogeny of rapid estrogen-mediated ERK1/2 signaling in the rat cerebellar cortex in vivo: potent non-genomic agonist and endocrine disrupting activity of the xenoestrogen bisphenol A. Endocrinology. First published August 25, 2005 as doi:10.1210/en.2005-0565.

26 Cardona-Gomez GP, Mendez P, Garcia-Segura LM. (2002) Synergistic interaction of estradiol and insulin-like growth factor-I in the activation of PI3K/Akt signaling in the adult rat hypothalamus. Brain Res Mol Brain Res 107: 80-88.

27 Zsarnovszky A, Belcher SM. (2004) Spatial, temporal, and cellular distribution of the activated extracellular signal regulated kinases 1 and 2 in the developing and mature rat cerebellum. Dev Brain Res 150: 199-209.

28 Zsarnovszky A, Belcher SM. (2003) Estrogen rapidly modulates the phosphorylation of ERK1/2 in the rat cerebellum in vivo. 33rd Annual Meeting of the Society for Neuroscience.

29 Sterio DC. (1984) The unbiased estimation of number and sizes in arbitrary particles using the disector. J Microsc 134:127–136.

30 Palay SL, Chan-Palay V. (1975) A guide to the synaptic analysis of the neuropil. Cold Spring Harbor Symposia Quantitative Biol 40: 1-16.

31 Colonnier M. (1968) Synaptic patterns on different cell types in the different laminae of the cat visual cortex. Brain Res 9: 268-287.

32 Norman RL, Lindstrom SA, Bangsberg D, Ellinwood WE, Gliessman P, Spies HG. (1984) Pulsatile secretion of luteinizing hormone during the menstrual cycle of rhesus macaques. Endocrinology 115: 261-266.

33 Ellinwood WE, Resko JA. (1980) Sex differences in biologically active and immunoreactive gonadotropins in the fetal circulation of rhesus monkeys. Endocrinology 107: 902-907.

34 Jakab RL, Wong JK, Belcher SM. (2001) Estrogen receptor-β immunoreactivity in differentiating cells of the developing rat cerebellum. J Comp Neurol 430: 396–409.

35 Wong JK, Kennedy PR, Belcher SM. (2001) Simplified serum- and steroid-free culture conditions for the high-throughput viability analysis of primary cultures of cerebellar neurons. J Neurosci Methods 110: 45–55.

36 Cunningham MG, McKay RD. (1993) A hypothermic miniaturized stereotaxic instrument for surgery in newborn rats. J Neurosci Methods 47: 105-114.

37 Wenthold RJ, Yokotani N, Doi K, Wada K. (1992) Immunocytochemical characterization of the non-NMDA glutamate receptor using subunit-specific antibodies. J Biol Chem 267: 501–507.

38 Sinkiewitz W, Majewski M, Kaleczyk J, Lakomy M. (1996) Distribution of catecholamine-synthesizing enzymes and some neuropeptides in the median eminence-arcuate nucleus complex (MEARC) of the immature female pig. Acta Histochem 98: 419–434.

39 Kawano H, Daikoku S. (1987) Functional topography of the rat hypothalamic dopamine neuron systems: retrograde tracing and immunohistochemical study. J Comp Neurol 265: 242–253.

40 Palay VC, Zaborszky L, Kohler C, Goldstein M, Palay SL. (1984) Distribution of tyrosin-hydroxylase-immunoreactive neurons in the hypothalamus of rats. J Comp Neurol 227: 467–496.

41 Silverman AJ, Antunes JL, Ferin M, Zimmerman EA. (1977) The distribution of luteinizing hormone-releasing hormone (LHRH) in the hypothalamus of the rhesus monkey. Light microscopic studies using immunoperoxidase technique. Endocrinology 101: 134-142.

42 Silverman AJ, Antunes JL, Abrams GM, Nilaver G, Thau R, Robinson JA, Ferin M, Krey LC. (1982) The luteinizing hormone-releasing hormone pathways in rhesus (Macaca mulatta) and pig-tailed (Macaca nemestrina) monkeys: new observations on thick, unembedded sections. J Comp Neurol 211: 309-317.

43 Leranth C, Shanabrough M, Naftolin F. (1991) Estrogen induces ultrastructural changes in progesterone receptor-containing GABA neurons of the primate hypothalamus. Neuroendocrinology 54: 571-579.

44 Witkin JW, Ferin M, Popilskis SJ, Silverman A-J. (1991) Effects of gonadal steroids on the ultrastructure of GnRH neurons in the Rhesus monkey: synaptic input and glial apposition. Endocrinology 129: 1083-1092.

45 Tappaz ML, Brownstein MJ. (1977) Origin of glutamate-decarboxylase (GAD)-containing cells in discrete hypothalamic nuclei. Brain Res 132: 95-106.

46 Wood KA, Dipasquale B, Youle RJ. (1993) In situ labeling of granule cells for apoptosis-associated DNA fragmentation reveals different mechanisms of cell loss in developing cerebellum. Neuron 11: 621–632.

47 Villalba M, Bockaert J, Journot L. (1997) Concomitant induction of apoptosis and necrosis in cerebellar granule cells following serum and potassium withdrawal. Neuroreport 8: 981–985.

48 Tanaka M, Marunouchi T. (1998) Immunohistochemical analysis of developmental stage of external granular layer neurons which undergo apoptosis in postnatal rat cerebellum. Neurosci Lett 242: 85–88.

49 Kitanaka C, Kuchino Y. (1999) Caspase-independent programmed cell death with necrotic morphology. Cell Death Differ 6: 508–515.

50 Yamashima T. (2000) Implication of cysteine proteases calpain, cathepsin, and caspase in ischemic neuronal death of primates. Prog Neurobiol 62: 273–295.

51 Razandi M, Oh P, Pedram A, Schnitzer J, Levin ER. (2002) ERs associate with and regulate the production of caveolin: implications for signaling and cellular actions. Mol Endocrinol 16: 100–115.

52 Laine J, Axelrad H. (2002) Extending the cerebellar Lugaro cell class. Neuroscience 115: 363-374.

53 Horvath TL, Naftolin F, Kalra SP, Leranth C. (1992) Neuropeptide Y innervation of beta-endorphin-containing cells in the rat mediobasal hypothalamus. A light- and electronmicroscopic double-immunostaining analysis. Endocrinology 131: 2461–2467.

54 Horvath TL, Kalra SP, Naftolin F, Leranth C. (1995) Morphological evidence for a galanin-opiate interaction in the rat mediobasal hypothalamus. J Neuroendocrinol 7: 579–588.

55 Horvath TL, Naftolin F, Leranth C. (1992) GABAergic and catecholaminergic innervation of mediobasal hypothalamic beta-endorphin cells projecting to the medial preoptic area. Neuroscience 51: 391–399.

56 Loose MD, Ronnekleiv OK, Kelly MJ. (1991) Neurons in the rat arcuate nucleus are hyperpolarized by GABAB and mu-opioid receptor agonists: evidence for convergence at a ligand-gated potassium conductance. Neuroendocrinology 54: 537–544.

57 Sahu A, Crowley WR, Tatemoto K, Balasubramaniam A, Kalra SP. (1987) Effects of neuropeptide Y, NPY analog (norleucine4-NPY), galanin and neuropeptide K on LH release in ovariectomized (ovx) and ovx estrogen, progesterone-treated rats. Peptides 8: 921–926.

58 Horvath TL, Naftolin F, Leranth C, Sahu A, Kalra SP. (1996) Morphological and pharmacological evidence for neuropeptide Y-galanin interaction in the rat hypothalamus. Endocrinology 137: 3069–3077.

59 Guy J, Pelletier G. (1988) Neuronal interactions between neuropeptide Y (NPY) and catecholaminergic systems in the rat arcuate nucleus as shown by dual immunocytochemistry. Peptides 9: 567–570.

60 Van den Pol A, Waurin J, Dudek F. (1990) Glutamate, the dominant excitatory transmitter in neuroendocrine regulation. Science 250: 1276–1278.

61 Olney JW, Cicero TJ, Meyer E, De Gubareff T. (1976) Acute glutamate-induced elevations in serum testosterone and luteinizing hormone. Brain Res 112: 420–424.

62 Horvath TL, Bechmann I, Naftolin F, Kalra SP, Leranth C. (1997) Heterogeneity in the neuropeptide Y-containing neurons of the rat arcuate nucleus: GABAergic and non-GABAergic subpopulations. Brain Res 756: 283–286.

63 Garthwaite G, Hajos F, Garthwaite J. (1992) Morphological response of endoplasmic reticulum in cerebellar Purkinje cells to calcium deprivation. Neuroscience 48: 681–688.

64 Leranth C, Sakamoto H, MacLusky NJ, Shanabrough M, Naftolin F. (1985) Estrogen-responsive cells in the arcuate nucleus of the rat contain glutamic acid decarboxylase (GAD): electron microscopic immunocytochemical study. Brain Res 331: 376–381.

65 Leranth C, Shanabrough M, Naftolin F. (1991) Estrogen induces ultrastructural changes in progesterone receptor-containing GABA neurons of the primate hypothalamus. Neuroendocrinology 54: 571–579.

66 Rizzuto R, Pinton P, Carrington W, Fay FS, Fogarty KE, Lifshitz LM, Tuft RA, Pozzan T. (1998) Close contacts with the endoplasmic reticulum as determinants of mitochondrial Ca responses. Science 280: 1763–1766.

67 Diano S, Naftolin F, Horvath TL. (1997) Gonadal steroids target AMPA glutamate receptor-containing neurons in the rat hypothalamus, septum and amygdala: a morphological and biochemical study. Endocrinology 138: 778–788.

68 Merchenthaler I. (1991) Neurons with access to the general circulation in the central nervous system of the rat: a retrograde tracing study with fluoro-gold. Neuroscience 44: 655–662.

69 Arnold AP, Breedlove SM. (1985) Organizational and activational effects of sex steroids on brain and behavior: a reanalysis. Horm Behav 19: 469–498.

70 MacLusky NJ, Naftolin F. (1981) Sexual differentiation of the central nervous system. Science 211: 1294–1303.

71 Arnold AP, Gorski RA. (1984) Gonadal steroid induction of structural sex differences in the central nervous system. Annu Rev Neurosci 7: 413–442.

72 Greenough WT, Carter CS, Steerman C, DeVoogd TJ. (1977) Sex differences in dendritic patterns in hamster preoptic area. Brain Res 126: 63–72.

73 Guillamon A, Segovia S, Del Abril A. (1988) Early effects of gonadal steroids on the neuron number in the medial posterior region and the lateral division of the bed nucleus of the stria terminalis in the rat. Dev Brain Res 44: 281–290.

74 Perez J, Naftolin F, Garcia-Segura LM. (1990) Sexual differentiation of synaptic connectivity and neuronal plasma membrane in the arcuate nucleus of the rat hypothalamus. Brain Res 527: 116–122.

75 Parducz A, Garcia-Segura LM. (1993) Sexual differences in the synaptic connectivity in the rat dentate gyrus. Neurosci Lett 161: 53–56.

76 Olmos G, Naftolin F, Perez J, Tranque PA, Garcia-Segura LM. (1989) Synaptic remodelling in the rat arcuate nucleus during the estrous cycle. Neuroscience 32: 663–667.

77 Frankfurt M, Gould E, Woolley CS, McEwen BS. (1990) Gonadal steroids modify dendritic spine density in ventromedial hypothalamic neurons: a Golgi study in the adult rat. Neuroendocrinology 51: 530–535.

78 Gould E, Woolley C, Frankfurt M, McEwen B. (1990) Gonadal steroids regulate dendritic spine density in hippocampal pyramidal cells in adulthood. J Neurosci 10: 1286–1291.

79 Theodosis DT, Poulain DA. (1993) Activity-dependent neuronal-glial and synaptic plasticity in the adult mammalian hypothalamus. Neuroscience 57: 501–535.

80 Parducz A, Perez J, Garcia-Segura LM. (1993) Estradiol induces plasticity of GABAergic synapses in the hypothalamus. Neuroscience 53: 395–401.

81 Kis Z, Horvath S, Hoyk S, Toldi J, Parducz A. (1999) Estrogen effects on arcuate neurons in rat: an in situ electrophysiological study. Neuroreport 10: 3649–3652.

82 Parducz A, Hoyk Z, Kis Z, Garcia-Segura LM. (2002) Hormonal enhancement of neuronal firing is linked to structural remodelling of excitatory and inhibitory synapses. Eur J Neurosci 16: 665–670.

83 Mellon PL, Windle JJ, Goldsmith PC, Padula CA, Roberts JL, Wiener RI. (1990) Immortalization of hypothalamic GnRH neurons by genetically targeted tumorigenezis. Neuron 5: 1-10.

84 Martinez de la Escalera G, Choi ALH, Weiner RI. (1992) Generation and synchronization of gonadotropin-releasing hormone (GnRH) pulses: intrinsic propertiesof the GT1-1 GnRH neuronal cell line. Proc Natl Acad Sci USA 89: 1852-1855.

85 Wetsel WC, Valenca MM, Merchenthaler I, Lipositz Z, Lopez FJ, Wiener RI, Mellon PL, Negro-Vilar A. (1992) Intrinsic pulsatile secretory activity of immortalized luteinizing hormone-releasing hormone secreting neurons. Proc Natl Acad Sci USA 89: 4149-4153.

86 Krsmanovic LZ, Stojilkovic SS, Merelli F, Dufour SM, Virmani MA, Catt KJ. (1992) Calcium signaling and episodic secretion of gonadotropinreleasing hormone in hypothalamic neurons. Proc Natl Acad Sci USA 89: 8462-8466.

87 Knobil E. (1980) The neuroendocrine control of the menstrual cycle. Rec Prog Horm Res 36: 53-88.

88 Terasawa E, Quanbeck CD, Schultz CA, Burich AJ, Luchansky LL, Claude P. (1993) A primary cell culture system of luteinizing hormone releasing hormone (LHRH) neurons derived from fetal olfactory placode in the rhesus monkey. Endocrinology 133: 2379-2390.

89 Burich AJ, Claude P, Terasawa E. (1994) LHRH neurons in vitro derived from the embryonic olfactory placod of the rhesus monkey release LHRH into medium in a pulsatile manner. Proc 24th Ann Meet Soc Neurosci 20: 272.

90 Depaolo LV, Shimonaka M, Ling N. (1992) Regulation of pulsatile gonadotropin secretion by estrogen, inhibin, and follistatin (activin-binding protein) in ovariectomized rats. Biol Reprod 46: 898-904.

91 Strobl FJ, Levine JE. (1988) Estrogen inhibits luteinizing hormone (LH), but not follicle-stimulating hormone secretion in hypophysectomized pituitary-grafted rats receiving pulsatile LH-releasing hormone infusions. Endocrinology 123: 622-630.

92 Condon TP, Dykshoorn-Bosch MA, Kelly MJ. (1988) Episodic luteinizinghormone release in the ovariectomized female guinea pig: rapid inhibition by estrogen. Biol Reprod 38: 121-126.

93 Weick RF, Noh KA. (1984) Inhibitory effects of estrogen and progesterone on several parameters of pulsatile LH release in the ovariectomized rat. Neuroendocrinology 38: 351-356.

94 Plant TM, Nakai Y, Belchetz P, Keogh E, Knobil E. (1978) The sites of action of estradiol and phentolamine in the inhibition of the pulsatile, circhoral discharges of LH in the rhesus monkey (Macaca mulatta). Endocrinology 102: 1015-1018.

95 Thind KK, Goldsmith PC. (1997) Expression of estrogen and progesteron receptors in glutamate and GABA neurons of the pubertal female monkey hypothalamus. Neuroendocrinology 65: 314-324.

96 Calabrese EJ, Baldwin LA. (2003) Hormesis: the dose–response revolution. Annu Rev Pharmacol Toxicol 43: 175–197.

97 Montano MM, Welshons WV, vom Saal FS. (1995) Free estradiol in serum and brain uptake of estradiol during fetal and neonatal sexual differentiation in female rats. Biol Reprod 53: 1198–1207.

98 Horvath TL, Wikler KC. (1999) Aromatase in developing sensory systems of the rat brain. J Neuroendocrinol 11: 77–84.

99 Gotoh Y, Nishida E, Yamashita T, Hoshi M, Kawakami M, Sakai H. (1990) Microtubule-associated protein (MAP) kinase activated by nerve growth factor and epidermal growth factor in PC12 cells. Identity with the mitogen-activated MAP kinase of fibroblastic cells. Eur J Biochem 193: 661–669.

100 Kao SC, Jaiswal RK, Kolch W, Landreth GE. (2001) Identification of the mechanisms regulating the differential activation of the MAPK cascade by epidermal growth factor and nerve growth factor in PC12 cells. J Biol Chem 276: 18169–18177.

101 Filardo EJ. (2002) Epidermal growth factor receptor (EGFR) transactivation by estrogen via the G-protein-coupled receptor, GPR30: a novel signaling pathway with potential significance for breast cancer. J Steroid Biochem Mol Biol 80: 231–238.

102 Singh M, Setalo Jr G, Guan XP, Warren M, Toran-Allerand CD. (1999) Estrogen-induced activation of mitogen-activated protein kinase in cerebral cortical explants: convergence of estrogen and neurotrophin signaling pathways. J Neurosci 19: 1179–1188.

103 Singh M, Setalo G, Guan X, Frail DE, Toran-Allerand CD. (2000) Estrogeninduced activation of the mitogen-activated protein kinase cascade in the cerebral cortex of estrogen receptor-α knock-out mice. J Neurosci 20: 1694–1700.

104 Wakeling AE, Bowler J. (1992) ICI182,780, a new antioestrogen with clinical potential. J Steroid Biochem Mol Biol 43: 173–177.

105 Parisot JP, Hu XF, Sutherland RL, Wakeling A, Zalcberg JR, DeLuise M. (1995) The pure antiestrogen ICI182,780 binds to a high-affinity site distinct from the estrogen receptor. Int J Cancer 62: 480–484.

106 Wakeling AE. (1995) Use of pure antioestrogens to elucidate the mode of action of oestrogens. Biochem Pharmacol 49: 1545–1549.

107 Pike AC, Brzozowski AM, Hubbard RE, Bonn T, Thorsell AG, Engstrom O, Ljunggren J, Gustafsson JA, Carlquist M. (1999) Structure of the ligandbinding domain of oestrogen receptor β in the presence of a partial agonist and a full antagonist. EMBO J 18: 4608–4618.

108 Pike AC, Brzozowski AM, Walton J, Hubbard RE, Thorsell AG, Li YL, Gustafsson JA, Carlquist M. (2001) Structural insights into the mode of action of a pure antiestrogen. Structure 9: 145–153.

109 Egner U, Heinrich N, Ruff M, Gangloff M, Mueller-Fahrnow A, Wurtz JM. (2001) Different ligands–different receptor conformations: modeling of the hERα LBD in complex with agonists and antagonists. Med Res Rev 21: 523–539.

110 Watters JJ, Campbell JS, Cunningham MJ, Krebs EG, Dorsa DM. (1997) Rapid membrane effects of steroids in neuroblastoma cells: effects of estrogen on mitogen-activated protein kinase signaling cascade and *c-fos* immediate early gene transcription. Endocrinology 138: 4030–4033.

111 Gu Q, Korach KS, Moss RL. (1999) Rapid action of 17β-estradiol on kainate-induced currents in hippocampal neurons lacking intracellular estrogen receptors. Endocrinology 140: 660–666.

112 Kuroki Y, Fukushima K, Kanda Y, Mizuno K, Watanabe Y. (2000) Putative membrane-bound estrogen receptors possibly stimulate mitogen-activated protein kinase in the rat hippocampus. Eur J Pharmacol 400: 205–209.

113 Dubal DB, Kashon ML, Pettigrew LC, Ren JM, Finklestein SP, Rau SW, Wise PM. (1998) Estradiol protects against ischemic injury. J Cereb Blood Flow Metab 18: 1253–1258.

114 Dubal DB, Shughrue PJ, Wilson ME, Merchenthaler I, Wise PM. (1999) Estradiol modulates Bcl-2 in cerebral ischemia: a potential role for estrogen receptors. J Neurosci 19: 6385–6393.

115 Singer CA, Figueroa-Masot XA, Batchelor RH, Dorsa DM. (1999) The mitogen-activated protein kinase pathway mediates estrogen neuroprotection after glutamate toxicity in primary cortical neurons. J Neurosci 19: 2455–2463.

116 Han BH, Holtzman DM. (2000) BDNF protects the neonatal brain from hypoxic–ischemic injury *in vivo* via the ERK pathway. J Neurosci 20: 5775–5781.

117 Dubal DB, Wise PM. (2001) Neuroprotective effects of estradiol in middleaged female rats. Endocrinology 142: 43–48.

118 Wise PM, Dubal DB, Wilson ME, Rau SW, Liu Y. (2001) Estrogens: trophic and protective factors in the adult brain. Front Neuroendocrinol 22: 33–66.

119 Schweichel JU, Merker HJ. (1973) The morphology of various types of cell death in prenatal tissues. Teratology 7: 253–266.

120 Sorimachi H, Ishiura S, Suzuki K. (1997) Structure and physiological function of calpains. Biochem J 328: 721–732.

121 Schnellmann RG, Williams SW. (1998) Proteases in renal cell death: calpains mediate cell death produced by diverse toxicants. Ren Fail 20: 679–686.

122 Nixon RA, Saito KI, Grynspan F, Griffin WR, Katayama S, Honda T, Mohan PS, Shea TB, Beermann M. (1994) Calcium-activated neutral proteinase (calpain) system in aging and Alzheimer's disease. Ann NY Acad Sci 747: 77–91.

123 Grewal SS, York RD, Stork PJ. (1999) Extracellular signal-regulated kinase signaling in neurons. Curr Opin Neurobiol 9: 544–553.

124 Glading A, Uberall F, Keyse SM, Lauffenburger DA, Wells A. (2001) Membrane proximal ERK signaling is required for M-calpain activation downstream of epidermal growth factor receptor signaling. J Biol Chem 276: 23341–23348.

125 Shiraha H, Glading A, Chou J, Jia Z, Wells A. (2002) Activation of M-calpain (calpain II) by epidermal growth factor is limited by protein kinase A phosphorylation of M-calpain. Mol Cell Biol 22: 2716–2727.

126 Altman J, Bayer SA. (1997) Development of the Cerebellar System. In Relation to its Evolution, Structure, and Function, CRC Press, Boca Raton, FL.

127 Thomas KL, Hunt SP. (1993) The regional distribution of extracellularly regulated kinase-1 and -2 messenger RNA in the adult rat central nervous system. Neuroscience 56: 741–757.

128 Seger R, Krebs EG. (1995) The MAPK signaling cascade. FASEB J 9: 726–735.

129 Sweatt JD. (2001) The neuronal MAP kinase cascade: a biochemical signal integration system subserving synaptic plasticity and memory. J Neurochem 76: 1–10.

130 Sanchez MC, Diaz-Nido J, Avila J. (1998) Regulation of a site-specific phosphorylation of the microtubule-associated protein 2 during the development of cultured neurons. Neuroscience 87: 861–870.

131 Schmid RS, Pruitt WM, Maness PF. (2000) A MAP kinase signaling pathway mediates neurite outgrowth on L1 and requires Src-dependent endocytosis. J Neurosci 20: 4177–4188.

132 Kawasaki H, Fujii H, Gotoh Y, Morooka T, Shimohama S, Nishida E, Hirano T. (1999) Requirement for mitogen-activated protein kinase in cerebellar long term depression. J Biol Chem 274: 13498–13502.

133 Llansola M, Felipo V. (2002) Carnitine prevents NMDA-receptor-mediated activation of MAP-kinase and phosphorylation of microtubule-associated protein 2 in cerebellar neurons in culture. Brain Res 947: 50–56.

134 Ragozzino D, Giovanelli A, Mileo AM, Limatola C, Santoni A, Eusebi F. (1998) Modulation of the neurotransmitter release in rat cerebellar neurons by GRO beta. Neuroreport 9: 3601–3606.

135 Fiore RS, Bayer VE, Pelech SL, Posada J, Cooper JA, Baraban JM. (1993) p42 mitogen-activated protein kinase in brain: prominent localization in neuronal cell bodies and dendrites. Neuroscience 55: 463–472.

136 Ito M. (1989) Long-term depression. Annu Rev Neurosci 12: 85–102.

137 Thompson RF. (1986) The neurobiology of learning and memory. Science 233: 941–947.

138 Sato M, Suzuki K, Nakanishi S. (2001) NMDA receptor stimulation and brain-derived neurotrophic factor upregulate Homer 1a mRNA via the mitogen-activated protein kinase cascade in cultured cerebellar granule cells. J Neurosci 21: 3797–3805.

139 Light KE, Belcher SM, Pierce DR. (2002) Time course and manner of Purkinje neuron death following a single ethanol exposure on postnatal day 4 in the developing rat. Neuroscience 114: 327–337.

140 Llansola M, Saez R, Felipo V. (2001) NMDA-induced phosphorylation of the microtubule-associated protein MAP-2 is mediated by activation of nitric oxide synthase and MAP kinase. Eur J Neurosci 13: 1283–1291.

141 Ramirez VD, Kipp JL, Joe I. (2001) Estradiol, in the CNS, targets several physiologically relevant membrane-associated proteins. Brain Res Rev 37: 141–152.

142 Das GD, Lammert L, McAllister JP. (1974) Contact guidance and migratory cells in the developing cerebellum. Brain Res 69: 13–29.

143 Bittigau P, Sifringer M, Genz K, Reith E, Pospischil D, Govindarajalu S, Dzietko M, Pesditschek S, Mai I, Dikranian K, Ikonomidou JW, Ikonomidou C. (2002) Antiepileptic drugs and apoptotic neurodegeneration in the developing brain. Proc Natl Acad Sci 99: 15089–15094.

144 Bordey A, Sontheimer H. (2003) Modulation of glutamayergic transmission by Bergmann glial cells in rat cerebellum in situ. J Neurophysiol 89: 979–988.

145 Iino M, Goto K, Kakegawa W, Okado H, Sudo M, Ishiuchi S, Miwa A, Takayasu Y, Saito I, Tsuzuki K, Ozawa S. (2001) Glia –synapse interaction through Ca2+-permeable AMPA receptors in Bergmann glia. Science 292: 926–929.

146 Kulik A, Haentzsch A, Luckermann M, Reichelt W, Ballanyi K. (1999) Neuron-glia signaling via alpha(1) adrenoceptor-mediated Ca(2+) release in Bergmann glial cells in situ. J Neurosci 19: 8401–8408.

147 Watanabe M. (2002) Glial processes are glued to synapses via Ca(2+)-permeable glutamate receptors. Trends Neurosci 25: 5–6.

148 Yamada K, Fukaya M, Shibata T, Kurihara H, Tanaka K, Inoue Y, Watanabe M. (2000) Dynamic transformation of Bergmann glial fibers proceeds in correlation with dendritic outgrowth and synapse formation of cerebellar Purkinje cells. J Comp Neurol 418: 106–120.

149 Jimenez AI, Castro E, Delicado EG, Miras-Portugal MT. (2002) Specific diadenosine pentaphosphate receptor coupled to extracellular regulated kinases in cerebellar astrocytes. J Neurochem 83: 299–308.

150 Bajetto A, Barbero S, Bonavia R, Piccioli P, Pirani P, Florio T, Schettini G. (2001) Stromal cell-derived factor-1alpha induces astrocyte proliferation through the activation of extracellular signal-regulated kinases 1/2 pathway. J Neurochem 77: 1226–1236.

151 Beyer C, Ivanova T, Karolczak M, Kuppers E. (2002) Cell type-specificity of nonclassical estrogen signaling in the developing midbrain. J Steroid Biochem Mol Biol 81: 319–325.

152 Zhang L, Li B, Zhao W, Chang YH, Ma W, Dragan M, Barker JL, Hu Q, Rubinow DR. (2002) Sex-related differences in MAPKs activation in rat astrocytes: effects of estrogen on cell death. Brain Res Mol Brain Res 103: 1–11.

153 Bulleit RF, Hsieh T. (2000) MEK inhibitors block BDNF-dependent and -independent expression of GABA(A) receptor subunit mRNAs in cultured mouse cerebellar granule neurons. Brain Res Dev Brain Res 119: 1-10.

154 Hallak H, Seiler AE, Green JS, Henderson A, Ross BN, Rubin R. (2001) Inhibition of insulin-like growth factor-I signaling by ethanol in neuronal cells. Alcohol Clin Exp Res 1058-1064.

155 Krainock R, Murphy S. (2001) Regulation of functional nitric oxide synthase-1 expression in cerebellar granule neurons by heregulin is post-transcriptional, and involes mitogen-activated protein kinase. J Neurochem 78: 552-559.

156 Thelen K, Kedar V, Panicker AK, Schmid RS, Midkiff BR, Maness PF. (2002) The neural cell adhesion molecule L1 potentiates integrin-dependent cell migration to extracellular matrix proteins. J Neurosci 22: 4918–4931.

157 VanderHorst VG, Holstege G. (1997) Estrogen induces axonal outgrowth in the nucleus retroambiguus-lumbosacral motoneuronal pathway in the adult female cat. J Neurosci 17: 122-136.

158 Mudd LM, Torres J, Lopez TF, Montague J. (1998) Effects of growth factors and estrogen on the development of septal cholinergic neurons from the rat. Brain Res Bull 45: 137-142.

159 Beyer C, Karolczak M. (2000) Estrogenic stimulation of neurite growth in midbrain dopaminergic neurons depends on cAMP/protein kinase A signaling. J Neurosci Res 59: 107-116.

160 Cambiasso MJ, Carrer HF. (2001) Nongenomic mechanism mediates estradiol stimulation of axon growth in male rat hypothalamic neurons in vitro. J Neurosci Res 66: 475-481.

161 Gollapudi L, Oblinger MM. (2001) Estrogen effects on neurite outgrowth and cytoskeletal gene expression in ERalpha-transfected PC12 cell lines. Exp Neurol 171: 308-316.

162 Murphy DD, Segal M. (1996) Regulation of dendritic spine density in cultured rat hippocampal neurons by steroid hormones. J Neurosci 16: 4059-4068.

163 Stone DJ, Rozovsky I, Morgan TE, Anderson CP, Finch CE. (1998) Increased synaptic sprouting in response to estrogen via an apolipoprotein E-dependent mechanism: implication for Alzheimer's disease. J Neurosci 18: 3180-3185.

164 Pozzo-Miller LD, Inoue T, Murphy DD. (1999) Estradiol increases spine density and NMDA-dependent Ca2+transients in spines of CA1 pyramidal neurons from hippocampal slices. J Neurophysiol 81: 1404-1411.

165 Lee MS, Zhu YL, Sun Z, Rhee H, Jeromin A, Roder J, Dannies PS. (2000) Accumulation of synaptosomal-associated protein of 25 kDa (SNAP-25) and other proteins associated with the secretory pathway in GH4C1 cells upon treatment with estradiol, insulin, and epidermal growth factor. Endocrinology 141: 3485-3492.

166 Brake WG, Alves SE, Dunlop JC, Lee SJ, Bulloch K, Allen PB, Greengard P, McEwen BS. (2001) Novel target sites for estrogen action in the dorsal hippocampus: an examination of synaptic proteins. Endocrinology 142: 1284-1289.

167 Rajendren G, Gibson MJ. (2001) A confocal microscopic study of synaptic inputs to gonadotropin-releasing hormone cells in mouse brain: regional differences and enhancement by estrogen. Neuroendocrinology 73: 84-90.

168 Horvath KM, Hartig W, Van der Veen R, Keijser JN, Mulder J, Ziegert M, Van der Zee EA, Harkany T. (2002) Luiten PG, 17beta-estradiol enhances cortical cholinergic innervation and preserves synaptic density following excitotoxic lesions to the rat nucleus basalis magnocellularis. Neuroscience 110: 489-504.

169 Marie H, Billups D, Bedford FK, Dumoulin A, Goyal RK, Longmore GD, Moss SJ, Attwell D. (2002) The amino terminus of the glial glutamate transporter GLT-1 interacts with the LIM protein Ajuba. Mol Cell Neurosci 19: 152-64.

170 Smith SS, Waterhouse BD, Woodward DJ. (1987) Sex steroid effects on extrahypothalamic CNS. I. Estrogen augments neuronal responsiveness to iontophoretically applied glutamate in the cerebellum. Brain Res 422: 40-51.

171 Smith SS, Waterhouse BD, Woodward DJ. (1988) Locally applied estrogens potentiate glutamate-evoked excitation of cerebellar Purkinje cells. Brain Res 475: 272-282.

172 Calabrese EJ. (2001) Estrogen and related compounds: Biphasic dose responses. Crit Rev Toxicol 31: 503-515.

THE AUTHOR'S PUBLICATIONS ON THE SUBJECT

Papers

Zsarnovszky A, Horvath TL, Naftolin F, Leranth L. (2000) AMPA-receptors colocalize with neuropeptide Y- and galanin-containing, but not with dopamine neurons of the female rat arcuate nucleus: a semiquantitative immunohistochemical colocalization study. Experimental Brain Research. 133 (4): 532-537.

Zsarnovszky A, Horvath TL, Garcia-Segura LM, Horvath B, Naftolin F. (2001). Oestrogen-induced changes in the synaptology of the monkey (Cercopithecus aethiops) arcuate nucleus during gonadotropin feedback. Journal of Neuroendocrinology. 13 (1): 22-28.

Belcher SM, **Zsarnovszky A.** (2001) Estrogenic actions in the brain: Estrogen, phytoestrogens and rapid intracellular signaling mechanisms. Journal of Pharmacology and Experimental Therapeutics. 299 (2) 408-414.

Parducz A., **Zsarnovszky A**, Naftolin F., Horvath TL. (2003) Estradiol affects axo-somatic contacts of neuroendocrine cells in the arcuate nucleus of adult rats. Neuroscience. 117 (4): 791-794.

Wong JK., Le HH., **Zsarnovszky A**, Belcher SM. (2003) Estrogens and ICI182,780 (Faslodex) modulate mitosis and cell death in immature cerebellar neurons via rapid activation of p44/p42 mitogen-activated protein kinase. The Journal of Neuroscience. 23 (12): 4984-4995.

Zsarnovszky A, Belcher SM. (2004) Spatial, temporal, and cellular distribution of the activated extracellular signal regulated kinases 1 and 2 in the developing and mature rat cerebellum. Developmental Brain Research. 150 (2): 199-209.

Naftolin F, Garcia-Segura LM, **Zsarnovszky A**, Demir N, Fadiel A, Horvath T. (2005) The estrogen-induced gonadotrophin surge (EIGS). AR Genazzani, J Schenker J, Artini PG, T Simoncini (Eds.): Human Reproduction: 12th World Congress, Venice, March 10-13, 2005, Rome, CIC Edizioni Internazionali, pp 188-197.

Zsarnovszky A, Le H. H, Wang H-S, Belcher S. M. (2005) Ontogeny of rapid estrogen-mediated ERK1/2 signaling in the rat cerebellar cortex in vivo: potent

non-genomic agonist and endocrine disrupting activity of the xenoestrogen bisphenol A. Endocrinology. 146 (12): 5388-5396.

Belcher S.M, **Zsarnovszky A**, Crawford P. A, Hemani H, Spurling L, Kirley T.L. (2006) Immunolocalization of ecto-nucleoside triphosphate diphosphohydrolase 3 (NTPDase3) in rat brain: Implications for modulation of multiple homeostatic systems including feeding and sleep-wake behaviors. Neuroscience. 137 (4): 1331-1346.

Scientific meetings

Zsarnovszky A, Horvath TL, Garcia-Segura LM, Horvath B, Naftolin F. (2000) Plasticity of the hypothalamic GABA system and its relationship to GnRH neurons during positive gonadotrophin feedback in non-human primates. Annual Meeting of the Society for Neuroscience, Abstract.

Zsarnovszky A, Horvath TL, Garcia-Segura LM, Horvath B, Naftolin F. (2000) Plasticity of the hypothalamic GABA system and its relationship to GnRH neurons during positive gonadotrophin feedback in non-human primates. Annual Meeting of the Endocrine Society, Abstract.

Zsarnovszky A, Horvath TL, Garcia-Segura LM, Horvath B, Naftolin F. (2000) Estrogen-induced changes in the synaptology of the monkey (Cercopithecus Aethiops) Arcuate nucleus. Annual Meeting of the Endocrine Society, Abstract.

Zsarnovszky A, Belcher SM. (2001) Estrogen receptor β (ERβ) in the female rat barrelfield: developmental and functional concerns. Annual Meeting of the Society for Neuroscience, Abstract.

Zsarnovszky A, Belcher SM. (2003) Estrogen rapidly modulates the phosphorylation of ERK1/2 in the rat cerebellum in vivo. Annual Meeting of the Society for Neuroscience.

Belcher SM, **Zsarnovszky A.** (2003) Distribution of activated extracellular signal regulated kinases 1 and 2 in the developing and mature rat cerebellum. Annual Meeting of the Society for Neuroscience.

Zsarnovszky A, Belcher SM (2004) Comparative analysis of rapid estrogen and bisphenol A activation of ERK-signaling in rat cerebellar neurons. Annual Meeting of the Society for Neuroscience.

Zsarnovszky A. (2005) Effects of endogenous and exogenous estrogens on the regulatory mechanisms of reproductive functions. 16. Annual Meeting of the Hungarian Associations for Buiatrics.

Publications related to the subject

Zsarnovszky A, Scalise TJ, Horvath TL, Naftolin F. Estrogen effects on tyrosine-hydroxylase-immunoreactive cells in the ventral mesencephalon of the female rat: further evidence for the two cell hypothesis of dopamine function. Brain Research. 868 (2): 363-366, 2000.

Zsarnovszky A, Belcher SM. (2001) Identification of a developmental gradient of estrogen receptor expression and cellular localization in the developing and adult female rat primary somatosensory cortex. Developmental Brain Research. 129 (1): 39-46.

Zsarnovszky A, Smith T, Hajos F, Belcher SM. (2002) Estrogen regulates GFAP-expression in specific subnuclei of the female rat interpeduncular nucleus: a potential role for estrogen receptor beta. Brain Research. 958 (2): 488-496.

Kirby M, **Zsarnovszky A**, Belcher SM. (2004) Estrogen receptor expression in a human primitive neuroectodermal tumor cell line from the cerebral cortex: estrogen stimulates rapid ERK1/2 activation and receptor-dependent cellular migration. Biochemical and Biophysical Research Communications 319: 753-758.

Papers in preparation

Zsarnovszky A, Horvath TL, Garcia-Segura LM, Horvath B, Naftolin F. Plasticity of the hypothalamic GABA system and its relationship to GnRH neurons during

positive gonadotrophin feedback in non-human primates. (Journal of Clinical Endocrinology and Metabolism)

Naftolin F, Horvath TL, **Zsarnovszky A**, Shanabrough M, Lewis C, Chang A, Garcia-Segura LM. Estrogen-induced synaptic plasticity and pituitary sensitization in the control of gonadotrophins. (Endocrine Reviews)

Acknowledgement

I am indebted to my colleagues, Drs. Frederick Naftolin, Tamas L. Horvath and Csaba Leranth at Yale University, Department of Obstetrics and Gynecology; Dr. Scott M. Belcher at University of Cincinnati College of Medicine, Department of Pharmacology and Cell Biophysics; they have provided invaluable professional support, guidance and friendship to support these experiments.

I would like to express my gratitude to Dr. Otto Szenci at Szent Istvan University Faculty of Veterinary Science, who guided me through the process of preparing this work and provided all the help and support necessary to finalize this thesis.

I am grateful for all the help I have received from Professor Endre Brydl at Szent Istvan University Faculty of Veterinary Science, who ensured the adequate environment I needed to prepare this paper, and helped me with his critical and constructive remarks.
Last but not least, I would like to thank Professor Peter Sótonyi for all the valuable help he provided to have this work done.